Application of an Energy-Like Stability Metric for Axial Compressor Design

by

Josep M. Dorca Luque

M.Eng.(Hons) Aerospace Engineering, University of Manchester, UK (2002)

Submitted to the Department of Aeronautics and Astronautics
in partial fulfillment of the requirements for the degree of

MASTER OF SCIENCE IN AERONAUTICS AND ASTRONAUTICS

at the

MASSACHUSETTS INSTITUTE OF TECHNOLOGY

September 2003

Author_____
Department of Aeronautics and Astronautics
August 22, 2003

Certified by_____
Professor Zoltán S. Spakovszky
C.R. Soderberg Assistant Professor of Aeronautics and Astronautics
Thesis Supervisor

Accepted by_____
Professor Edward M. Greitzer
H.N. Slater Professor of Aeronautics and Astronautics
Chair, Committee on Graduate Students

Application of an Energy-Like Stability Metric for Axial Compressor Design

by

Josep M. Dorca Luque

Submitted to the Department of Aeronautics and Astronautics
on August 22, 2003, in partial fulfilment of the
requirements for the degree of
Master of Science in Aeronautics and Astronautics

Abstract

This thesis constitutes the continuation of a line or work stemming from a joint project between Snecma Moteurs, ENSAE, ECL and MIT aimed at the conception of an integrated design methodology for enhanced compressor stability, motivated by the *a posteriori* treatment of compressor stability in the traditional industrial practice. Previous work on the project was geared towards the implementation of an existing reduced-order, modular dynamic compressor model to multi-stage configurations, dissecting the dynamics associated to individual stages and their role in the overall compression system. For the feasible development of an inverse design scheme, however, novel metrics to ascertain the true dynamic stability and robustness of a compressor remain to be defined, together with expedient methods for their practical evaluation in large-scale design processes.

The available dynamic model is extended using existing theory to analyse the temporal behaviour of an energy-like quantity (the disturbance-kinetic energy, in incompressible flows) as a single-valued indicator of dynamic stability. The discrete contribution of each blade-row to the system dynamics is assessed through its emission power of this disturbance-energy. The dynamic consequences of inter-blade-row gap length re-distribution, established by previous research, are re-visited from this energetic standpoint. Elongation of the intra-stage gaps produces a uniform reduction in disturbance-powers, stabilising the compressor, whereas longer inter-stage gaps lead to reduced dynamic stability, mainly due to an increase in power of the blade-rows on the edge of the compressor.

In parallel, a new set of metrics for the degree of dynamic stability and its robustness to flow changes is defined, based on the resonant amplification of disturbances under aerodynamic forcing.

With these tools, a unified relation is uncovered between the flow range to a given level of dynamic stability and an equivalent measure of the performance characteristic curvature, which can be arrived at through the flow-sensitivity of the pre-stall dynamics, characterised either by the growth rate of perturbations or the disturbance-energy. The Equivalent Curvature relation is used as a stepping-stone to formulate a framework that simultaneously links the concepts of stable flow range, dynamic instability margin and dynamic robustness to flow changes. This has been proved valid for incompressible machines, regardless of particular design features, so long as they are captured by the formulation of the dynamic compressor model.

The new metrics and their unified Equivalent Curvature framework are used to define relevant design requirements and cost functions for loading, dynamic stability and robustness to be applied within a multi-objective optimisation. This process is demonstrated in a computationally efficient manner for the integrated preliminary design of a 2-stage compressor. Expedient design changes based on the disturbance-energy power distribution are suggested for a faster progression through the design space. State-of-the-art multi-variable optimisation techniques remain to be incorporated into the scheme, thus completing the effort to create the practical design tool envisioned at the onset.

Thesis Supervisor: Professor Zoltán Spakovszky
Title: C.R. Soderberg Assistant Professor of Aeronautics and Astronautics

Acknowledgements

I am indebted, first of all, to Professor Spakovszky for his timely, systematic dedication to this research and the many enlightening discussions that we have had over the last few months.

As a newcomer to the project, Emmanuel Blanvillain was invaluable in providing the necessary tips and assistance during the initial steps of the implementation efforts.

I am grateful to my office colleagues Sebastien, Deborah and Jay, and the rest of the faculty and staff for contributing to the Gas Turbine Laboratory's motivating, yet familiar working environment. In particular, Vincent Perrot has been an outstanding research partner. It has been a pleasure to work and establish a friendship with him, which I am positive will endure during the years ahead.

I should also thank Dr. Dave Lambie for introducing me to the world of turbo-machinery aerodynamics and his gentleman's treatment before, during and after my stay at MIT. Similarly, Francesc Arbós has given me technical expertise, but above all a solid, encouraging friendship throughout my academic life.

Xevi and Adrià's visit halfway through the academic year was a welcome breath of fresh air. I must thank them and the rest of my friends for their persistent contact throughout this time.

The final and deepest thanks must go to Gemma and my parents, whose wholehearted, constant presence and support has shrunk the distance between the new and the old continents.

Contents

Abstract 3

List of Figures 11

List of Tables 15

1 Introduction 21

1.1 Technical Background 21
1.2 Previous Work 22
1.3 Thesis Framework 23
1.3.1 Joint Project 23
1.3.2 Past and Present Efforts within the Project 24
1.4 Objectives and Thesis Structure 25
1.5 Contributions 25

2 Analysis of Compressor Stability through Energy-Based Considerations 26

2.1 Organisation of the Chapter 26
2.2 The Need for Compressor Dynamics and their Modelling through Modal Oscillations and Disturbance-Energy Conservation 27
2.3 Analytical Development of the Disturbance-Energy Balance Framework 29
2.3.1 Conservation Law for Disturbance-Energy 29
2.3.2 Disturbance-Energy Balance in an Axial Flow Compressor 30
2.3.3 Compressor Dynamic Stability Prediction through Disturbance-Energy 31
2.4 Practical Calculation of DEB for Axial Flow Compressors at Specified Operating Conditions 32
2.4.1 Compressible Mean Flow Model 33

2.4.2 Dynamic Compressor Model 34
2.4.2.1 Theoretical Outline 34
2.4.2.2 Computational Cost in the Context of DEB 37
2.4.2.3 Perturbation Modeshapes Calculation 49
2.4.3 Evaluation of the Disturbance-Energy Balance 44
2.5 Application of *DE* Theory to Compression Systems 44
2.5.1 Moore-Greitzer Compressor Model 45
2.5.2 Standard 1-stage Model with Inter-Blade-Row Gap & Unsteady Loss Effects 48
2.5.2.1 DEB Analysis 48
2.5.2.2 Intra-Stage Gap Length Effects on Dynamic Behaviour 50
2.5.3 Standard 2-stage Model 51
2.5.3.1 Intra-Stage Gap Size Effects in a Multi-Stage Environment 51
2.5.3.2 Inter-Stage Gap Size Effects 53
2.6 Concluding Remarks on the Application of the *DEB* concept 54

3 Stability Metrics Definition and a New Framework for Their Implementation 56

3.1 Motivation for a Unified Set of Dynamic Stability Metrics 56
3.2 Prediction of the Stable flow range to Stall from the Evolution of System Dynamics 58
3.2.1 Physical Basis for a Unique Function to Predict the Stable flow range 58
3.2.2 Development of the Equivalent Curvature Relation 59
3.2.3 Physical Interpretation of Equivalent Curvature K_e 63
3.2.4 Generation of an alternative Equivalent Curvature Relation from Disturbance-Energy Information Only 63
3.2.5 Parametric Deviations from the Equivalent Curvature Relation 65
3.2.5.1 Loss Bucket Effects 65
3.2.5.2 Compressibility Effects 66
3.2.5.3 Gap Length and Blade Geometry Effects 67
3.3 How much σ is enough dynamic stability? 68
3.3.1 The Q-Factor Analogy for the Amplification of Disturbances 68
3.3.2 Practical Application of the Analogy 71
3.4 Robustness of Dynamic Stability to Flow Changes 73
3.5 Summary 77

4 Integrated Design Process for Stability 79

4.1 Introduction 79

4.1.1 The Need for an Integrated Design Methodology 79

4.1.2 A Unified Framework for Compressor Dynamics 79

4.1.3 Organisation of the Chapter 81

4.2 Cost Function Definition 82

4.2.1 Design Requirements 82

4.2.2 Loading Contribution to the Cost Function 83

4.2.3 Dynamic Stability Contribution to the Cost Function 83

4.2.4 Dynamic Robustness Contribution to the Cost Function 86

4.2.5 Overall Cost Function and Potential Errors 86

4.3 Application of the Integrated Optimisation Scheme 87

4.3.1 Unfeasible Design Iteration 89

4.3.1.1 Performance Check 89

4.3.1.2 Stability Check 90

4.3.1.3 Robustness Check 91

4.3.1.4 Overall Cost Function and Required Changes 93

4.3.2 Successful Design Iteration 94

4.3.3 Effects of Individual Changes in Intermediate Iterations 96

4.4 Use of DE power distribution within the integrated scheme 98

4.5 Summary 102

5 Conclusions and Future Work 104

5.1 Summary and conclusions 104

5.1.1 Application of the Disturbance-Energy Analysis within the Existing Dynamic compressor model Framework 104

5.1.2 Stability and Robustness Metrics Definition and Standard Relations for their Assessment 105

5.1.3 Integrated Design Optimisation Scheme for Stability 106

5.2 Recommendations for future work 107

5.2.1 Dynamic compressor model Refinements towards the Application of the *DEB* to a Wider Range of Dynamic Systems and Operating Conditions 107

5.2.2 Extensions to the Equivalent Curvature Relation 108
5.2.3 Integrated Design Optimisation for Enhanced Stability 108

APPENDICES

A Analytical Derivation of the Disturbance-Energy Conservation Law **109**

A.1 Conservation law for Disturbance-Energy 109
A.2 Integral Disturbance-Energy Theorem 111

B Analytical Evaluation of the Terms Contributing to the DE Balance **112**

B.1 Fluxes 112
B.2 Unsteady Term - DEB 114

C 1-D Mean Line Flow Analysis **116**

C.1 Geometric Model and Input Parameters 116
C.2 Flow through a Generic Rotor 118
C.3 Flow through a Generic Stator 119

D Loss and Deviation Models **120**

D.1 Definitions 120
D.2 3D Interpolation Technique 121
D.3 Mapping Inaccuracies 123
D.4 Evaluation of Loss Sensitivity from the Analytic Surface 123

Bibliography **125**

List of Figures

1-1 Inverse Design for Stability – information flow 24

2-1 Schematic of static and dynamic stability 31
2-2 Control Volume definition for the *DE* analysis of a generic axial flow compressor 31
2-3 2-stage compressor dynamic model geometry and definitions 35
2-4 Feasibility of various circumferential modeshapes
to satisfy Longley's spatial resolution requirement 37
2-5 Flow schematic for the calculation of the reduced frequency 38
2-6 Moore-Greitzer eigenvalue map 40
2-7 Eigenvalue map for a 1-stage compressor with 5%
inter-blade-row gap, $4xR_{mean}$ inlet and exit ducts in stable operation 41
2-8 δP modeshape for 2-stage repeating-stage compressor with 5%
inter-blade-row gaps near neutral stability 43
2-9 δV_x & δV_θ modeshapes for 2-stage repeating-stage compressor with
5% inter-blade-row gaps 43
2-10 Dynamic stability evolution as predicted by
critical eigenvalue growth rate (σ) and DEB 46
2-11 Disturbance-Energy Flux distribution for the 1-stage repeating-stage
compressor with 0% R1-S1 gap 46
2-12 Elemental *DE* balance showing zero source/sink powers for inlet and exit ducts 47
2-13 *DEB* unsteady-term numerical convergence for various spatial resolutions 47
2-14 Graphical representation of the elemental *DEB* convergence
for 5,10,25 & 50 intervals per gap 48
2-15 Disturbance-Energy Flux distribution (1-stage repeating-stage compressor,
50% gap, 0 inlet and exit swirl) 49
2-16 Elemental DE Balance showing zero source/sink powers for inlet and exit
ducts (1-stage repeating-stage compressor, 50% gap, 0 inlet and exit swirl) 49

2-17 DEB unsteady-term numerical convergence for various spatial resolutions (1-stage repeating-stage compressor, 50% gap, 0 inlet and exit swirl) 50
2-18 3rd-harmonic dynamic evolution for a range of inter-blade-row spaces 51
2-19 Inter- and intra-stage gaps nomenclature 52
2-20 DEB and σ histories for the 2-stage repeating-stage compressor with varying intra-stage blade-row gaps 53
2-21 Dynamic history for the 2-stage repeating-stage compressor with varying inter-stage blade-row gaps 54

3-1 Relation between characteristic curvature, dynamic stability, stable flow range and stall margin 56
3-2 Definition of surge margin 57
3-3 Logarithmic Equivalent Curvature relation for σ = -0.5 using σ as stability metric 61
3-4 Equivalent Curvature relation for σ=-0.5 using σ as stability metric 62
3-5 Equivalent Curvature relation for σ=-0.5 generated from DEB information 64
3-6 Nondimensional performance characteristics and DEB history for the 1-stage standard compressor with 1% inter-blade-row gaps, at 35% corrected speed and with increasingly narrow loss buckets 65
3-7 Position of compressors from the loss-factor parametric study on the Equivalent Curvature relation 66
3-8 Close-up of deviations from Equivalent Curvature relation due to inter-blade-row gap size and engine speed 67
3-9 Nondimensional characteristics and DEB history for 1-stage standard compressor with 1% inter-blade-row gap at different rotational speeds 67
3-10 Range prediction error for the 1-stage standard compressor with varying inter-blade-row gap 68
3-11 Stability margin rule relating the maximum allowable Q-factor to its corresponding σ/ω contour on the complex eigenvalue map 71
3-12 Rotation rate sensitivity studies 73
3-13 Average curvature error with differente degrees of compressibility for σ_{OP} =-0.3 76
3-14 Polynomial interpolation surfaces with 3(a), 4(b), 5(c) and 6(d) terms 77

4-1 Logical path to the Equivalent Curvature relation 80
4-2 Unified Equivalent Curvature relation for various dynamic stability levels 80
4-3 Comparison between $\Delta\phi$ computations for compressors with excessive (1), insufficient (2) and correct (3) Q-factors at the operating point 84
4-4 Outline of procedures in one optimisation iteration 88
4-5 Loading check for unfeasible 2-stage compressor 89
4-6 Eigenvalue history for unfeasible 2-stage compressor 90
4-7 Nondimensional σ-history for unfeasible 2-stage compressor 90
4-8 Range prediction error for unfeasible 2-stage compressor 92
4-9 Loading check for feasible 2-stage compressor 94
4-10 Comparison of eigenvalue migration paths 95
4-11 Reduced and complete dynamic history for the 2-stage compressor before and after optimisation 96
4-12 Evolution of limit-stability point for usccessive optimisation steps 97
4-13 Disturbance-energy power distribution for unrefined solution at design and neutral stability mass flow 98
4-14 Performance variation for individual blade-row enhancements from initial optimiser solution 99
4-15 Dimensional σ-histories for individual blade-row enhancements from initial optimiser solution 100
4-16 Non-dimensional σ-histories for individual blade-row enhancements from initial optimiser solution 100
4-17 Dynamic stability and robustness for individual blade-row enhancements from initial optimiser solution 101
4-18 Comparison of DE-power distributions between initial optimiser solution and enhanced stator 2 configuration 101

B-1 Flux integration schematic 113
B-2 Unsteady term integration procedure 115

C-1 Mean flow model – nomenclature and definitions 117

D-1 Sample loss dataset obtained from CFD or empirical tests 120
D-2 Analytic surface mapping of experimental/computational data 122
D-3 Least-squares mapping error for sample experimental data 123

List of Tables

2-1 Transient timescales for standard series of compressors 39

3-1 Compressors studied towards identification of the Equivalent Curvature relation 59
3-2 Mach number dependency of Equivalent Curvature logarithmic errors 61

4-1 Design requirements summary of the 2-stage compressor integrated optimisation for stability 87
4-2 Design features before and after optimisation 89
4-3 Predicted and actual performance values for optimised solution 95

Nomenclature

Acronyms

CFD Computational Fluid Dynamics

CREATE Compresseur de Recherche pour l'Etude des effets Aerodynamiques et TEchnologiques (Research Compressor for the study of Aerodynamic and Technological Effects)

ECL Ecole Central de Lyon

ENSAE Ecole Nationale Supérieure de l'Aéronautique et de l'Espace

DE Disturbance-Energy

DEB Disturbance-Energy Balance

GTL Gas Turbine Laboratory

NS Neutral Stability

KE Kinetic Energy

UAV Unmanned Air Vehicle

SM Surge Margin

PR Pressure Ratio

MG Moore-Greitzer

RMS Root Mean Square

Greek

α absolute flow angle

β relative flow angle, reduced frequency

δ deviation angle, perturbation, damping frequency

ε disturbance-energy density

ϕ flow coefficient

γ ratio of specific heats, stagger angle

ι incidence

φ phase

λ rotor blade-row inertia, blade passage inertia

μ rotor + stator blade-row inertia

ρ air density

Ω rotational speed

σ_n growth rate

ω loss coefficient, frequency

ω_d damped frequency

ω_{res} resonant frequency

ω^r rotation rate

ω_n natural frequency

Ψ_{TS} total-to-static pressure ratio

τ unsteady-loss time lag, characteristic time

ξ damping ratio

Roman

a speed of sound

A cross-sectional area

$\mathcal{B}$ transmission matrix

c_P specific heat at constant pressure

c blade-row chord, damping

$\mathcal{C}$ cost function

$\mathcal{E}$ error

F forcing amplitude

$\mathcal{F}$ disturbance-energy flux

i index

I disturbance-energy intensity

j index, $j=\sqrt{-1}$

J polar inertia

k stiffness

K curvature

L loss coefficient, neck length in a Helmholtz resonator

m mass

$\dot{m}$ mass flow

M Mach number

n harmonic number

N rotation speed, number of stages

P pressure

$\mathcal{P}$ disturbance-energy power

Q amplification factor

r radius

r ratio between forcing and natural frequencies

R mean radius

s entropy, growth rate, blade pitch

T temperature

U wheel speed

V velocity, integration volume

x axial location

X displacement amplitude

$\mathcal{X}$ transmission matrix

$\mathcal{Y}$ transmission matrix

Superscripts

^{TS} total-to-static

$^{-}$ mean quantity

$'$ in relative frame

Subscripts

$_{acc}$ acceleration

$_{AVE}$ averaged value

$_{corr}$ corrected value

$_{des}$ at design

$_{e}$ equivalent

$_{f}$ forced

$_{H}$ Helmholtz

$_{in}$ at inlet

$_{KE}$ kinetic energy term

$_{NS}$ at neutral stability

$_{OP}$ at the operating point

$_{out}$ at exit

$_{P}$ pressure term

$_{\theta}$ in tangential direction

$_{res}$ at resonance

$_{R}$ rotor

$_{S}$ stator

$_{x}$ in axial direction

$_{T}$ stagnation quantity

Chapter 1

Introduction

1.1 Technical Background

The issue of dynamic stability in axial flow compressors has been the subject of intensive study as the use of gas turbine engine technology has become widespread. When the aerodynamic conditions are such that instability develops in compression systems, severe performance, mechanical, operational and economic penalties can be incurred.

Cumpsty [2] broadly classifies instabilities between stall and surge. Surge is essentially a 1-D oscillating, engine-wide phenomenon in which the average mass flow through the system oscillates in time, at a frequency that is typically between 3-10Hz, leading to large changes in performance (see Greitzer [6]). The event can be so abrupt that, in some instances, flow reversal takes place and flow from the hot engine sections can be expelled through the inlet. Surge can result in widespread mechanical damage and/or catastrophic failure of the engine. To put this in perspective, Blanvillain [1] estimated that a non-fatal in-flight surge event can generate $3.5M in costs to a typical airline.

Rotating stall, on the other hand, is a non-uniform, long-circumferential-wavelength oscillation instigated by a region of the annulus that contains reduced flow. This region of low velocity, known as the stall cell, rotates at a fraction of the rotor speed (20-50%) and one or more blades experience stall as they pass through it. Depending on the spanwise extent of the stall cells, one or more of them can be present, and it is not unusual for rotating stall to be a precursor of surge, in which case the instability extends longitudinally along the whole machine.

It is crucial to understand the paths through which stall can be triggered. Camp and Day [2] identified two distinct inception mechanisms: spike-like stalling of a particular blade-row, which can lead to an overall compressor stall, and modal stall inception, caused by long-wavelength circumferential modes of oscillation that extend through the entire compressor length. It is on the latter that this work is focused.

Extensive efforts over the past two decades have been directed towards the physical prediction of the inception of surge and rotating stall, and the understanding of their underlying dynamics. In the meantime, the common industrial design practice regarding compressor stability has been to use the surge margin as a safety measure, limiting the pressure ratio to a fraction of its maximum value at a particular flow condition. While this steady-state, conservative approach ensures safe operation of the machine, it implies having to sacrifice potential aerodynamic performance and efficiency. On the other hand, one cannot afford to lower the surge margin requirements without knowledge of the actual system dynamics; according to Blanvillain [1], a reduced-stability fleet could entail annual maintenance and management costs of $10M, a good proportion of the airline's revenues.

As a result of all these present deficiencies, the motivation for accurate modelling of compressor dynamics and their incorporation in the design process is thus established.

1.2 Previous Work

This thesis makes extensive use of a line of work started by Moore and Greitzer [10], who analysed the behaviour of small disturbances in compressor flow fields, understood as natural modes of resonance of the compression system. The time-evolution of these oscillations is linked to the mean background flow, which governs the damping of the system. When this becomes negative, the compressor becomes unstable, through either rotating stall or surge.

Spakovszky [12] further elaborated a modular application of the same low-order concept, through which the dynamics of both blade-rows (considered as semi-actuator disks) and gaps/ducts are cast in the form of transmission matrices, capturing their dynamic interaction effects. This more evolved model renders far greater flexibility, allowing for the construction of a compressor consisting of any combination of the previous elements. Because of its analytical nature, this model also lends well to the treatment and physical understanding of the individual dynamic mechanisms involved in the stall phenomenon. Such capability was exploited by Spakovszky [13] to explain, for the first time, the existence of backward travelling rotating stall waves in centrifugal compressors. It is this model that is used in this thesis as the primary tool for the analysis of dynamic stability.

Fréchette [4] pursued a further line of thinking based on the same modelling framework. He started by proving that there exists a perturbation energy-like quantity that is conserved in any region of a turbomachinery flow where blade-rows are absent. For incompressible flows, this quantity is the kinetic energy of the fluid due to the disturbance-velocity field, characterised by the corresponding modal oscillations. The compressor-wide variation of this energy in time can be used as an analogous metric to ascertain whether the compressor is in a stable or unstable operating condition: it grows in the first case and decays in the second.

Furthermore, the conservation law for this disturbance-energy lends well to the application of a control volume analysis, through which the individual blade-row disturbance powers can be found. This provides a power distribution along the machine that relates to the stability-impact of each rotor and stator.

In this thesis, attention is turned to the application of Fréchette's energy-based analysis to Spakovszky's dynamic compressor model, with a view of benchmarking their stability predictions and to apply the localised dynamic information within an integrated design process.

1.3 Thesis Framework

1.3.1 Joint Project

A joint effort between the French aerospace propulsion company Snecma Moteurs, the French universities Ecole Nationale Supérieure de l'Aéronautique et de l'Espace (ENSAE) and Ecole Central de Lyon (ECL), and the Massachusetts Institute of Technology (MIT) was initiated in 2001 in order to put together a design framework for an advanced core compressor to be used in an unmanned air vehicle (UAV). The details of this agreement and the delineation of the expertise contributed by each of the parties are reviewed in Blanvillain [1].

Given the comprehensive expertise in compressor stability gained over the last two decades by the Gas Turbine Laboratory (GTL), MIT's key role is the practical implementation of the knowledge base acquired over these years. Representing a departure from traditional industry procedures, dynamic stability considerations are to be embedded in the design process from the onset.

Inverse Design for Stability

The architecture for the proposed inverse design for stability is shown below. The initial aerodynamic design can be used to obtain the performance characteristics, which provide the mean flow information for the evaluation of the dynamic behaviour through Spakovszky's reduced order model. Having obtained the eigenvalues for the flow modal oscillations, an objective set of metrics should be used to assess the dynamic stability and robustness of the system at the required operating condition. The shape of the loss buckets can then be altered in an inner optimisation loop until the required stability margins have been satisfied.

The final task is the definition of a geometry that is capable of delivering the required loss buckets. To this effect, a series of CFD studies should be carried out to establish what type of blade profile changes modify the loss buckets in the desired manner.

The new blading can be fed to the mean flow solver and the dynamic compressor model, repeating the iterative procedure until convergence in performance and stability has been achieved.

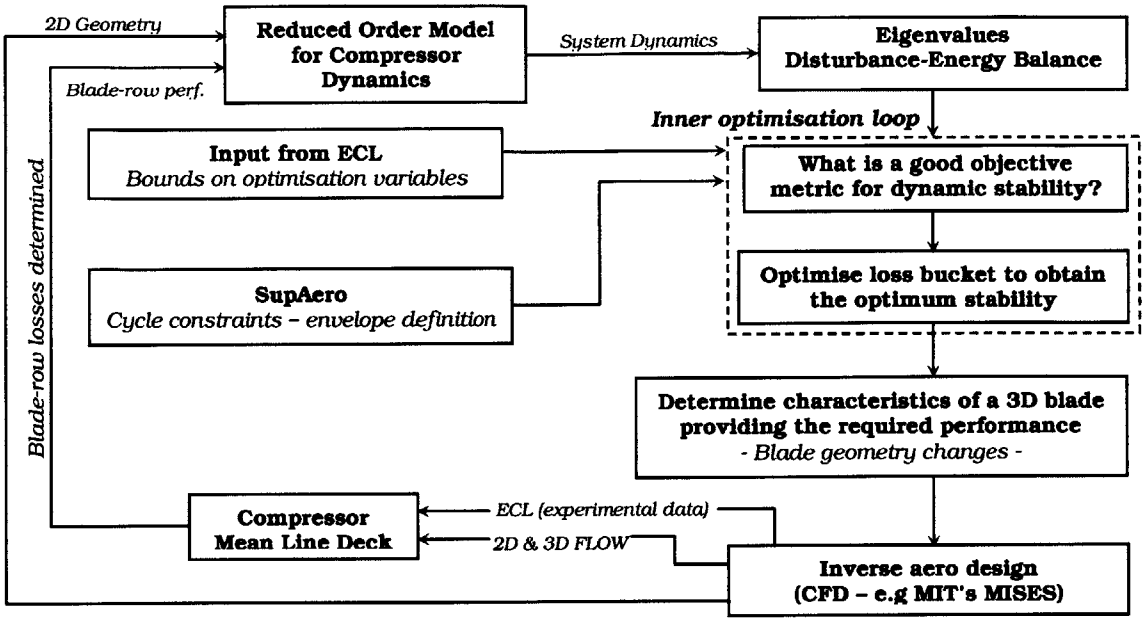

Figure 1-1 Inverse Design for Stability – information flow

1.3.2 Past and Present Efforts within the Project

Blanvillain's work [1] represented the first-year effort in the construction of the inverse design scheme. Spakovszky's reduced order model was systematically implemented, and its capabilities used to analyse the stability characteristics of a candidate compressor for the Joint Project, Snecma's CREATE (Compresseur de Recherche pour l'Etude des effets Aérodynamiques et TEchnologiques).

Preliminary design guidelines for stability were issued, stemming from a series of parametric studies. In summary, it was found that increasing the inertia of a blade-row has a negligible effect on the growth rate of the perturbation waves, and that increasing the separation between blade-rows in the same stage enhanced stability, whereas enlarging the gaps between different stages had the opposite effect.

The efforts of this research are centred on the inner optimisation loop shown in Figure 1-1. This thesis deals with the development of a new set of stability metrics based on compressor dynamics, and the demonstration of their use within an optimisation loop.

In parallel, Perrot [10] examines the design changes required to manipulate the shape of the loss buckets, develops systematic ways to implement these alterations and explores the use of multi-variable optimisation techniques for the inner loop.

1.4 Objectives and Thesis Structure

This thesis deals with three successive objectives. Each chapter is devoted to one of these:

- Applying the results from Spakovszky's model to Fréchette's disturbance-energy balance, and benchmarking the relative merits of each method as an indicator of system stability.
- Using the available dynamics information to derive a set of new physics-based metrics that provide a true measure of the degree of stability and its robustness to changes in operating condition.
- Demonstrating the use of the new metrics within an integrated design scheme for stability in a computationally efficient fashion, using dynamic compressor model outputs and standard relations to derive the compliance of the machine with the pre-specified stability and robustness margins.

1.5 Contributions

In summary, the three key contributions of the present work are:

1. The development of a simple relationship between stable flow range, compression system damping and robustness to instability for low-speed axial compressors, denoted as the equivalent curvature characteristic.
2. The application of the concept of equivalent curvature to derive a set of novel physics-based metrics for dynamic stability and its robustness to flow variations.
3. The implementation of the novel metrics and the unified equivalent curvature relation to a practical design architecture incorporating simultaneous performance and stability requirements, together with the delineation of dynamically beneficial design guidelines.

Chapter 2

Analysis of Compressor Stability through Energy-Based Considerations

2.1 Organisation of the Chapter

This chapter presents the sequence of steps required to determine the dynamic history of an axial flow compressor, which is necessary for the systematic definition of the new stability metrics put forward in Chapter 3. Only the essential theoretical scope is given in the overview of the various models employed, with a fundamentally practical orientation, while the core of the derivations can be found in the relevant Appendices. Additional insights are provided when specifically related to the problem at hand, particularly in the areas of numerical cost and accuracy, central to the optimisation task ahead.

The final aim of the procedural architecture described here is the assessment of the Disturbance-Energy Balance (*DEB*) for the machine in question, a pivotal tool developed by Fréchette [4] that provides a localised stability-performance distribution as well as the overall machine degree of stability. Its key theoretical concepts are outlined at the onset. This is useful to identify the information that must be produced beforehand and in which order:

- Background flow field → *Mean line flow solver*
- Characterisation of the fundamental aerodynamic oscillations → *Dynamic model*
- Velocity and pressure disturbance flow field → *Perturbation modeshapes*

  [The work presented here stems from an incompressible formulation. However, a compressible dynamic compressor model would entails the characterisation of an entropy wave, too.]

Each of these differentiated tasks is given a concise subsection, together with the associated methods and implementation issues.

The complete course of action is benchmarked against former stability studies performed by Blanvillain [1], related to the effects of various gap spacings on the overall stability. The trends are reproduced from a *DEB* standpoint and the work is taken a step further by analysing the contributions of the different blade-rows to the stability gains/losses through the model's extended capabilities.

2.2 The Need for Compressor Dynamics and their Modelling through Modal Oscillations and Disturbance-Energy Conservation

The stability of a compression system designed following the usual industry practice is guaranteed through the use of the traditional surge margin concept, based on static stability considerations (see Chapter 3 for a thorough discussion of its validity). This represents a conservative, *brute-force* approach that sacrifices aerodynamic performance for alleged levels of safety.

Before discussing the different modelling approaches for compressor dynamics, their importance must be highlighted through the concepts of static and dynamic stability in a compression system (see Greitzer [6] for a more comprehensive overview).

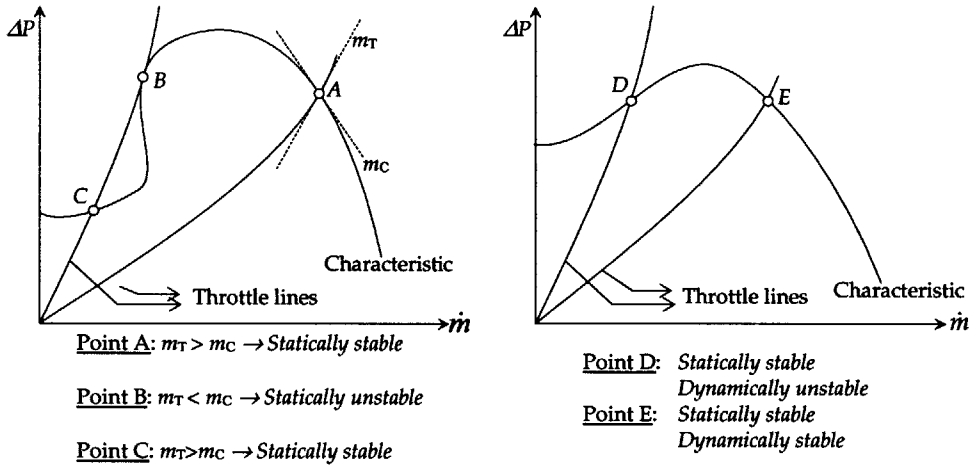

Point A: $m_T > m_C \rightarrow$ *Statically stable*

Point B: $m_T < m_C \rightarrow$ *Statically unstable*

Point C: $m_T > m_C \rightarrow$ *Statically stable*

Point D: *Statically stable*
Dynamically unstable

Point E: *Statically stable*
Dynamically stable

Figure 2-1 Schematic of static and dynamic stability

- Static instability is related to the departure from the operating point in a non-oscillatory fashion. In order to avoid this behaviour, an increase in mass flow along the system throttle line must always produce a greater increase in pressure ratio than if one followed the compressor characteristic. Thus, if the slope m of the characteristic is greater than that of the throttle line, the system is statically unstable.
- Dynamic stability, on the other hand, determines whether oscillations that grow in time develop in the flow field. As the operating point oscillates about point *D* above, there is a pressure ratio increase when the mass flow goes up, and vice-versa. Therefore, the two

perturbations are in phase and the energy input ($\delta P \cdot \delta \dot{m}$) into the system is positive, so the disturbance has a positive growth rate in time. Conversely, when the characteristic has a decreasing slope, as in point *E*, the pressure ratio goes down as the mass flow through the machine increases. These two perturbations have a phase difference of one half-cycle and there is no net energy being introduced into the flow field: the system is damped.

The key issue about this discussion is that an operating point that is statically stable may well be dynamically unstable. Static stability is *necessary but not sufficient* to ensure overall compressor stability; dynamics must be considered, too. In fact, it is the dynamic stability requirement that tends to be violated first

The dynamic compressor model used by Blanvillain [1] is the direct predecessor of this work and was developed by Spakovszky [12] as an incompressible, modular extension of the small-disturbance approach adopted by Moore and Greitzer [10]. Essentially, small disturbances in an incompressible flow field – namely vorticity and pressure perturbations – are analysed on a system-wide basis, considering their natural modes of oscillation within the compressor. The damping of these system resonances is governed by the background mean flow, the conditions of which determine whether perturbations grow or decay in time. This lends well to a standard eigenvalue problem formulation, through which the different modes of oscillation can be analysed.

Fréchette [4] used this information to arrive at an alternative way to understand compressor dynamics. Assuming small disturbances in density, velocity and entropy (for the compressible case) within the Navier-Stokes transport equations, it was shown that an energy-like perturbation quantity also obeys the Reynolds Transport Theorem in a flow field without blade-rows. In the incompressible case, this quantity is simply the additional fluid kinetic energy due to the disturbance velocities, and is referred to as *Disturbance-Energy* (*DE*). It will be shown, as was established by Fréchette, that both the modal representation of the disturbances and the temporal behaviour of *DE* can be used to assess the stability characteristics of a compression system: in the unstable regime, at least one natural flow resonance exhibits positive damping, and at the same time, the *DE* contained within the entire compressor is seen to grow in time; the opposite happens when the machine is in a stable operating condition.

In the illustrative, incompressible examples provided throughout this thesis, it will always be found that one particular, lightly-damped resonance mode is critical to dynamic stability. The rest of the modes are assumed to be damped enough that their contributions to the perturbation fields are negligible. Thus, *DEB* will be based only on the disturbance velocity associated with the critical mode. However, in systems with multiple, lightly-damped modes of oscillation, *DEB* represents the additional kinetic energy associated with all of them in conjunction. The beauty of this stability-metric

is that it represents the dynamic state of the machine through only *one* number and avoids having to deal with the growth rates of all the perturbation modes separately.

There is an additional advantage in the use of *DEB* as a pointer to stability. Because one is now concerned with the transport of an additional kinetic energy in the flow field, it is possible to determine how much *DE* is convected by the mean flow into and out of any arbitrary control volume. If this control volume contains a blade-row, the difference in the *DE* that comes in and that which goes out, per unit time, is not the same as its rate of change in that region. This is because blade-rows are capable of introducing or removing disturbance-energy from the system, effectively acting as *DE* source/sink terms, in the standard control volume terminology. It is the ability to determine the individual blade powers that offers an advantage over the standard eigenvalue information: this makes it possible to know the extent to which each independent blade-row impacts the overall dynamics of the system.

Therefore, the motivation to incorporate Fréchette's *DE* analysis into Spakovszky's dynamic compressor model is clear: to allow for the use and comparison of both concepts in the definition of new stability metrics, and to apply the localised dynamic information in an integrated design process.

2.3 Analytical Development of the Disturbance-Energy Balance Framework

2.3.1 Conservation Law for Disturbance-Energy

The physical definition of disturbance-energy can be arrived at by straightforward manipulations of the Navier-Stokes equations, the details of which are summarised in Appendix A.

Through appropriate combination of the linearised transport equations for mass, momentum and energy, Fréchette showed that for incompressible flow the quantity $\varepsilon = \rho(\delta V)^2/2$ obeys the following conservation law

$$\frac{D\varepsilon}{Dt} + \nabla \cdot \vec{I} = 0 \tag{2.1}$$

where:
$$\vec{I} = \delta P \delta \vec{V} \tag{2.2}$$

Therefore, ε is defined as *Disturbance-Energy Density* and has units of energy per unit volume. If one carries out a similar compressible analysis, *DE* is found to possess an internal-energy-like term of the form $(\delta P)^2/2\overline{\rho a}^2$. However, in the simplified incompressible case, *DE* is simply the additional fluid kinetic energy per unit volume due to the perturbation velocities.

The flux term $\vec{I}$, known as the *Disturbance-Energy Intensity*, represents the time rate of change of disturbance-pressure work per unit area exerted on a given cross-section of the compressor.

Integral Disturbance-Energy Theorem

In view of an application of the *DE* transport concept in a control-volume analysis, the conservation law is best viewed in integral form over a generic volume *V*, the final form of which is

$$\frac{\partial}{\partial t}\iiint_{CV} \varepsilon dV + \oiint_{CV}\left(\varepsilon\bar{\bar{V}} + \bar{\bar{I}}\right)\cdot\vec{n}dA = 0 \qquad (2.3)$$

The control volume analysis can be applied to discrete regions of the domain at will, in order to assess the local contributions of the various terms to the Volumetric Rate of Increase in *DE*. From this point onwards, this quantity will be referred to as *Disturbance-Energy Balance (DEB)*,

$$DEB = \frac{\partial}{\partial t}\iiint_{V} \varepsilon dV = \frac{\partial}{\partial t}\iiint_{V} \rho\frac{(\delta V)^2}{2}dV \qquad (2.4)$$

In an incompressible model, the sum of the net *DE* increase due to convection and the disturbance-pressure work per unit time must be equal to the rate of change of disturbance-kinetic energy inside any given control volume, which is analogous to *DE*. If compressible effects were taken into account, then the net energy balance put into the system would be split between kinetic and internal disturbance energy.

The boundaries on which the disturbance-intensity term, $\bar{\bar{I}}$, acts are the annular cross-sections that define the longitudinal limits of the control volume, i.e. the same surfaces through which the convective term is calculated. Therefore, the term in the second integral in (2.3) can be thought of as an overall *DE* flux $\mathcal{F}$, although strictly only the convective term really fits that description, being transported by the mean flow velocity.

$$\mathcal{F} = \oiint_{CV}\left(\varepsilon\bar{\bar{V}} + \bar{\bar{I}}\right)\cdot\vec{n}dA = \oiint_{CV}\left(\rho\frac{(\delta V)^2}{2}\bar{\bar{V}} + \delta P\delta\bar{\bar{V}}\right)\cdot\vec{n}dA \qquad (2.5)$$

Both the mean and the perturbation velocities are parallel to the wall at the hub and case, so their product with the normal vector at those two bounding surfaces is zero. Therefore, the inlet and exit fluxes reduce to the integral over the respective annuli

$$\mathcal{F} = \mathcal{F}_{in} - \mathcal{F}_{out} = \iint_{Ain}\left(\rho\frac{(\delta V)^2}{2}V_x + \delta P\delta V_x\right)dA - \iint_{Aout}\left(\rho\frac{(\delta V)^2}{2}V_x + \delta P\delta V_x\right)dA \qquad (2.6)$$

2.3.2 Disturbance-Energy Balance in an Axial Flow Compressor

The equations presented so far are representative of flow fields without source or sink terms, such as blade-rows. However, our control volume of interest is that of a standard axial-flow compressor (see Figure 2-2).

The *DE* conservation law only holds in the form presented in *(2.2)* within the various ducts. However, when blade-rows are included inside the domain, their *DE* power $\mathcal{P}_{row}$ must be accounted for when calculating the overall energetic balance.

In the absence of source terms, the overall *DEB* in any arbitrary control volume must be equal to the net flux, $\mathcal{F}_{in} - \mathcal{F}_{out}$. When that is not the case, i.e. when a blade-row *is* present in the control volume, the difference must be accounted for by a *DE* power, $\mathcal{P}$, defined as

$$\mathcal{P} = \frac{\partial}{\partial t}\iiint_V \varepsilon dV - \left(\mathcal{F}_{in} - \mathcal{F}_{out}\right) \tag{2.7}$$

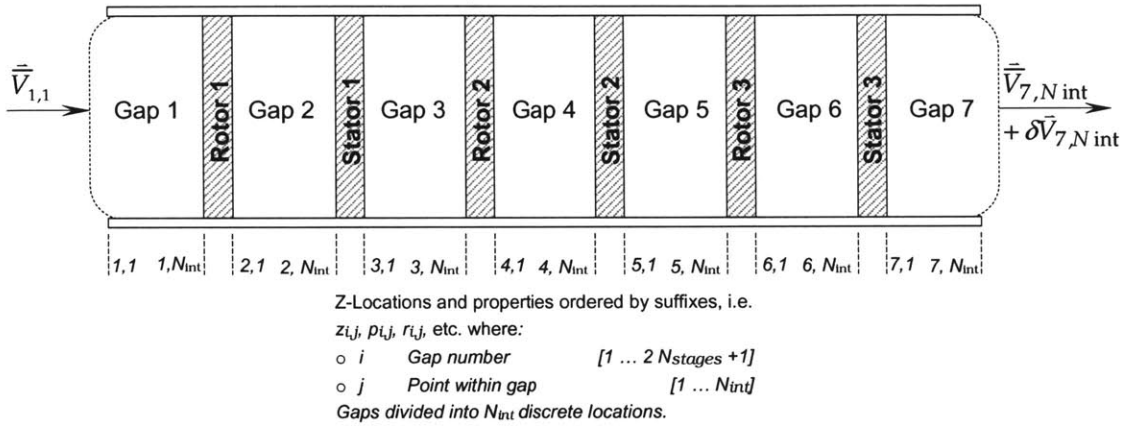

Figure 2-2 Control Volume definition for the DE analysis of a generic axial flow compressor

The growth rate of the modal oscillations is zero at neutral stability. Therefore, the perturbation velocities remain constant in time and *DE* cannot possibly change. Any net flux across the entire compressor must be accounted for by the cumulative power of all the blade-rows. Hence the equivalence between instability prediction through eigenvalues and *DE*.

When analysing individual gaps or ducts, one finds that the net flux is not zero if the machine is operating away from neutral stability. In that case, this non-zero effective flux must be balanced by the rate of change of *DE*, since there is no physical mechanism for additional energy creation/destruction without blade-rows being present, other than through unsteadiness.

As the system damping increases, the perturbation quantities start to decay in time, and consequently there must be an overall decrease in disturbance-energy. The net flux, in this case, need not be balanced only by the sum of all the blade-row powers, but also by the temporal evolution of *DE*.

2.3.3 Compressor Dynamic Stability Prediction through Disturbance-Energy

In a more general form, the Integral *DE* Conservation Law for a Compressor can be written as

$$\frac{\partial}{\partial t}\iiint_V \rho\frac{(\delta V)^2}{2}dV + \iint_{Aout}\left(\rho\frac{(\delta V)^2}{2}V_x + \delta P\delta V_x\right)dA - \iint_{Ain}\left(\rho\frac{(\delta V)^2}{2}V_x + \delta P\delta V_x\right)dA = \sum_{i=1}^{Nrows}\mathcal{P}_i \tag{2.8}$$

Once the longitudinal and circumferential perturbation modeshapes have been determined, the power of each of the individual blade-rows can be calculated, together with the local modular value of *DE* growth. The details of this procedure are outlined in Section 2.4.3.

By means of these computations, *DEB* is found, as expected, to exhibit additive properties: the sum of the net growth of *DE* of each individual compressor region amounts to the total system *DEB*. This overall growth is linked to the growth rate of the stability-critical eigenvalue (the one reaching zero-damping first as the machine is throttled down). Therefore, one must expect that the *DEBs* for any control volume within the compressor will have the same sign. If the machine is in a stable operating condition, the net growth of *DE* must be negative throughout the domain (regardless of the portion of the machine enclosed by the boundaries of the control volume in question) and vice-versa.

On the other hand, the *DE* powers need not comply with any particular trend and will be shown to be the true indicators of stability-related performance. One would hope to reduce the $\mathcal{D}$ levels for all blade-rows, ideally reaching negative values for all of them. In that situation, all modules would be acting as *DE* sinks.

Gysling [7] and Fréchette [4] demonstrated that, for a Moore-Greitzer type compressor, the *DE* conservation law could be used analogously to predict the onset of dynamic instability.

Neutral Stability:
$$DEB = \frac{\partial}{\partial t}\iiint_V \mathcal{E}\,dV = 0 \quad \Leftrightarrow \quad \frac{\partial \Psi^{TS}}{\partial \phi} = 0\,,\ i.e.\ \sigma = 0 \tag{2.9}$$

Stable Condition:
$$DEB = \frac{\partial}{\partial t}\iiint_V \mathcal{E}\,dV < 0 \quad \Leftrightarrow \quad \frac{\partial \Psi^{TS}}{\partial \phi} < 0\,,\ i.e.\ \sigma < 0 \tag{2.10}$$

Unstable Condition:
$$DEB = \frac{\partial}{\partial t}\iiint_V \mathcal{E}\,dV > 0 \quad \Leftrightarrow \quad \frac{\partial \Psi^{TS}}{\partial \phi} > 0\,,\ i.e.\ \sigma > 0 \tag{2.11}$$

In other words, there is no net growth or decay of disturbance-kinetic energy in the control volume at the onset of instability. Expansion of (2.9) gives the *DEB Criterion for Neutral Stability*

$$\iint_{Aout}\left(\rho\frac{(\delta V)^2}{2}V_x + \delta P\,\delta V_x\right)dA - \iint_{Ain}\left(\rho\frac{(\delta V)^2}{2}V_x + \delta P\,\delta V_x\right)dA = \mathcal{F}_{out} - \mathcal{F}_{in} = \sum_{i=1}^{Nrows}\mathcal{D}_i \tag{2.12}$$

2.4 Practical Calculation of DEB for Axial Flow Compressors at Specified Operating Conditions

The *DEB* control-volume analysis necessitates the resolved perturbation flow field. This, in turn, can only be attempted when the mean background flow has been characterised. Therefore, the logical sequence of steps leading to the determination of *DEB* is as follows:

(i) Calculation of the background flow quantities via, for instance, a 1-D mean line flow solver. Inputs to the subsequent dynamic compressor model include the average velocity & pressure fields and the loss-curve derivative at the operating point of interest.

(ii) Determination of the modal eigenvalues through, for example, Spakovszky's [12] incompressible dynamic model for compression systems. This enables a systematic isolation of the critical eigenvalue, which is carried forward for the *DEB* analysis.

(iii) Development of the longitudinal and circumferential modeshapes for perturbation pressure and velocities (both axial and angular).

(iv) Calculation of individual $\mathcal{P}$ and $\mathcal{F}$ for each modular compressor element, following the methodology established in 2.3.

(v) Overall *DE* analysis and stability assessment according to the criterion set forth in 2.3.3.

Steps (i) through (iii) are discussed in detail in the following sections.

2.4.1 Compressible Mean Flow Model

A compressible mean line solver has been implemented to more accurately represent the performance characteristic of any axial flow compressor, although the dynamic compressor model devised by Spakovszky [12] is incompressible in nature.

The mean line tool handles compressors of any number of stages and generic loss and deviation distributions, obtained either empirically, through CFD computations or by simple estimations. The variations of loss and deviation with both blade incidence and relative Mach number are captured. As well as a closer approximation to the performance levels, the analytical treatment of the loss surface enables a direct calculation of the loss-sensitivity $\partial L/\partial\beta_1$, which is to be fed to the aforementioned dynamic compressor model. Deviation sensitivity is not incorporated in the dynamics.

The aforementioned compressible additions do not enhance the physics that can be captured by Spakovszky's analysis. However, the background flow dictates the dynamic behaviour of the perturbation modeshapes, and the additional compressible considerations provide more accurate mean velocity and mean pressure fields. In addition, the loss sensitivity is evaluated at the correct Mach number plane. While there are no disturbance quantities linked to the degree of compressibility, this additional degree of freedom enables the slope of the loss to vary as the blade-rows undergo different operating speeds.

Given the extensive coverage of mean flow models in the literature, the detailed structure of the mean line solver is only briefly discussed in Appendix C. Separately, Appendix D is dedicated to the

three-dimensional analytical mapping of the loss and deviation buckets, and the extraction of the required sensitivity from the former.

2.4.2 Dynamic Compressor Model

2.4.2.1 Theoretical Outline

The dynamic compressor model devised by Spakovszky [12] captures the compressor-wide natural modes of flow oscillation that control the dynamic behaviour of the compression system. This is achieved by suitable manipulation of the linearised flow equations leading to an eigenvalue problem, assuming incompressible flow and a semi-actuator disk description of the blade-rows.

Separate dynamic analyses can be performed for ducts, rotor/stator blade-rows and inter-blade-row gaps. For each of these entities, the unsteady, incompressible, small-perturbation governing equations are solved exactly for the perturbation values of pressure, axial and angular velocities. The spatial structure of the flow oscillations is broken down into spatial Fourier harmonics, each n^{th} spatial harmonic being dealt with separately, whereas the temporal behaviour is captured by conversion of the equations to the frequency domain using a Laplace-transform. This solution can be compacted into the so-called *transmission matrix* for the component in question (for a detailed derivation, see Spakovszky[12]).

Transmission matrix for an axial duct

$$\mathcal{T}_{n,ax} = \begin{bmatrix} e^{nx} & e^{-nx} & e^{-\left(\frac{s}{\overline{V}_x}+jn\frac{\overline{V}_\theta}{\overline{V}_x}\right)x} \\ je^{nx} & -je^{-nx} & \left(-\frac{sj}{\overline{\overline{V}}_x n}+\frac{\overline{V}_\theta}{\overline{\overline{V}}_x}\right)e^{-\left(\frac{s}{\overline{V}_x}+jn\frac{\overline{V}_\theta}{\overline{V}_x}\right)x} \\ \left(-\frac{s}{n}-\overline{V}_x-j\overline{V}_\theta\right)e^{nx} & \left(\frac{s}{n}-\overline{V}_x+j\overline{V}_\theta\right)e^{-nx} & 0 \end{bmatrix} e^{jn\theta} \qquad (2.13)$$

Transmission matrix for a rotor blade-row

$$\mathcal{B}_{rot,n} = \begin{bmatrix} 1 & 0 & 0 \\ \tan\beta_2 & 0 & 0 \\ \begin{bmatrix} \tan\beta_2 - \tan\alpha_1 - \lambda_r(s+jn) \\ +\frac{\partial L_R}{\partial \tan\beta_2}\frac{\tan\beta_1}{\overline{\overline{V}}_x(1+\tau_R\cdot(s+jn))} - \overline{V}_{\theta 2}\tan\beta_2 \end{bmatrix} & -\frac{\partial L_R}{\partial \tan\beta_1}\frac{1}{\overline{\overline{V}}_x(1+\tau_R\cdot(s+jn))} + \overline{V}_{\theta 1} & 1 \end{bmatrix} e^{jn\theta} \qquad (2.14)$$

Transmission matrix for a stator blade-row

$$\mathcal{B}_{sta,n} = \begin{bmatrix} 1 & 0 & 0 \\ \tan\alpha_2 & 0 & 0 \\ -\lambda_S s + \dfrac{\partial L_S}{\partial \tan\alpha_1}\dfrac{\tan\alpha_1}{\overline{V}_x(1+\tau_S\cdot s)} - \overline{V}_{\theta 2}\tan\alpha_2 & -\dfrac{\partial L_S}{\partial \tan\alpha_1}\dfrac{1}{\overline{V}_x(1+\tau_S\cdot s)} + \overline{V}_{\theta 1} & 1 \end{bmatrix} e^{jn\theta} \quad (2.15)$$

The axial duct transmission matrix relates inlet boundary conditions and perturbation values at the exit of the duct, whereas the rotor and stator matrices relate perturbations across the blade-row in question.

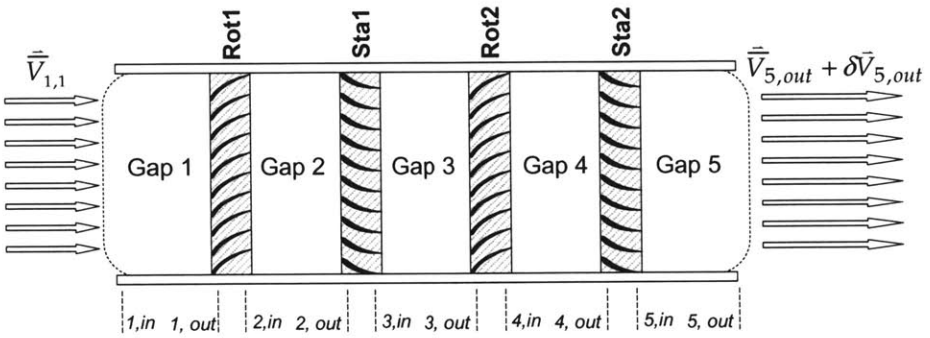

Figure 2-3 2-stage compressor dynamic compressor model geometry and definitions

Larger compression systems consisting of arbitrary combinations of the previous modules can be built by successive multiplication of their respective transmission matrices. Specification of suitable inlet and exit boundary conditions suffices to finalise the eigenvalue problem formulation. These arise from the necessity that, for infinitely long upstream and downstream ducts, potential waves decay away from the compressor and the assumption of irrotational upstream flow. The closed system of equations can be expressed as an eigenvalue problem

$$\det\begin{bmatrix} EC\cdot\mathcal{X}_{sys} \\ IC \end{bmatrix} = 0 \quad (2.16)$$

where $$EC = \begin{bmatrix} 1 & 0 & 0 \end{bmatrix} \qquad IC = \begin{bmatrix} 0 & 1 & 0 \\ 0 & 0 & 1 \end{bmatrix} \quad (2.17)$$

and $\mathcal{X}_{sys}$ is the overall system transmission matrix.

In general, this is assembled as follows

$$\mathcal{X}_{sys} = \mathcal{T}_{ax,n}\left(x_{last\ stage,in}, s\right)^{-1} \cdot \prod_{i=2Nstages}^{i=2}\left[\mathcal{B}_{sta,i,n}\cdot\mathcal{B}_{gap,2i,n}\cdot\mathcal{B}_{rot,i,n}\cdot\mathcal{B}_{gap,2i-1,n}\right]\cdot \cdot\mathcal{B}_{sta,1,n}\cdot\mathcal{B}_{gap,2,n}\cdot\mathcal{B}_{rot,1,n}\cdot\mathcal{T}_{ax,n}\left(x_{1,out}, s\right) \quad (2.18)$$

For the 2-stage machine depicted above, this would become:

$$\mathcal{X}_{sys} = \mathcal{T}_{ax,n}(x_{5,in}, s)^{-1} \cdot \mathcal{B}_{sta,2,n} \cdot \mathcal{B}_{gap,4,n} \cdot \mathcal{B}_{rot,2,n} \cdot \mathcal{B}_{gap,3,n} \cdot \mathcal{B}_{sta,1,n} \cdot \mathcal{B}_{gap,2,n} \cdot \mathcal{B}_{rot,1,n} \cdot \mathcal{T}_{ax,n}(x_{1,out}, s) \quad (2.19)$$

Analytical and numerical methods to solve for the eigenvalues arising from the eigenvalue problem were proposed by Spakovszky [12]. Blanvillain [1] further explored the potential of commercially available optimisation-based routines to find the various roots of the determinant. The Nelder-Mead direct search algorithm, included as a standard Matlab function, proves efficient enough, allowing for the calculation of all the roots for a given harmonic in a timescale of seconds, for one stage, and a few minutes for two, three or four-stage machines, so long as one stays reasonably close to the peak of the characteristic, which roughly coincides with the neutral stability condition. The issue of computational expense is revisited later in the discussion.

Having specified the harmonic number that one wishes to study, *(2.16)* returns eigenvalues for all the flow resonance modes

$$s = \sigma_n - j\omega_n \quad (2.20)$$

where σ_n and ω_n are the growth and rotation rates of the wave, respectively.

Spatial Flow Field Resolution

An important constraint to 2-D compressor modelling is the spatial flow field resolution. The question is how large the ratio of non-uniformity wavelength to blade pitch has to be to obtain a local blade-row performance in non-uniform flow similar to that in uniform flow for the same local conditions.

Longley [9] gives the following rough constraint as a guideline: a blade and its neighbours – i.e. two pitches – have similar flow conditions, within a quarter wavelength, when the circumferential lengthscale of the flow non-uniformity is large enough. In other terms,

$$\frac{1}{4}\lambda_{non-unif.} \succ 2s \quad (2.21)$$

where s is the blade pitch. In terms of the highest feasible harmonic, this criterion can also be expressed as

$$\frac{N_{blades}}{n_{\max}} \succ 8 \quad (2.22)$$

For a typical row of 50~60 blades, one should, at most, use the dynamic compressor model to calculate up to around 6~7 harmonics.

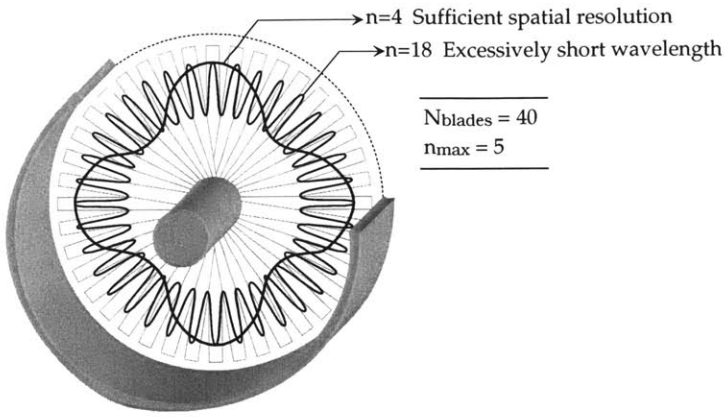

Figure 2-4 Feasibility of various circumferential modeshapes to satisfy Longley's spatial resolution requirement

Temporal Flow Field Resolution

An additional limit on the perturbation wavelength is imposed by the requirement that the blades see quasi-steady conditions, so that the actuator disc description can be employed. In simple terms, the flow change time due to the circumferential mode of oscillation must be larger than the travel time of the flow along the passage. This effectively means that the reduced frequency β is below unity, in which case the blade-rows behave in a quasi-steady manner.

Considering a periodic oscillation of wavelength λ upstream of a rotor blade row, as seen in Figure 2-5, the radian frequency of the unsteadiness, as seen by the rotor, is

$$\omega = \frac{2\pi\Omega R}{\lambda} \tag{2.23}$$

On the other hand, the travel time of a fluid particle along the passage is

$$\tau_{passage} = \frac{L}{U} \tag{2.24}$$

The reduced frequency is obtained by comparison of these two timescales, i.e.

$$\beta = \frac{2\pi\Omega R \cdot L}{\lambda U} \tag{2.25}$$

The tangential speed of the rotor Ωr and the fluid velocity along the passage U are comparable in many fluid devices, so the reduced frequency can be roughly expressed as

$$\beta \approx \frac{2\pi L}{\lambda} \tag{2.25}$$

However, it should be noted that the circumferential perturbations have an integer number of lobes. Therefore, the reduced frequency can be viewed in terms of

$$\beta \approx \frac{nL}{R} \prec 1 \tag{2.25}$$

This sets the value of the maximum harmonic that complies with the temporal resolution requirement.

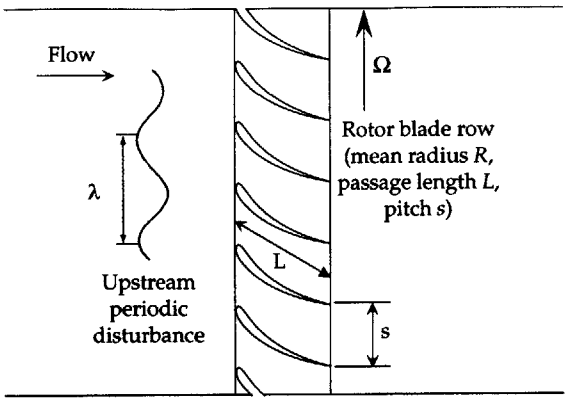

Figure 2-5 Flow schematic for the calculation of the reduced frequency

Validity of the Model for Engine Transient Cycles

One of the aspects that will be investigated in Chapter 3 is the change in stability that the compressor experiences during engine acceleration cycles, which take the operating point above the running line until a steady mean flow condition is reached again at a higher speed.

This dynamic compressor model assumes steady-state, axi-symmetric performance characteristics (i.e. with a steady 2D background flow). Therefore, when the operating point has to be changed and a transient is undergone, one needs to ascertain that the mean flow change timescales are sufficiently large, compared to the blade convection time.

For the full-compressor, the timescale that one must control is the characteristic acceleration time τ_{acc}, which can be arrived at by considering the torque exerted by the fluid on the blading and the overall polar inertia to be accelerated from a given speed.

Kerrebrock [8] expressed the characteristic acceleration time from speed N as

$$\tau_{acc} = \frac{4\pi^2 J N^2 \frac{\gamma}{\gamma-1}}{c_p T_{T2} \dot{m}_2 \left(T_{out}/T_{in}\right)_{comp,o}} \qquad (2.23)$$

where J is the rotor polar inertia and T_{T2} denotes the stagnation temperature at the compressor face.

This timescale is calculated for the repeating-stage compressor used for all studies henceforth , varying the number of stages (see 2.5.1 for a full description of the standard compressor).

The characteristic *accel* time is computed from a low speed of 3350rpm ($M_{rel,R1} < 0.2$). The estimate is in fact conservative, for only the blades and a cylindrical disk are taken into account in the calculation of the polar inertia.

The results for the machines of interest are summarised below:

Number of stages	Accel time, τ_{acc}	β_{acc}
1	6.668	5.908E-05
2	7.892	4.992E-05
3	9.116	4.321E-05
4	10.339	3.810E-05
5	11.563	3.407E-05

Table 2-1 Transient timescales for *standard* series of compressors

In conclusion, it is clear from inspection of the reduced frequency that the acceleration time is different in order of magnitude from the flow travel time through the blade passages. As the engine accelerates, the flow field responds more rapidly than the changes in mass flow and the instantaneous conditions vary smoothly enough for the quasi-steady assumption to be valid even in transient operation.

2.4.2.2 Computational Cost in the Context of DEB

Having put in place all the necessary tools, one can attempt the calculation of the modal eigenvalues at various harmonics. The issue of computational expense is of importance at this point, since of the resulting eigenvalue map, only the least stable pole is taken forward to the DEB calculation. A minimum of resources should be spent in the identification of such pole

In a simplified, Moore-Greitzer type model, where all blade-rows are lumped into a single semi-actuator disk and the effects of unsteady loss-lags are neglected, one expects only one mode per spatial harmonic. It can be shown that when the compressor is in stable operation, the first harmonic leads all others, while the opposite is true in the unstable regime. As expected from this behaviour, all harmonics align along the imaginary axis at the point of neutral stability. One can confidently neglect higher order harmonics and track the first one only as it progresses towards instability.

When blade-rows are separated from each other, the gap dynamics are accounted for and the unsteady time lags are incorporated into the analysis one finds two different modes of oscillation per blade-row (see Spakovszky [12]). The eigenvalue map becomes more complicated if the number of blade-rows is increased. Blanvillain [1] dissected the eigenvalue map of a multi-stage compressor and grouped modes with similar dynamic characteristics into strings of eigenvalues.

The convergence of the currently available, reasonably efficient search routines for the solution of the eigenvalue problem is highly dependent on the starting point of the iterative process. Once the first harmonic of a particular mode has been found, this solution is used as the initial guess for the iteration of the immediately higher harmonic, thus generating a string of eigenvalues.

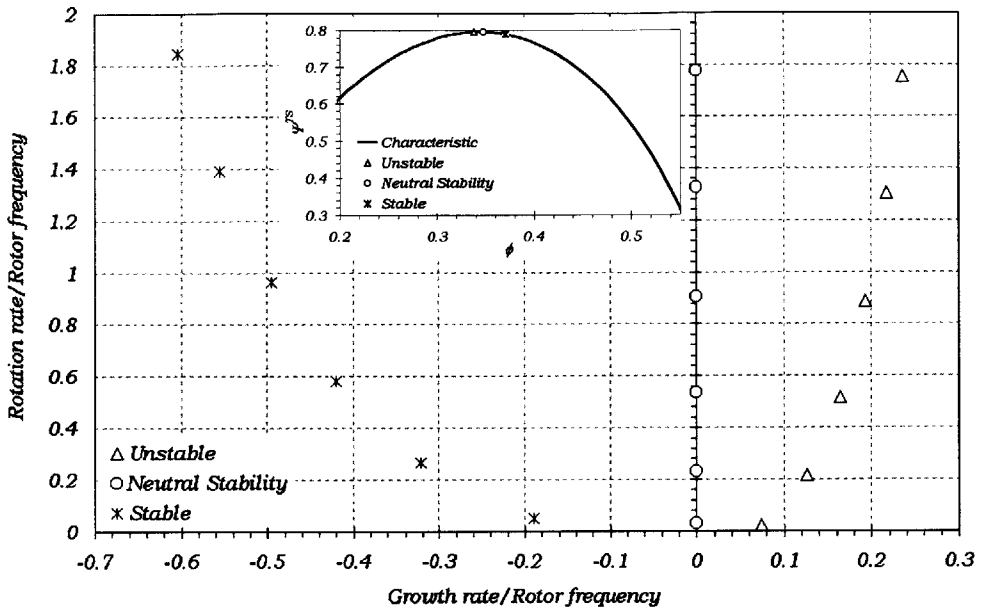

Figure 2-6 Moore-Greitzer eigenvalue map

However, it has been observed that an iteration starting with a harmonic solution from a given string might well converge to the next harmonic of a different one. This is especially acute when two different sets of eigenvalues intersect, but jumps have also been observed between strings lying in well-differentiated regions of the complex plane. At present, no systematic method for the exact calculation of all the harmonics of a given string of modes has been devised. One must therefore solve for the entire set of eigenvalues and decide, by geometric concatenation of the various poles, the topology and dynamics associated to each different string.

Fortunately, despite this proliferation of different strings of modes for one given machine, the first harmonic in each set of eigenvalues is found to lead its own string, so long as one looks at the stable operating region. The fundamental difference with the Moore-Greitzer map is that, since the relative locus of each mode is unknown initially, one must find the first harmonic of all the families before deciding which is the critical one.

Such an endeavour can be exceedingly expensive, particularly far away from neutral stability. Convergence of the optimisation algorithm to a root of the determinant is largely sensitive to the starting point of the gradient search. In many instances, one encounters that the initial guess is in a flat region of the domain, where no progress towards the pole is possible, in which case the guess must be updated and the process restarted.

However, as one restricts the analysis between $\sigma \sim -0.15$ and $\sigma = 0$, the critical eigenvalue becomes the main attractor and the Nelder-Mead algorithm converges towards it invariably from an initial guess of $(\sigma,\omega) = (0,0)$. Consequently, it would be desirable to exploit the relatively cheap

information from the vicinity of the vertical axis in the eigenvalue map and employ it to predict dynamic behaviour away from this region.

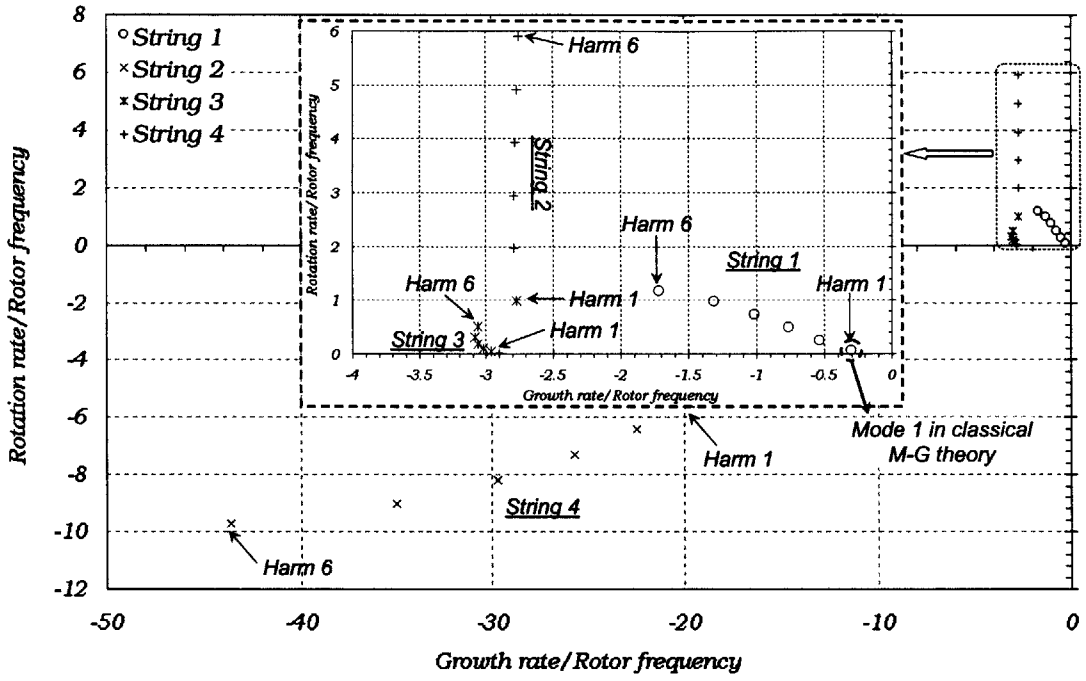

Figure 2-7 Eigenvalue map for a 1-stage compressor with 5% inter-blade-row gap and long inlet & exit ducts, in stable operation

2.4.2.3 Perturbation Modeshapes Calculation

The dynamic analysis described so far, leading to the growth rate and rotation rate of each of the eigenvalues, is insufficient to proceed to the evaluation of *DEB*. With a view of employing the velocity and pressure perturbations in integral expressions used to calculate the different terms in the control-volume analysis, the compressor ducts and gaps can be subdivided into an arbitrary number of points, at each of which δV_x, δV_θ and δP must be evaluated. This discretisation is necessary for the evaluation of the disturbance-energy balance, which requires these flow quantities at the various axial positions in order to determine the local values of *DE* flux and *DEB*.

The transmission matrix for an infinite upstream duct is used to find the i^{th} perturbations in Duct 1

$$\begin{bmatrix} \delta V_x \\ \delta V_\theta \\ \delta P \end{bmatrix}_{1,i} = T_{n,ax}\left(s, x_{1,i}\right) \begin{bmatrix} 1 \\ 0 \\ 0 \end{bmatrix} \qquad (2.24)$$

Once the edge of the first blade-row is reached, the perturbations at the first point of the following gap are simply

$$\begin{bmatrix} \delta V_x \\ \delta V_\theta \\ \delta P \end{bmatrix}_{j+1,1} = \mathcal{B}_{rot,k,n} \begin{bmatrix} \delta V_x \\ \delta V_\theta \\ \delta P \end{bmatrix}_{j,N\text{int}} \tag{2.25}$$

Elemental gap transmission matrices can be assembled to relate perturbations across successive points between any two blade-rows

$$\begin{bmatrix} \delta V_x \\ \delta V_\theta \\ \delta P \end{bmatrix}_{j,i+1} = \left[\mathcal{T}_{n,ax}\left(s, x_{j,i+1}\right)\right] \cdot \left[\mathcal{T}_{n,ax}\left(s, x_{j,i}\right)\right]^{-1} \cdot \begin{bmatrix} \delta V_x \\ \delta V_\theta \\ \delta P \end{bmatrix}_{j,i} \tag{2.26}$$

Typical modeshapes for a standard, repeating-stage 2-stage compressor with zero inlet and exit swirl, 5% inter-blade-row gaps ($\Delta x/R = 0.05$) and long upstream and downstream ducts are shown in the following page. For incompressible flow, potential waves, which decay away from the source, propagate in all directions, whereas vortical disturbances are convected downstream by the mean velocity. As a result, it is seen that all perturbations decay away from the compressor face in the inlet duct. In this region, the axial and circumferential perturbation velocities are in quadrature.

In the exit duct, however, the effect of vorticity is patent. The pressure wave decays away from the last blade-row because it is solely governed by potential effects. However, the perturbation velocities exhibit changes in the exit duct, as the vorticity shed from the last blade-row is convected downstream. At neutral stability, δV_x remains constant, whereas in stable operation the wave is seen to increase along the duct, following the vorticity wave, which also exhibits this behaviour. This means that the magnitude of the perturbation decays in time, which is expected if the growth rate is negative. The opposite is true for an unstable operating point.

The angular velocity perturbation, on the other hand, shows a smaller growth in time as the machine is throttled along the speed line to higher mass flows, i.e. into the stable operating region.

It should be noted that in the illustrative plots, the blade-rows are identified by blocks of a finite axial length due to the structure of the code; in fact, the actuator-disks should be infinitely short.

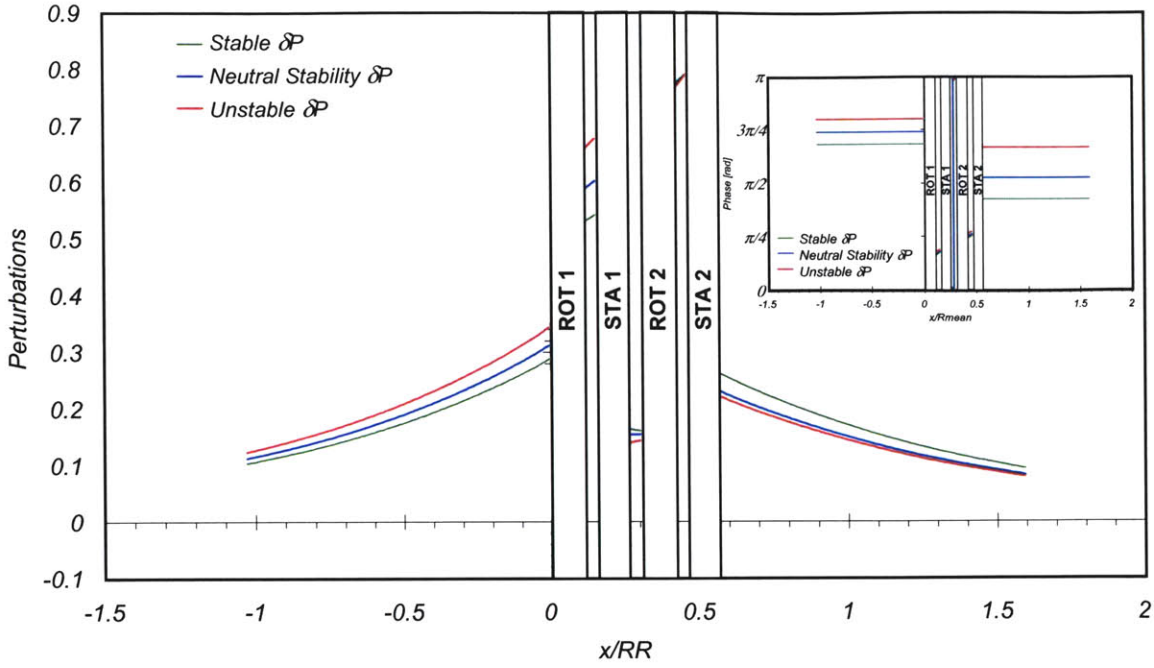

Figure 2-8 δP modeshape for 2-stage repeating-stage compressor with 5% inter-blade-row gaps near neutral stability

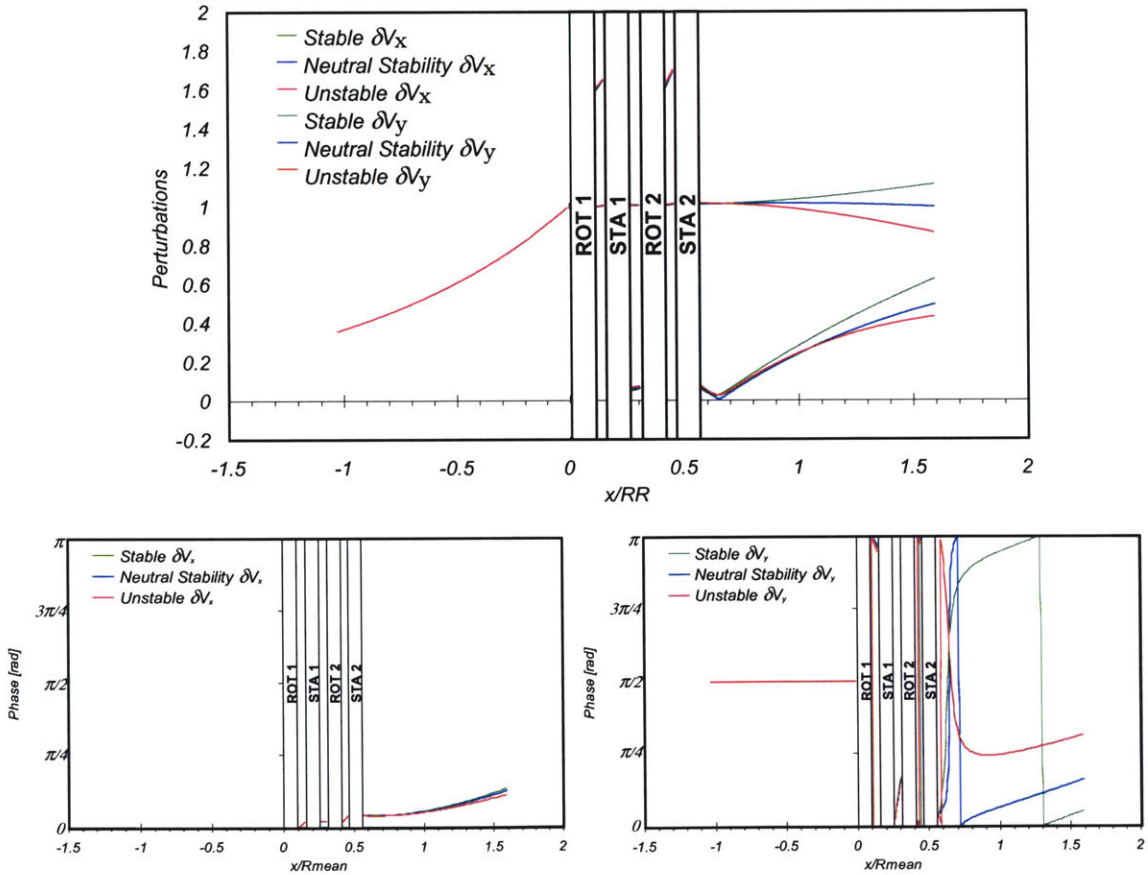

Figure 2-9 δV_x & δV_θ modeshapes for 2-stage repeating-stage compressor with 5% inter-blade-row gaps

2.4.3 Evaluation of the Disturbance-Energy Balance

The full derivation of the integrals involved in the calculation of the *DE* fluxes and unsteady term is too cumbersome to describe here, and is developed in full detail in Appendix B. To preserve the continuity of the argument, the final expressions for the terms involved in the *DE* Balance are provided.

There are two physical mechanisms contributing to the *DE* flux: the disturbance-pressure work exerted on the area under consideration and the disturbance-kinetic energy entering the control volume across this surface through convection by the mean velocity. In summary,

$$\mathcal{F} = \mathcal{F}_P + \mathcal{F}_{KE} = \frac{A}{2}\left(|\delta P||\delta V_x|\cos(\varphi_P - \varphi_{Vx}) + \frac{\rho V_x}{2}|\delta V_x|^2|\delta V_\theta|^2 \right) \tag{2.27}$$

The *DEB* term, i.e. the time rate of change of DE in the control volume, is shown to be

$$DEB = \frac{\sigma}{2}\int_{xin}^{xout} \rho(x)A(x)|\delta V_x(x)|^2|\delta V_\theta(x)|^2\,dx \tag{2.28}$$

This is the quantity that is used as a stability metric analogous to the critical growth rate stemming from the eigenvalue formulation. Clearly, the integral is always positive and its magnitude, for incompressible flow and a fixed control volume, is governed by the magnitude of the perturbation velocities in the flow field. The sign of *DEB*, therefore, is totally controlled by the growth rate of the critical eigenvalue. Thus, when σ reaches a value of zero, so will the *DEB*, as long as a single, stability-critical eigenvalue is considered; hence their equal validity for the onset of instability.

As a matter of fact, if only the overall system stability were of concern, there would be no need to evaluate flux terms, as enough information is available from the perturbation modeshapes to establish the value of the *DEB*. The only reason to go over the additional step of the flux calculation, under the assumption that the system dynamics are governed by a single eigenvalue, is to determine the *DE* powers of each of the blade-rows. These issues are better viewed in the following section.

2.5 Application of *DE* Theory to Compression Systems

This section deals with the detailed application of the theory presented so far to specific axial flow compressor configurations. This helps to elucidate some of the implementation issues, especially on the numerical side, as well as depicting the physical behaviour of the different terms involved in the *DE* conservation.

Further to this, multi-stage machines are analysed in order to assess, through *DE* considerations, stability trends for varying inter-blade-row gaps previously pointed out by Blanvillain [1].

2.5.1 Moore-Greitzer Compressor Model

The most elemental model to examine the basic features of DEB is the Moore-Greitzer compressor, in which:

- All blade-rows are lumped onto a single semi-actuator disk
- There exists no inlet or exit swirl
- Unsteady loss effects are neglected

A series of compressors has been created to carry out these analyses, the blade-rows of which can simply be appended to each other to generate multi-stage machines. These will be referred to as the *standard* machines. The stages are aerodynamically repeating and have 50% reaction, i.e. their velocity triangles are the same throughout the compressor. For the M-G case, the 1-stage version of this standard compressor is used, reducing the inter-blade-row gap to zero.

The *DE* balance is calculated at various mass flows along the 35% corrected speed line, where the flow is markedly incompressible. The maximum relative Mach number seen by the first rotor varies between 0.234 and 0.318 throughout the range of mass flows considered, among which the largest overall static density ratio is only 1.035. The distortions introduced by higher speeds and mass flows into the compressible mean line solver, which in turn feeds data to the incompressible dynamic compressor model, are examined in later sections.

The direct correspondence between *DE* and the system dynamics set out in Section 2.3.3 is demonstrated by tracking the two stability metrics along the speed line, as shown in Figure 2-10. The Disturbance-Energy and the critical eigenvalue growth rate σ reach neutral stability at precisely the same flow condition. It is interesting to note, however, that while the eigenvalue exhibits a proportional evolution with flow coefficient, this is not the case for the disturbance-energy. This is expected, since *DEB* is inherently an integral quantity related to the square of the velocity perturbations, whereas σ is a system-wide growth rate of disturbances.

The local topology of *DEB* can be more clearly dissected using the detailed *DE* distribution through the compression system. This is shown in Figure 2-11 for the three different dynamic conditions, analogously to Fréchette [4]. At neutral stability the $\mathcal{F}$ distribution is completely flat, which ensures that any arbitrary control volume in the ducts has a zero net flux, and therefore a steady level of disturbance-kinetic energy. In this instance, the actuator-disk *DE* power is simply the step change in $\mathcal{F}$. In the stable operating condition, however, there is always a net positive flux leaving any control volume, which must be balanced precisely by the rate of increase of *DE*, thus ensuring that the ducts or gaps do not possess a net *DE* power, for which no physical mechanism exists. The opposite is observed when the compressor is dynamically unstable.

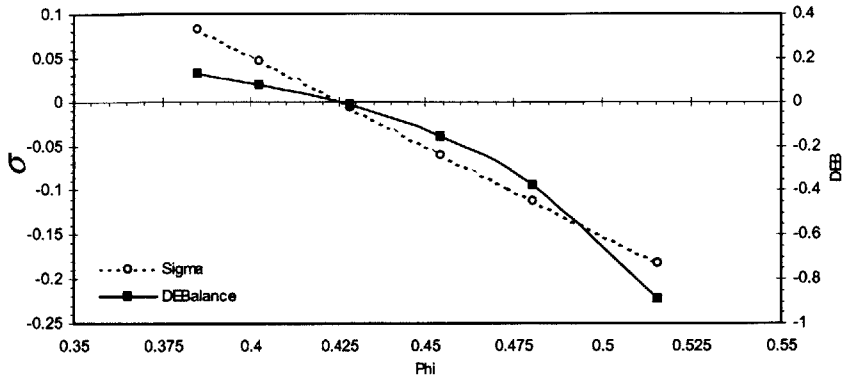

Figure 2-10 Dynamic stability evolution as predicted by critical eigenvalue growth rate (σ) and *DEB*

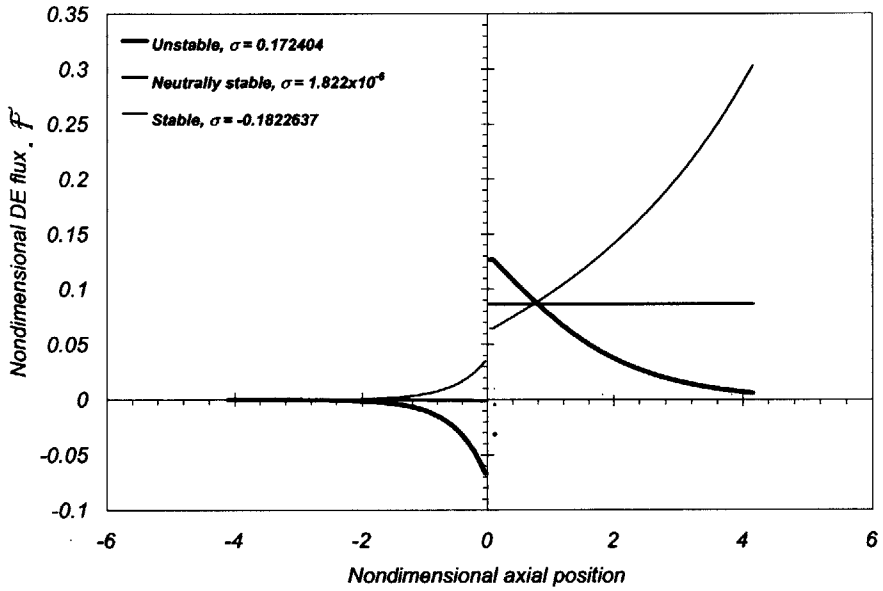

Figure 2-11 Disturbance-Energy Flux distribution for the 1-stage repeating-stage compressor with zero gap length

From this argument, it follows that the gradient of the f curves is directly related to the magnitude of the local rate of growth of *DE*. A stable compressor, therefore, experiences the largest dissipation of *DE* in the final region of the exit duct, whereas an unstable machine has a localised area of large *DE* growth immediately around the actuator-disk. The influence of the source power, therefore, decays away from the blade-rows, whereas their sink influence is felt more intensely at greater distances, as seen in Figure 2-12. As the number of elements becomes very large, the local DE balance overlaps with the slope of the f distribution, which must always be the case.

Since ∇f is tied to the local rate of change of *DE*, it must have the same sign over the entire domain at any given operating point. This relates to the fact that the eigenvalue governs the growth of disturbances on a system-wide scale and therefore *DE* must either grow, decay or remain steady everywhere, albeit at different rates.

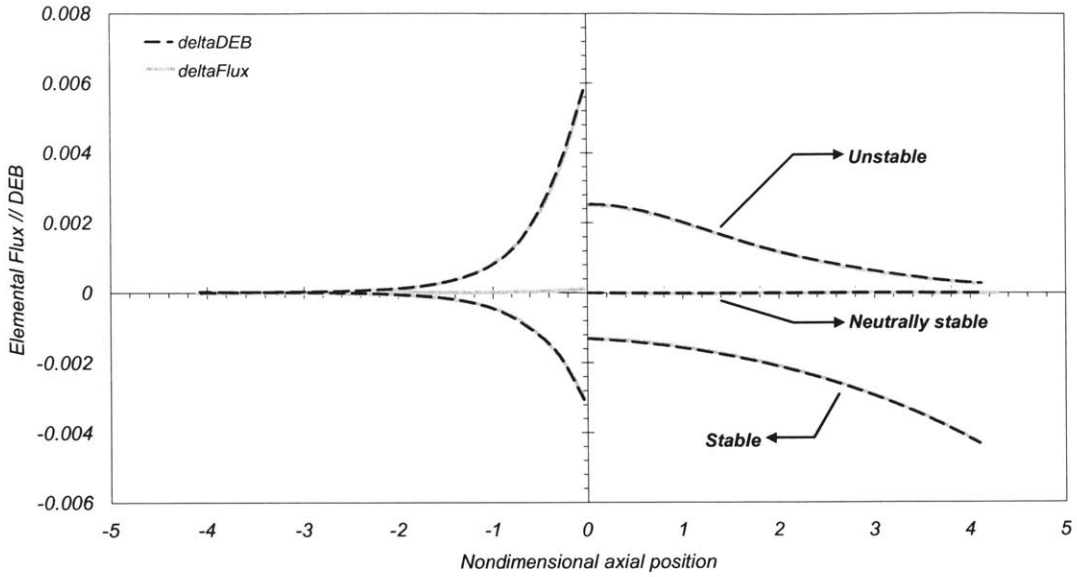

Figure 2-12 Elemental *DE* balance showing zero source/sink powers for inlet and exit ducts

The condition that gaps and ducts must in no case contribute a net power to the *DE* balance can be used as a convergence criterion for the numerical scheme used to calculate the elemental *DEB*, as discussed in 2.3.3. At very coarse discretisations, the unsteady term does not follow the net elemental flux well, and the ducts appear to have a net power. This is used as the error function, nondimensionalised by the net flux, which is an analytically exact quantity that does not involve longitudinal integration,

$$\varepsilon_{duct} = p_{duct} = \frac{\iiint_{duct} \rho \frac{(\delta V)^2}{2} dV - \left(\mathcal{F}_{Nintervals,duct} - \mathcal{F}_{1,duct}\right)}{\left(\mathcal{F}_{Nintervals,duct} - \mathcal{F}_{1,duct}\right)} \tag{2.29}$$

The convergence of this error depends on the spatial resolution achieved by the discretisation of the duct lengths. For the 1-stage standard compressor with long inlet and exit ducts, the parabolic fitting of the perturbation modeshapes gives an error of under 2%, as one operates beyond the very reasonable resolution of 25 intervals per duct/gap. It remains constant thereafter for finer spatial subdivisions.

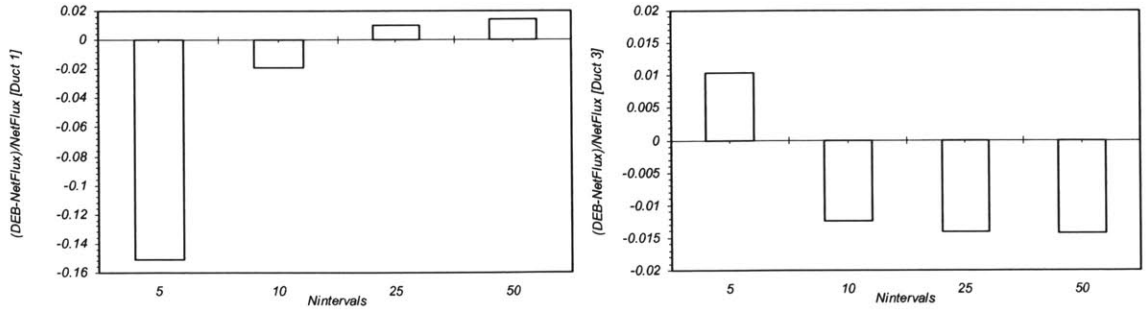

Figure 2-13 DEB Unsteady-term numerical convergence for various spatial resolutions

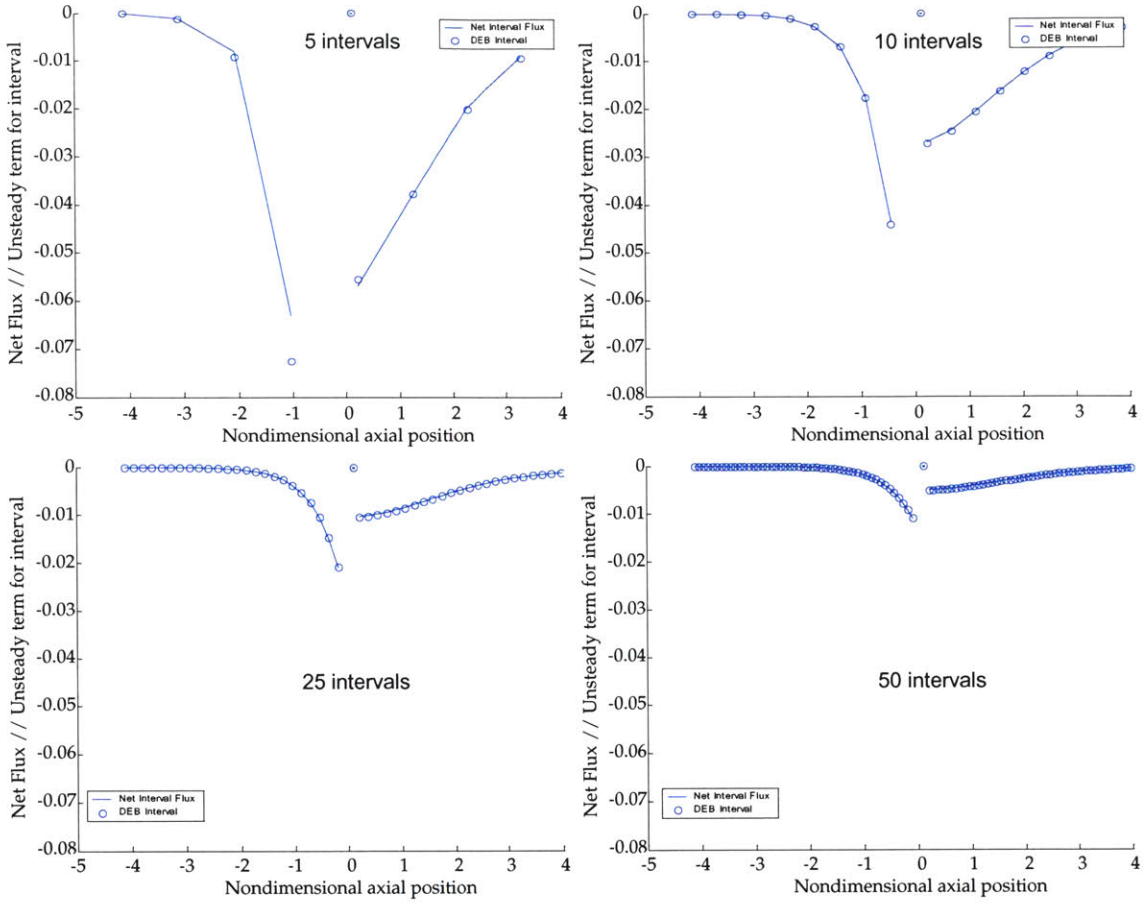

Figure 2-14 [a-d] Graphical representation of the elemental DE Balance convergence for 5, 10, 25 & 50 intervals per gap

2.5.2 Standard 1-stage Model with Inter-Blade-Row Gap & Unsteady Loss Effects

2.5.2.1 *DEB* Analysis

When the full capabilities of the dynamic compressor model are taken into consideration, some further observations can be made with respect to the nature of the *DE* balance.

Because the perturbations are now resolved in the inter-blade-row gaps, the flux distribution is known there as well. As expected, this follows the same trend as the inlet and exit ducts as far as the sign of $\partial \mathcal{F}/\partial x$ is concerned. However, the flux is found to be very steep in the gaps immediately after a rotor. This is due to the large magnitude of the circumferential velocity perturbation, which contributes greatly to the disturbance-kinetic energy.

The gaps located after stators, on the other hand, have a smoother behaviour. If the last stator fails to extract all the swirl from the airflow, the flux in the exit duct is also seen to vary more steeply, be it in the stable condition or otherwise.

This behaviour is patent in Figure 2-15, where the high sensitivity of the post-rotor flux is evident. The flux distribution is *almost* flat, but not exactly, despite the fact that the growth rate σ is only significant in the fifth decimal place. This is enough for δV_θ to be appreciable in this gap, thus making the slope slightly positive, and becomes more pronounced at higher rotational speeds. At precisely neutral stability, the flux distribution is *exactly* flat.

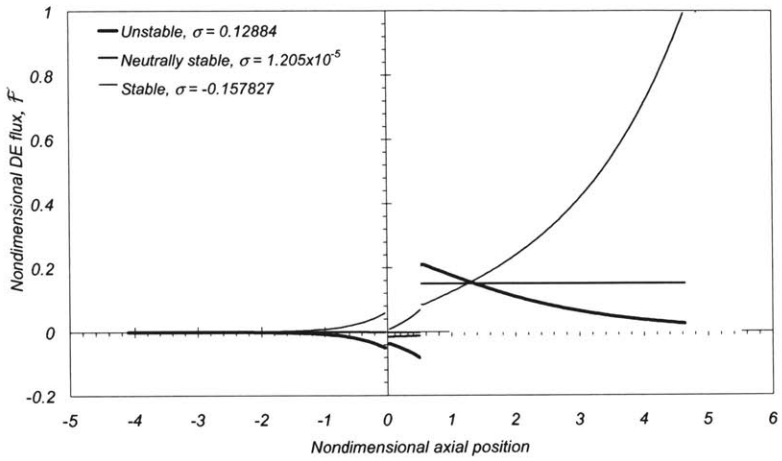

Figure 2-15 Disturbance-Energy Flux distribution (1-stage repeating-stage compressor, 50% gap, 0 inlet and exit swirl)

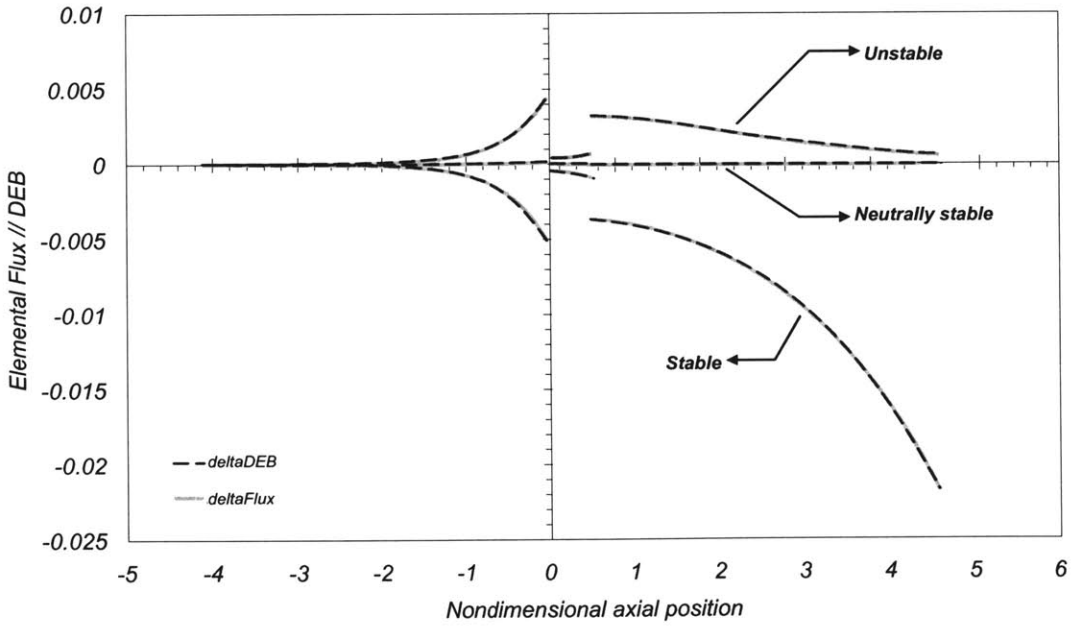

Figure 2-16 Elemental *DE* balance showing zero source/sink powers for inlet and exit ducts (1-stage repeating-stage compressor, 50% gap, 0 inlet and exit swirl)

Because of the more rapid variation of perturbation quantities in gaps with high amounts of swirl, it is wise to assign more integration points to these inter-blade-row regions. The shallower convergence rate for the inter-blade-row gap is obvious from the graph below. While the numerical error settles below 1.5% using as few as 25~30 intervals for the inlet and exit duct, the effective inter-blade-row gap power is still larger than 5% of its net flux, with 25 integration points (see Figure 2-17). Settling of the error for gap 2 does not take place until one employs on the order of 100 integration points.

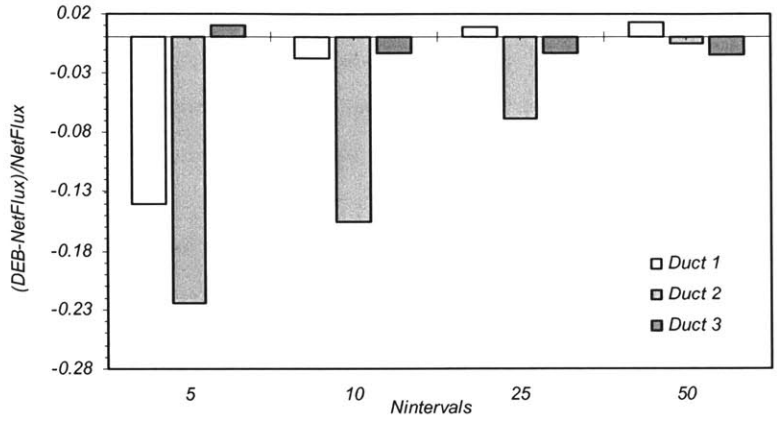

Figure 2-17 DEB Unsteady-term numerical convergence for various spatial resolutions (1-stage repeating-stage compressor, 50% gap, 0 inlet and exit swirl)

2.5.2.2 Intra-Stage Gap Length Effects on Dynamic Behaviour

Spakovszky [12] studied the evolution of rotor and stator-related modes in a 1-stage compressor as the inter-blade-row gap is increased from the Moore-Greitzer configuration up to essentially an uncoupled rotor-stator system, with an infinitely long gap. In particular, the critical eigenvalue, related to the stator, was found to follow a curved trajectory in this process, where the disturbances can even follow the counter-blade rotation for a certain range of gap lengths. From a dynamic standpoint, the growth rate becomes more negative, reaches a minimum (its most stable condition), then increases again to a positive maximum (its least stable condition) and settles at a constant value for very large gaps, when the two blade-rows are uncoupled.

This phenomenon was also observed in the 1-stage repeating-stage compressor, as seen in Figure 2-18. Indeed, until an elongation of $\Delta x = 15\%$ is reached, increasing the inter-blade-row gap has a stabilising effect of up to $\Delta\sigma = -0.08$. Intra-stage gaps, i.e. those separating a rotor and a stator belonging to the same stage, were also identified as having this effect in a multi-stage environment by Blanvillain [1], and the analysis will be repeated using *DEB* results in 2.5.3.1.

It is hardly imaginable that re-positioning of the compressor blades during the design process with the object of improving stability would be allowed to increase the gap length beyond a few

millimetres. As a result, one can say that small allowable extensions of the intra-stage gap in a given design will generally have beneficial effects from a dynamic point of view.

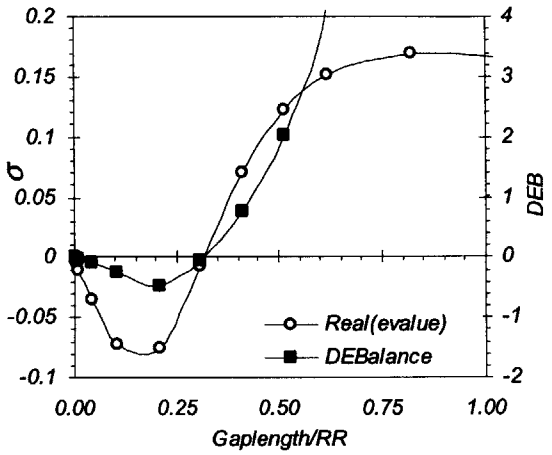

Figure 2-18 3rd-harmonic, critical mode dynamic evolution for a range of inter-blade-row spaces

The trend of *DEB* with varying gap length capture the evolution of the eigenvalue growth rate, as well as the crossing of neutral stability at a gap length of just over 30%. However, as the eigenvalue growth rate asymptotes towards a constant value of around 0.152, the overall disturbance-energy growth rate in the system rapidly rises towards infinity, because the compressor length becomes infinitely large. The critical growth rate, in this instance, is a more meaningful stability metric, as it gives a true indication of the relative dynamic performance between compressors of different size. However, this dependence on the individual components' characteristics makes *DEB* attractive to identify the relative dynamic importance of the various moduli.

Beyond a certain threshold (~75%), the growth rate of the perturbations does not vary for additional extensions of the gap, as rotor and stator are uncoupled from here onwards. However, as the compressor becomes longer, the total growth of disturbance-energy per unit time also becomes larger, but purely because the length of the compressor has increased, and not because the growth rate is altered. Therefore, it would be misleading to relate the absolute value of *DEB* to the actual stability of the machine, because its value is influenced by both the dynamics and the overall length.

The difference between the geometric growth of gaps separating blade-rows in the same stage and those separating adjacent stages is further enlightened in the next section, where the *DEB* analysis is carried over to a multi-stage machine.

2.5.3 Standard 2-stage Model

The starting point for the analysis of the relative effect of inter- and intra-stage gaps is the 2-stage repeating-stage compressor with long inlet and exit ducts [*Gaps 1 & 5*] and 5% inter-blade-row gaps

[*Gaps 2,3 & 4*]. First of all, the intra-stage gaps [*2 & 4*] are enlarged whilst keeping the inter-stage gap [4] at the benchmark dimension.

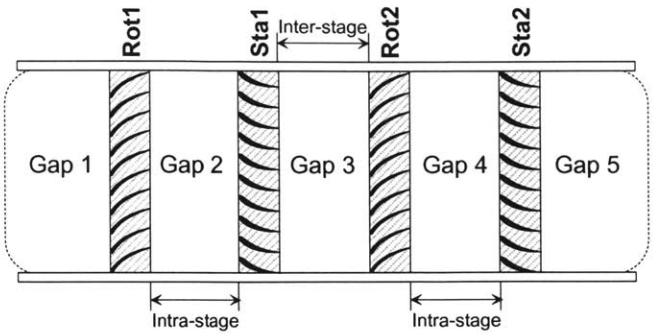

Figure 2-19 Inter- and intra-stage gaps nomenclature

2.5.3.1 Intra-Stage Gap Size Effects in a Multi-Stage Environment

Starting with the baseline configuration at neutral stability, one can detect an improvement in the growth rate of the least stable mode with larger intra-stage gap length, as long as this does not exceed 8% of the mean radius. This is about half the permissible gap size found in the 1-stage machine and suggests that the elongation of these gaps may be additive. In other words, it is conjectured that regardless of the number of stages, one appears to have to distribute a maximum extra compressor length among the various intra-blade-row gaps. The extent to which this limits the geometric changes on large multi-stage machines, and the relative impact of increasing the size of these gaps towards the front or rear ends of the compressor are issues to be studied, and lie beyond the scope of this thesis.

The local effects of this gap elongation are better visualised in the form of *DE* powers. Rotors are seen to act as sinks, whereas stators constitute sources of disturbance-energy. As the stabilising effect of the increasing gap length becomes more pronounced, the sink terms become stronger and the source powers of the stators diminish in magnitude. In relative terms [see Figure 2-20c], the increase in rotor sink powers is more acute than the decrease in stator source intensity. On the other hand, the second stage is seen to contribute much more to the compression system dynamics. This must be related to the effective flux redistribution around the compressor, which itself is directly linked to the changes in perturbation modeshapes. However, one cannot easily split the contribution of the potential and vortical portions of the perturbations to the flux distribution; a more detailed analysis is needed to understand the exact role of each of these interacting waves.

Blanvillain [1] carried out a similar analysis on a 4-stage compressor, in which the intra-stage gaps were doubled from their initial dimensions, while the rest of the gaps were reduced to maintain a constant compressor length. A maximum stability gain of 4.6% with respect to a stable, baseline operating conditions was achieved. The maximisation of intra-stage gap lengths for enhanced stability was established as a recommended design practice.

The same conclusions can be reached from a disturbance-energy standpoint. In summary, for small extensions, up to 8% for each intra-stage gap, the perturbation decay rate increases, up to a maximum of 5.5% of the rotor frequency. These elongations have a system-wide effect on the disturbance-energy re-distribution, all blade-rows having their *DE* powers reduced. The maximum cumulative gap length for which a dynamic benefit is recorded, and the extent to which stability is improved, are expected to vary across different compressors.

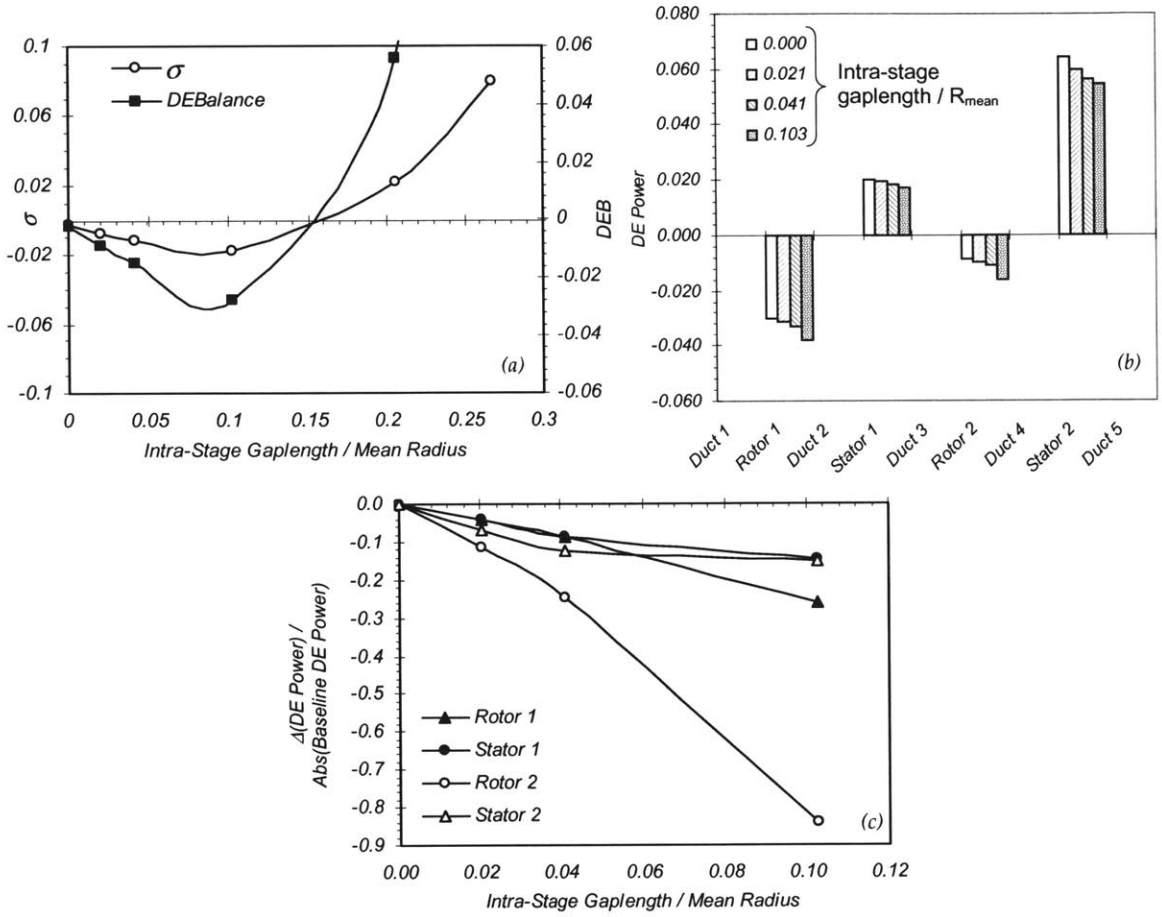

Figure 2-20 [a-c] DEB and σ histories for 2-stage repeating-stage compressor with varying intra-stage blade-row gaps

2.5.3.2 Inter-Stage Gap Size Effects

The next parametric study must be carried out on the gap separating stages 1 and 2. Having fixed gaps 2 and 4 to their baseline level, the size of the inter-stage gap is increased up to 40% of the mean radius, maintaining a constant operating condition that contains the compressor in the stable operating region throughout the whole analysis.

Recalling that in a practical design situation one is unlikely to be able to vary the dimensions by more than a few percents of the mean radius, it is reasonable to concern ourselves to the lower end of Figure 2-21[a], before the extrema in dynamic behaviour.

In that region, extending the inter-stage gap produces a deterioration in perturbation decay rate. This reaches a maximum of 5.6% in critical growth rate around a gap length of 16%, the same cumulative maximum extension recorded for the intra-stage gaps in previous studies.

The redistribution of *DE* power seen in Figure 2-21 [b] shows that the blade-rows adjacent to the gap in question actually experience a beneficial effect, their source powers being appreciably reduced. However, the edge rows experience a relatively larger increase in *DE* emission, which brings down the overall growth rate of the critical eigenvalue. The individual wave interactions leading to this distinct behaviour between inner and outer rows cannot be isolated with the tools used for this higher-level study.

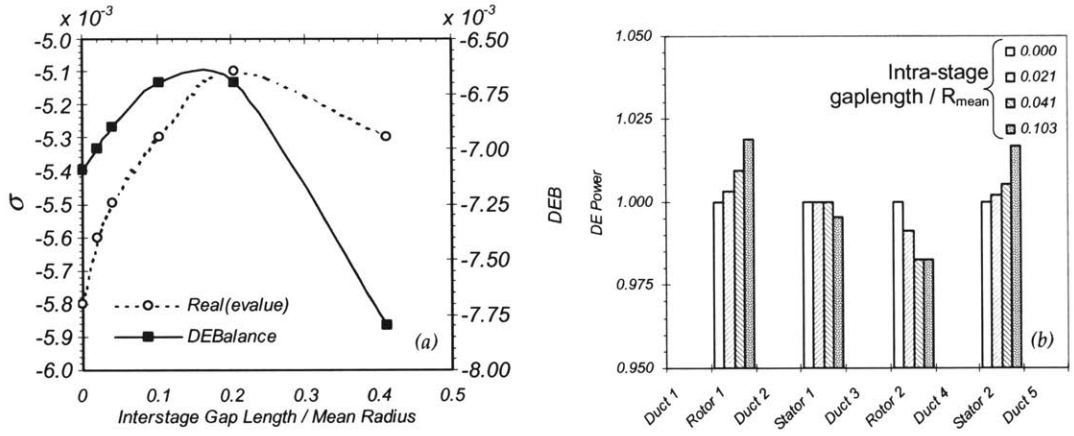

Figure 2-21 [a-b] Dynamic history for 2-stage repeating-stage compressor with varying inter-stage blade-row gaps

To sum up, the inter-stage gaps should be kept at minimal length in order to incur the lowest penalty in perturbation growth rate. If other factors impose an extension of these gaps and design changes are required to mitigate the loss in dynamic stability (change of blade profile, etc.), modifications should be applied to the first and last blade-rows of the compressor.

2.6 Concluding Remarks on the Application of the *DEB* concept

The key conceptual issues and design implications that must be carried forward to the exploration of new stability metrics can be briefly summarised as follows:

- *DEB* provides an assessment of compressor stability that coincides with that obtained from the modal analysis of the flow perturbations. Both approaches have been shown to predict the onset of instability identically. Under incompressible flow assumptions, the

additional fluid kinetic energy due to the perturbation velocities in the entire compressor grows when it is in the unstable regime and decays when the compressor is in a stable condition.

- The perturbation velocity and pressure fields are found by resolving the modeshape of the stability-critical mode. At present, the mode with the smallest decay rate can only be found, in a computationally efficient manner, for mass flows close to the point of instability ($|\sigma| < 0.15$). New metrics for compressor stability and dynamic robustness should rely on this information, if they are to be applied in a feasible design process.
- The additional motivation for the use of *DEB* is the fact that disturbance-energy is conserved in any duct that does not contain blade-rows. A control volume analysis can be used to reveal the *DE* power of each individual rotor and stator, indicating the region of the compressor that most contributes to the overall system dynamic instability.
- The sensitivity analyses performed by Blanvillain [1] to determine the impact of inter- and intra-stage gap dimensions on the dynamics have been carried out from *DEB* considerations. For a repeating-stage compressor, it has been confirmed that extending the gaps between rotors and stators belonging to the same stage leads to increased dynamic stability, whereas the opposite is true if the gaps separating different stages are elongated. An increase in intra-stage gaps is seen to reduce the *DE* powers of all blade-rows uniformly, whereas the reduction in dynamic stability experienced with longer inter-stage gaps can be attributed to an increase in *DE* power of the edge blade-rows.

Chapter 3

Stability Metrics Definition and a New Framework for Their Implementation

3.1 Motivation for a Unified Set of Dynamic Stability Metrics

A straightforward way to visualise the meaning of dynamic stability is to relate the temporal behaviour of the perturbation waves to the shape of the non-dimensional compressor characteristic. In simple terms, the growth rate of the critical eigenvalue is proportional to the slope of the pressure-rise characteristic. As a matter of fact, in the Moore-Greitzer formulation, $\sigma \propto \partial \Psi^{TS} / \partial \phi$.

By virtue of this concept, it is clear that compressors with more curved characteristics will exhibit very different flow ranges between the surge point, which is known to be roughly around the peak of the characteristic (exactly on the extremum, for the Moore-Greitzer case), and an operating point with a given level of dynamic stability.

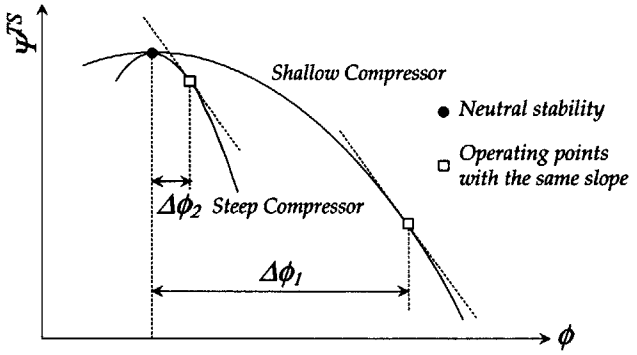

Figure 3-1 Relation between characteristic curvature, dynamic stability, stable flow range and surge margin

Based on the above comparison, one can comment on the validity of the Surge Margin (*SM*), which has slightly different definitions in the industry and NASA standards. The latter additionally accounts for the flow range between the operating point and surge along a given speed line.

$$SM_{ind} = \left.\frac{PR_{surge} - PR_{operating}}{PR_{surge}}\right|_{\dot{m}corr} \qquad SM_{NASA} = 1 - \left\{\frac{PR_{operating}}{PR_{surge}} \times \frac{\dot{m}_{corr,surge}}{\dot{m}_{corr,operating}}\right\} \qquad (3.1)$$

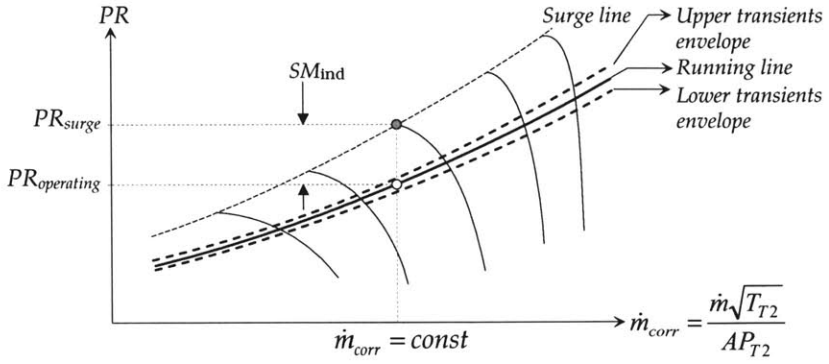

Figure 3-2 Definition of surge margin

In any case, Figure 3.1 compares two compressors with characteristics of different curvature. The operating points for both have the same dynamic stability. However, their surge margin, in either the industry or NASA definition, is nowhere near the same: that of the steep compressor is much smaller, although dynamically, the growth rate of the perturbations is the same as in the operating point for the shallower compressor.

Specifying a stall margin limits the pressure ratio to a fraction of its maximum value at that particular corrected mass flow. This ensures that the static stability requirement is always met (see 2.2), but one cannot ascertain whether operation at a given stall margin has the same dynamic meaning at different speeds. Furthermore, the operating point deviates from the steady-state running line as the machine undergoes accel/decel cycles. Common practice accommodates this by certain permissible reductions in stall margin for the transient envelope, as shown in Figure 3-2, so that a minimum safety threshold is never surpassed. However, there is no direct physical way to relate a change in stall margin to a meaningful quantity that depicts the true dynamic state of the system, such as *DEB* or σ, the growth rate of the least stable eigenvalue.

Performance-wise, it is clear that one would want to operate as close to the maximum pressure-rise as possible, if there was no penalty in dynamic stability. In that sense, the steeper compressor would be desirable. However, because of its higher curvature, one is faced with a smaller dynamic robustness to changes in the operating point: for the same flow variation, the change in slope is much

larger than in the compressor with a shallow characteristic, and correspondingly, the rate at which disturbances grow in time varies more sharply in the compressor with a steep characteristic.

In a practical design framework, it would be desirable to possess a relation between the stable flow range for a given dynamic stability level and the sensitivity of the dynamics at neutral stability, measured for instance by means of the *DEB*, which is essentially an equivalent measurement of the curvature of the characteristic.

With this in mind, and given the lack of coherence of the current stability metrics paradigm – the stall margin – the main objectives of this chapter are to:

1. Explore the relationship between some common, non-dimensional curvature of the performance characteristic and the stable flow range to a certain level of dynamic stability.
2. Identify an unambiguous, non-machine specific metric that provides a measure of *absolute dynamic stability*. This will be tackled by relating the dynamic compressor model formulation to a forced oscillatory system and the concept of dynamic response at resonance, much in the way that vibration problems are handled in structural mechanics.
3. Find a second metric to assess the *robustness* of the machine, in terms of dynamic stability, to changes in mass flow at the design operating conditions.
4. Suggest a physical interpretation of these metrics and *safety margins* for each of them.
5. Derive a set of *simple relationships* to assess the compliance of a given compressor with the dynamic stability and robustness requirements formulated using the new metrics. These must enable straightforward conversion between dynamic compressor model results in the neighbourhood of neutral stability and the relevant stability and robustness metrics at the operating mass flow, thus minimising the use of computational resources.
6. Devise a framework that is useful to the designer in order to understand these metrics in terms of conventional concepts.

3.2 Prediction of the Stable flow range to Stall from the Evolution of System Dynamics

3.2.1 Physical Basis for a Unique Function to Predict the Stable flow range

As set out by the comparative reasoning above, the stable flow range to a certain σ-level is to be compared with an equivalent curvature of the performance characteristics for a range of compressors, with a view of unveiling a common relation between the two that is fulfilled by all machines. The sensitivity of the dynamics has been shown to be an analogue to such curvature.

The asymptotic nature of this unique relation can be deduced *a priori* from simple arguments. Compressors with a high rate of change of σ, i.e. large characteristic curvature, are expected to have a smaller stable flow range. In the limiting cases, if one wanted to design a compressor with an infinite $\Delta\phi$, the growth rate of the perturbations σ, and the slope $\partial\sigma/\partial\phi$ should be zero. Conversely, a compressor with zero stable flow range should have a σ-history that changed infinitely fast with flow coefficient. Thus, these two limits must hold

$$\lim_{\Delta\phi\to 0}\frac{\partial\sigma}{\partial\phi}=\lim_{\Delta\phi\to 0}K_e=-\infty \qquad \lim_{\Delta\phi\to\infty}\frac{\partial\sigma}{\partial\phi}=\lim_{\Delta\phi\to\infty}K_e=0 \tag{3.2}$$

At this point, one has to decide the σ-level with respect to which the stable flow range is calculated. A value of σ = -0.5 will be used for the relation presented here. The physical significance of the eigenvalue growth rate is discussed in section 3.3, where an analogy between the eigenvalue locus in terms of σ and ω and the amplification of disturbances if formulated. In an industrial set-up, the function should be derived for a range of σ-levels, which would then be available in the design process.

3.2.2 Development of the Equivalent Curvature Relation

To validate the above hypothesis, a battery of tests on compressors with systematic configuration changes is performed, as laid out in Table 3-1. For each of them, the σ-sensitivity at neutral stability and the stable flow range to σ = -0.5 are calculated, following the steps detailed in this section.

Study	Stages	N_{corr} [%$N_{corr,des}$]	$M_{relative,R1}$	Gap size [% R_{mean}]	Blade-Row Inertias	Loss bucket *[baseline=standard comp]*
(a)	1	35%	0.230	1%	1x Baseline	1x,...,6x Baseline
(b)	1	35%	0.230	1%	2x Baseline	1x Baseline
(c)	1	35%	0.230	1%	1x Baseline	2x Rotor 1 losses
(d)	2	35%	0.230	1% ... 50%	1x Baseline	1x Baseline
(e)	1	35–100%	0.230 - ... – 0.860	1%	1x Baseline	1x Baseline
(f)	2	35 – 100%	0.276 - ... – 0.822	1%	1x Baseline	1x Baseline
(g)	3	20 – 100%	0.171 – ... - 0.858	1%	1x Baseline	1x Baseline
(h)	5	11 – 100%	0.114 - ... - 0.984	1%	1x Baseline	1x Baseline

Table 3-1 Compressors studied towards identification of the Equivalent Curvature relation

First of all, the performance characteristic at constant speed is calculated with the mean line model. With this, one can guess the approximate position of the neutral stability mass flow: in the

Moore-Greitzer scheme, it is located at the peak of the Ψ_{TS} vs ϕ characteristic, whereas it can be slightly to the left of the peak when all the extra modelling additions are made (non-zero inter-blade-row gaps and unsteady loss effects). One can safely start some distance to the left of this peak, finding that the system is just unstable, i.e. σ is small and positive. Then, the mass flow can be increased along the characteristic until the σ-limit is reached.

The disturbance-energy balance in the system is zero at the point of neutral stability, becoming more negative as the compressor works at more stable conditions. While one could be tempted to calculate the slope of the *DEB* vs ϕ curve, both of these quantities are machine-specific. The disturbance-energy in the system depends on both the aerodynamic conditions and the size of the compressor. The flow rate at which the compressor stalls varies with engine size, profile characteristics, etc.

To avoid these issues and to bring all compressors to a common non-dimensional space, where the sensitivity of their dynamics can be compared, the *DEB* history must be non-dimensionalised on both axes. The flow coefficient is normalised by its value at neutral stability. *DEB* is zero at that condition so, instead, one can choose as a normalisation quantity the *DEB* level when the eigenvalue growth rate is at its specified limit. The normalised quantities are denoted as $\tilde{DEB}$ and $\tilde{\phi}$.

Finally, an analytic curve is fitted to the non-dimensional *DEB* evolution and its slope at unity $\partial \tilde{DEB}/\partial\tilde{\phi}_{NS} = K_e^{DEB}{}_{NS}$ evaluated. Because the stable flow range $\Delta\phi$ arises from straightforward examination of the performance characteristic, the coordinates of the particular compressor on the Equivalent Curvature domain are thus established.

In parallel, the same procedure can be followed with the variation of the critical perturbation growth rate along the characteristic. In this case, only the stable flow range needs to be non-dimensionalised, and the sensitivity $\partial\sigma/\partial\tilde{\phi}_{NS}$ constitutes the σ-based measure for equivalent characteristic curvature at neutral stability, $K_{e,NS}$.

Derivation of the Equivalent Curvature Power Law Relation

This analysis is carried out for all the compressors in Table 3-1. The general character of this relation is most striking when one examines the resultant distribution of datapoints in logarithmic space, all the incompressible points forming a distinct linear function, as shown in Figure 3-3.

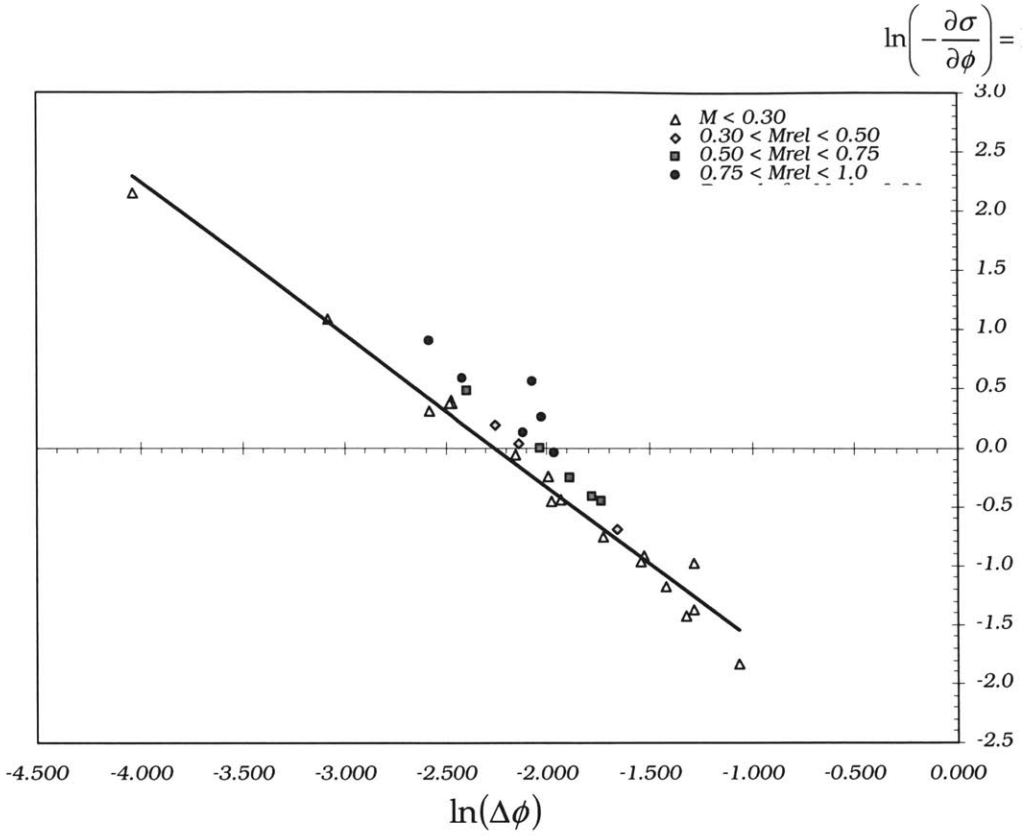

Figure 3-3 Logarithmic Equivalent Curvature relation for σ= -0.5 using σ as stability metric

The error appears to be directly related to the degree of compressibility, which is logical since the range is measured from a characteristic produced from a compressible mean line model, whereas the dynamics are solved from a purely incompressible formulation. The RMS errors for the different Mach number ranges are broken down as follows:

Compressibility	*Logarithmic slope RMS error*
$0 < M_{rel,R1} < 0.3$	0.088
$0.3 < M_{rel,R1} < 0.5$	0.110
$0.5 < M_{rel,R1} < 0.75$	0.221
$0.75 < M_{rel,R1} < 1$	0.517

Table 3-2 Mach number dependency of Equivalent Curvature logarithmic errors

The final tool that should be provided to a designer is an analytical expression for the Equivalent Curvature function, which is the solid line in Figure 3-4, in natural scales. It is noticed, once again, that all the cases running well into the incompressible flow regime, regardless of the other variations summarised in Table 3-1, are constrained to a very narrow band, asymptoting towards both axes, as defined by the limits set forth in Equation 3.2.

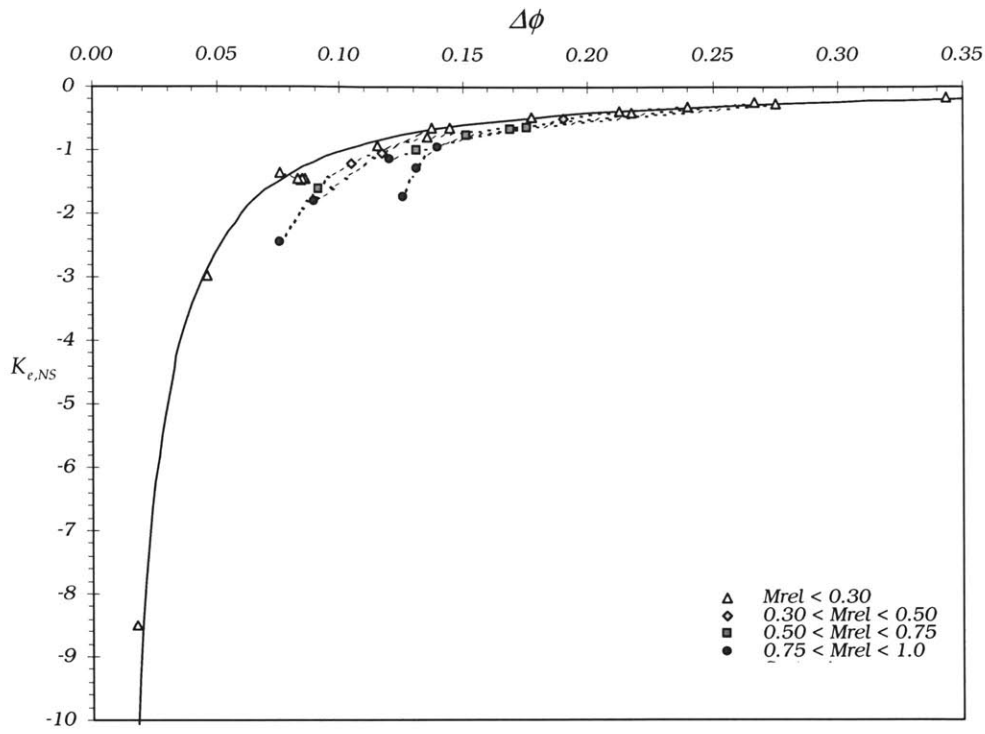

Figure 3-4 Equivalent Curvature relation for σ = -0.5 using σ as stability metric (dotted lines show the equivalent curvature path of different compressors as they are throttled up their running line)

The analytical function for the Equivalent Curvature relation can be derived from the above correlations by assuming the following functional behaviour, and discarding all points above the compressibility threshold of M_{rel}>0.30,

$$K_e = -\frac{k_1}{\Delta\phi^{K_2}} \tag{3.3}$$

Defining a pair of new variables $\beta = -K_e$, $\theta = \Delta\phi$ and taking their logarithms, the above expression is reduced to the linear dependency corresponding to the incompressible curve-fit shown in Figure 3-3, from which the value of the constants can be extracted.

$$\ln(\beta) = \ln(k_1) - k_2 \ln(\theta) \tag{3.4}$$

For the σ = -0.5 case, the Equivalent Curvature relation is

$$K_e = -\frac{0.07136}{\Delta\phi^{1.25113}} \tag{3.5}$$

By repeating the entire analysis for the desired values of σ_{limit} one can generate a succession of hyperbolae which, when linked together, form the *Equivalent Curvature Surface*. In an industrial design architecture, this data set would be available and a particular σ-slice of it would be applied to

each candidate compressor, depending on the required dynamic stability margin and the dynamic characteristics of the machine, in particular the rotation rate of its critical disturbances.

3.2.3 Physical Interpretation of Equivalent Curvature K_e

The rate at which the disturbance-energy approaches the zero-stability point when mass flow is reduced is the crucial *equivalent curvature* that relates to the machine stable flow range. However, by making *DEB* non-dimensional, one does away with the integral nature of this metric. In other words, the non-dimensional *DEB* does not relate to the absolute magnitude of the perturbations in the system any more. Instead, it represents an independent measure of overall dynamic stability, an analogue to the disturbance growth rate characterised by σ.

We recall that, in the Moore-Greitzer model, the eigenvalue growth rate depends on the slope of the total-to-static pressure rise characteristic, i.e. $\sigma \propto \partial\Psi^{TS}/\partial\phi$. Therefore, the rate of change of growth rate with flow $\partial\sigma/\partial\phi$ is truly a measure of $\partial^2\Psi^{TS}/\partial\phi^2$, the curvature of the characteristic. To first order, we would expect the dynamic sensitivity to have a hyperbolic behaviour, of the form

$$\frac{\partial\sigma}{\partial\tilde{\phi}} \propto \frac{const.}{\Delta\phi^2} \tag{3.6}$$

The exponent of the power law has been found to be 1.25, which is of the same order and reasonable, taking into account that the dynamic compressor model is a more evolved characterisation of the compression system dynamics. By this argument, since $D\tilde{E}B = f(\sigma)$, it follows that a similar link between $D\tilde{E}B$ and $\Delta\phi$ must exist, because the stable flow range is also a description of the curvature of the non-dimensional performance characteristic. One cannot expect the mapping to be exact for all compressors, because of the additional variables that affect the evolution of the perturbation flow field, such as gap length or unsteady loss-lags, and overall size. Divergences due to the latter are obliterated through the non-dimensionalisation of $D\tilde{E}B$, whereas the other variations are responsible for the 8% scatter of the points in the Equivalent Curvature relation.

3.2.4 Generation of an alternative Equivalent Curvature Relation from Disturbance-Energy Information Only

Because of the equivalence between σ and $D\tilde{E}B$, it is possible to reach a similar set of Equivalent Curvature relations through examination of the DEB sensitivity with flow rate at neutral stability. If

we concern ourselves with the relation between $\partial D\tilde{E}B/\partial\tilde{\phi}\big|_{NS}$, i.e. $K_e^{DEB}{}_{NS}$, and $\Delta\phi$, a hyperbola of the same topology is uncovered, as seen in Figure 3-5.

Given that obtaining the *DEB* requires the additional control volume analysis, it is not advisable to use this quantity for the calculation of the Equivalent Curvature Surface. This emphasises the point that, when the overall system stability is to be assessed, the growth rate σ is a much more efficient metric. *DEB* should be used in a component-by-component fashion, when the relative contributions of each blade-row to the whole stability balance need to be determined.

This argument is only valid when the dynamics are governed mainly by one lightly damped mode, all others being negligible. In systems with multiple critical modes of similar growth rate, or acoustic modes in the case of compressible conditions, then the only way to obtain an equivalent curvature is to represent the system dynamics through a single number by the use of *DEB*.

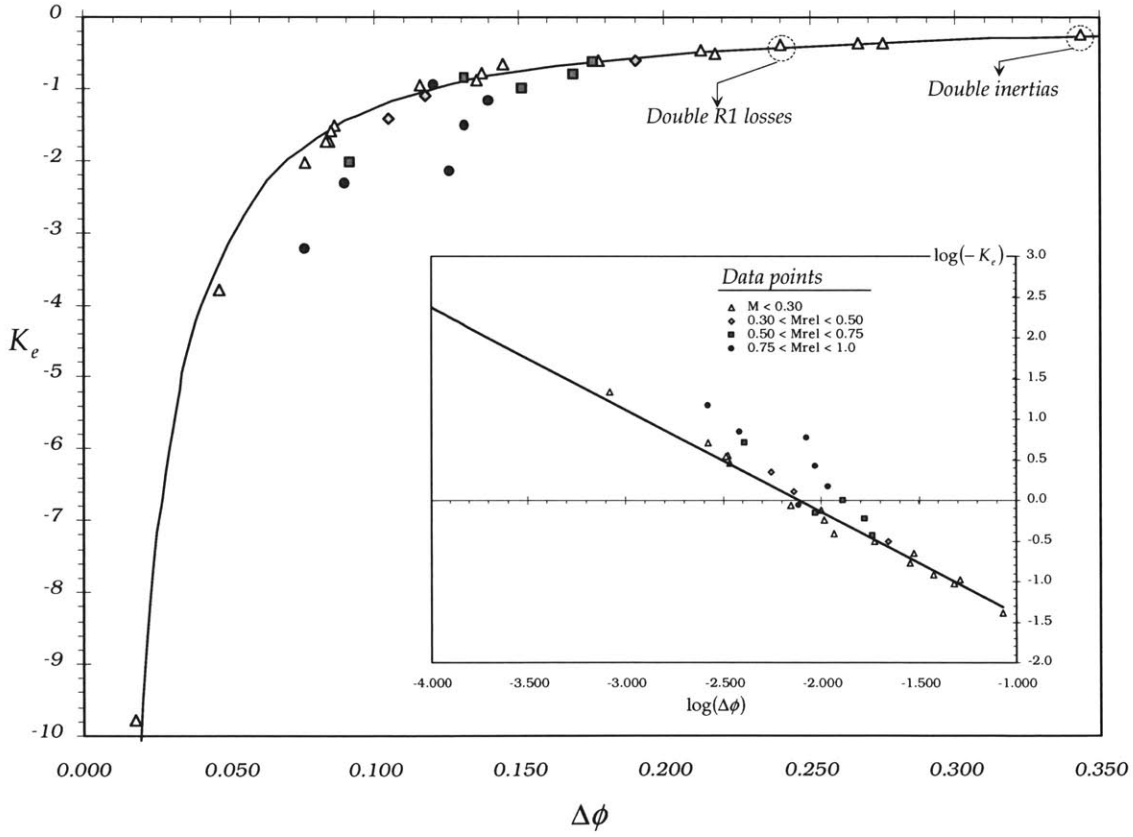

Figure 3-5 Equivalent Curvature relation for σ_{limit} = -0.5 generated from DEB information

3.2.5 Parametric Deviations from the Equivalent Curvature Relation

This subsection points out the effects of the individual design changes – loss buckets, gap size and compressibility – on the accuracy of the Equivalent Curvature relation. The insights gained from these parametric studies are essential to decide which points should be used to find the coefficients of the power law.

3.2.5.1 Loss Bucket Effects

A preliminary study that enables a wide spread in terms of range, whilst maintaining the required low compressibility, is the progressive modification of the loss curves for all the profiles in the compressor; the curvature of the characteristics is modified directly, without affecting the operating speed. Starting from the baseline 1-stage standard compressor at 35% corrected speed, the loss levels in the bucket are multiplied by integer factors, as detailed in Table 3-1, Study (a). As a consequence, the peak performance decays accordingly and the characteristics become steeper, as demonstrated in Figure 3-6. The non-dimensional DEB histories also change more steeply as the losses are increased. All these compressors fall almost exactly on the Equivalent Curvature relation (see Figure 3-7), with an average RMS error of 7.24%. Repeating this for multi-stage configurations of different geometry returns errors within the incompressible bound shown in Table 3-2.

This implies that the generation of the rest of curves for different σ limits can be sped up by taking low-speed compressors and changing their loss characteristics to cover the flow-range domain.

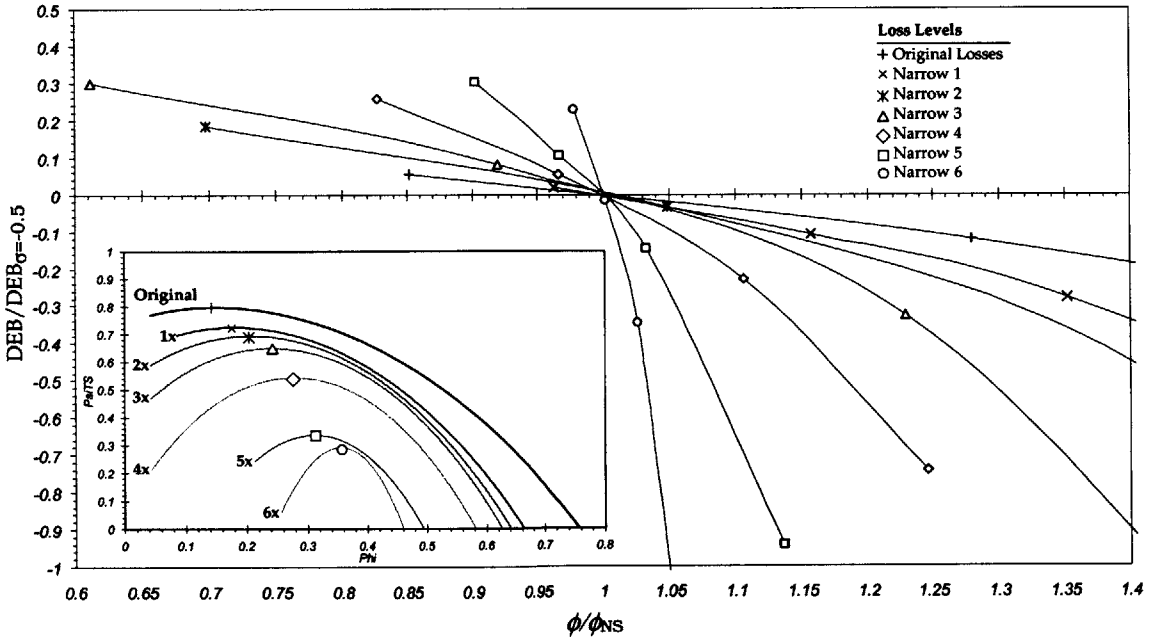

Figure 3-6 Nondimensional performance characteristics and DEB history for the 1-stage standard compressor with 1% inter-blade-row gaps, at 35% corrected speed and with increasingly narrow loss buckets

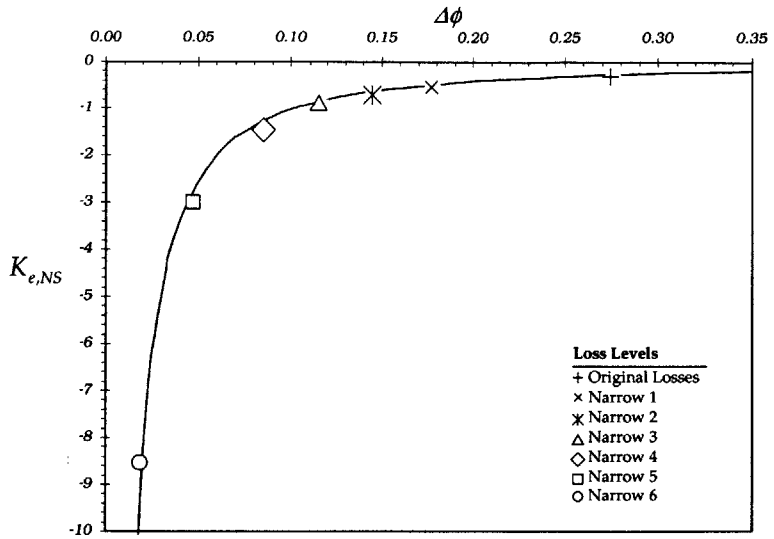

Figure 3-7 Position of compressors from the loss-factor parametric study on the Equivalent Curvature relation

3.2.5.2 Compressibility effects

As one examines progressively higher mass flows along a constant-σ running line, the characteristics become steeper and so do the dynamic histories, as seen in Figure 3-9 for the 1-stage standard compressor. A detailed view of the running line path on the *Equivalent Curvature* plot is provided in Figure 3-8 for the 1-, 2-, 3- and 5-stage cases.

The performance characteristic becomes much narrower as the engine is throttled up, and therefore the stable flow range as measured from the compressible characteristics is smaller than what would be found through an incompressible flow analysis. Therefore, one would expect the analysis to *under-predict* the range for a given DEB-slope.

The opposite is true, in fact, and all the compressor running-lines portray the same type of departure from the power law at high speeds, over-predicting the *DEB*-slope at neutral stability. To explain this, one must recall that compressible effects are not captured by the dynamic compressor model, except for the Mach number dependency of the loss buckets.

At high speeds, in fact, it is possible that an acoustic-like compressible system mode becomes critical to dynamic stability. It is unclear whether a fully compressible dynamic compressor model, in which the *DEB* related to the acoustic modes should be derived, may offset this over-prediction in range.

In conclusion, one is forced to stay within the prescribed speed range in order to use the Equivalent Curvature relation with confidence.

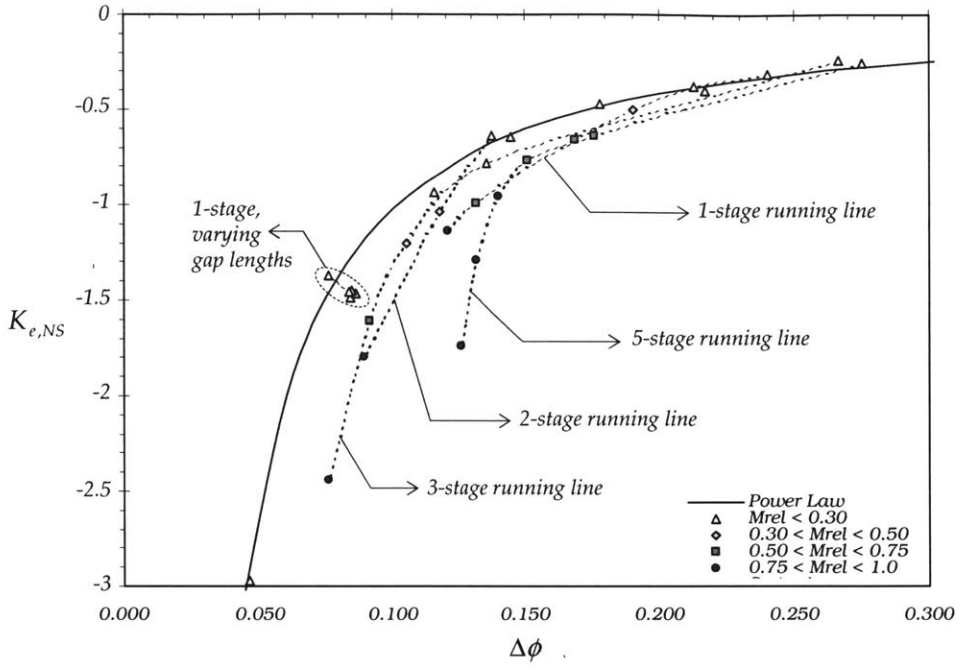

Figure 3-8 Close-up of deviations from Equivalent Curvature relation due to inter-blade-row gap size and engine speed

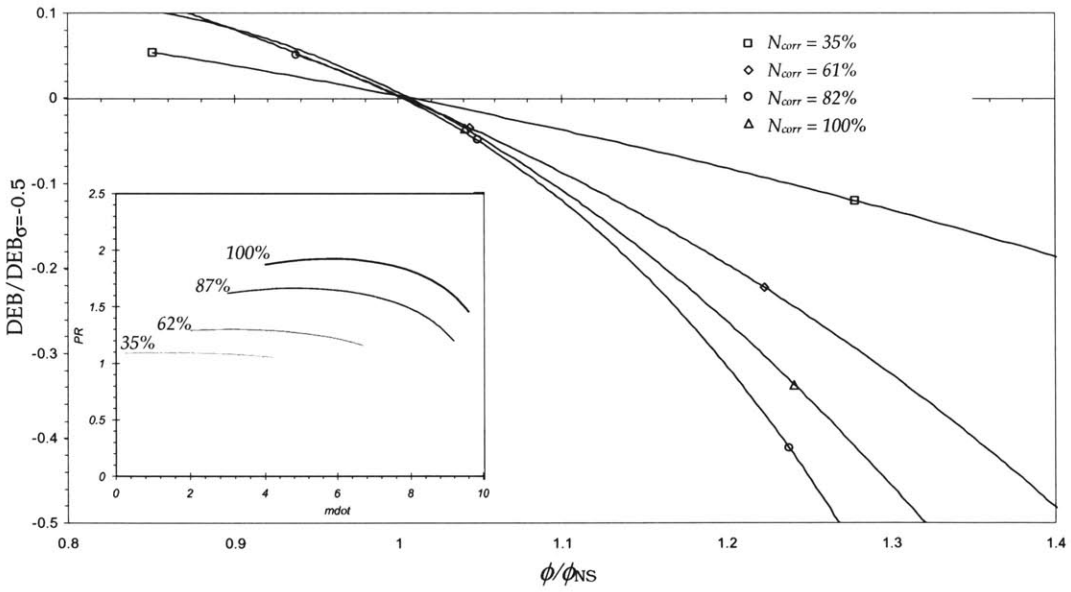

Figure 3-9 Nondimensional characteristics and DEB history for 1-stage standard compressor with 1% inter-blade-row gap at different rotational speeds

3.2.5.3 Gap Length and Blade-Geometry Effects

The dynamic variation induced by increasing inter-blade-row gap dimensions does not affect the validity of the K_e relation, to first order. Figure 3-8 shows the trace on the Equivalent Curvature map

of the 1-stage standard compressor with increasing gap size. The position of the compressor on the K_e map is found to be fairly constant for reasonable gap lengths of up to 15% of the mean radius for any incompressible machine, as depicted by the error curve on Figure 3-10. In other words, the incompressible error of the compressor at zero gap length is maintained up to a certain size. Beyond this, the error changes rapidly as the blade-row spacing becomes larger. In the case presented below, this means that the error actually becomes zero at a gap length of about 40%, but it increases markedly after that. In summary, reasonable gap lengths of under 15% contain the compressor within the incompressible error bounds.

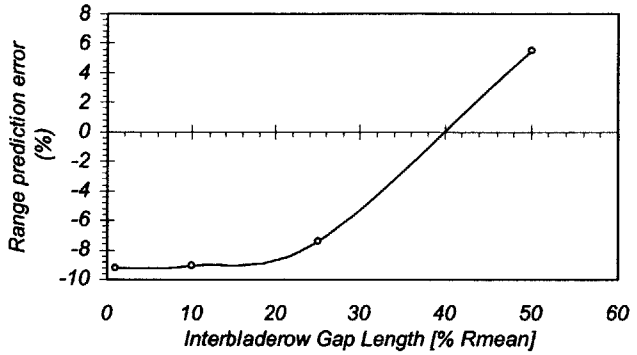

Figure 3-10 Range prediction error for the 1-stage standard compressor with varying inter-blade-row gap

It should finally be said that isolated changes to individual rows, such as variations in the blade dimensions or localised degradations of the loss buckets (see Table 3-1 (b) & (c)) do not produce significantly larger errors in range prediction, as both features are well captured by the dynamic compressor model. The locations of these two analyses are pointed out in the curve on Figure 3-5.

3.3 How much σ is enough dynamic stability?

3.3.1 The Q-Factor Analogy for the Amplification of Disturbances

After successfully developing a common pointer between the compression system dynamics and the stable flow range to a given degree of dynamic stability, the obvious issue that arises is the meaning of any particular value of σ. This is the question tackled in this section. It is easier to understand the reasonable dynamic safety margin that a compressor should comply with, if the information from the usual eigenvalue maps, i.e. σ and ω, is translated into a relevant quantity related to the amplification of perturbations under aerodynamic forcing. The quantity used to that end is the so-called *Q-factor*, which denotes the ratio of resonant to static disturbance amplitude.

First of all, an analogy between the compressor dynamics and a damped oscillator must be formulated. The standard solution for a single-degree-of-freedom motion of an unforced, damped harmonic system is found to be

$$x(t) = A_{\pm} \cdot e^{\left(-\delta \pm i\sqrt{\omega_n^2 - \delta^2}\right)t} \tag{3.7}$$

where $\delta = c/2m$ is the damping constant and is related to the commonly used damping ratio by $\xi = \delta/\omega_n$. The damped frequency of the motion is $\omega_d = \sqrt{\omega_n^2 - \delta^2} = \omega_n\sqrt{1-\xi^2}$.

On the other hand, the general solution for the behaviour of velocity and pressure perturbations in the compressor flow field is of the form

$$\delta\varphi(t) \propto e^{(\sigma - i\omega)t} \tag{3.8}$$

Here, the frequency ω is the rotation rate of the perturbations, and must not be confused with the natural or damped frequency of the system. As a matter of fact, the purpose of this analogy is establishing a relationship between the natural frequency and damping, and the growth/rotation rates obtained through the dynamic compressor model. The equivalence is

$$\sigma = -\delta \tag{3.9}$$

$$\omega = \sqrt{\omega_n^2 - \delta^2} \quad \leftrightarrow \quad \omega_n = \sqrt{\omega^2 + \sigma^2} \tag{3.10}$$

$$\xi = \frac{\delta}{\omega_n} = \frac{\sigma}{\sqrt{\omega^2 + \sigma^2}} \tag{3.11}$$

One can now turn the attention to an oscillatory system under sinusoidal forcing of frequency ω, the rotational frequency of the disturbance waves. Using the relations above, the ratio of forced to static amplitude can be shown to be a function of the damping and the frequency ratios ($r = \omega/\omega_n$), which can be substituted by expressions involving the perturbations' growth and rotation rates.

$$\frac{\left|\tilde{X}_f\right|}{\left|\tilde{X}_{static}\right|} = \frac{1}{\sqrt{\left(1-r^2\right)^2 + (2\xi r)^2}} = \frac{1 + (\sigma/\omega)^2}{\sqrt{(\sigma/\omega)^4 + 4(\sigma/\omega)^2}} \tag{3.12}$$

The dependency is solely on the ratio σ/ω, i.e. this analogy suggests that the amplification factor is constant along any ray going through the origin of the complex eigenvalue plane.

Both the amplitude of the resonant motion and the frequency at which it happens depend on the forcing and the natural frequency, as well as the damping. Differentiation of *(3.12)* enables one to find the resonant frequency

$$r_{res} = \sqrt{1 - 2\xi^2} \tag{3.13}$$

Or, in dimensional form

$$\omega_{res} = \sqrt{\omega_n^2 - 2\delta^2} = \sqrt{\omega^2 - \sigma^2} \tag{3.14}$$

It is clear that amplification of the static displacement can only occur when the damping is below a certain critical level. For the root in *(3.13)* to exist, then

$$\xi = \xi(\sigma/\omega) = \frac{(\sigma/\omega)}{\sqrt{1+(\sigma/\omega)^2}} \le \sqrt{1/2} \quad \Rightarrow \quad (\sigma/\omega) \le 1 \tag{3.15}$$

The resonant amplification can be arrived at by substitution of *(3.13)* in *(3.12)*. This is the Q-factor

$$Q = \frac{1}{2(\sigma/\omega)} + \frac{(\sigma/\omega)}{2} \tag{3.16}$$

Therefore, if we permit a maximum amplification Q, the location of the limit stability point in the complex plane in terms of the σ-to-ω ratio can be determined from

$$\frac{1}{2(\sigma/\omega)} + \frac{(\sigma/\omega)}{2} < Q \quad \Rightarrow \quad (\sigma/\omega)^2 - 2Q(\sigma/\omega) + 1 < 0 \quad \Rightarrow \quad |\sigma/\omega|_{\text{limit}} = Q - \sqrt{Q^2 - 1} \tag{3.17}$$

The regions of the complex plane where the allowed Q-factor will not be exceeded have been successfully established. If no resonant amplification is allowed to exist (Q=1), then the growth rate of the critical eigenvalue must be the same as its rotation rate (and of course, of opposite sign), which for typical machines lies in the range of 30% to 80% of the rotor frequency. In a one-stage configuration, for instance, the Moore-Greitzer solution is known to have a rotation rate of roughly $\omega \sim 0.5$, so for such compressor, a growth rate of $\sigma \sim -0.5$ would guarantee that the perturbations do not exceed their static values. On such grounds, this value was chosen as a σ limit for the derivation of the Equivalent Curvature relation in the previous section.

Alternatively, one could deem acceptable an amplification of the disturbances of, say, 10% over their static levels. In that case, the required σ-ω ratio is smaller, so the required growth rate for the least stable eigenvalue to satisfy the dynamic stability requirement is also lower, as long as ω remains constant.

While the concept of Q-factor is easily visualised in structural mechanics, experimental and/or computational work should be aimed at determining plausible values of Q that can be expected from the flow perturbations in an axial compressor. This lies beyond the scope of this work, which is aimed at the conception of the design philosophy. For all subsequent illustrative purposes, disturbances will only be allowed to grow an additional 10% from their steady values, i.e. a dynamic instability margin of $Q = 1.1$ will be prescribed in all designs.

The analogy between Q and the system dynamics is illustrated in the following figure, which shows the feasible regions where the critical eigenvalue must lie to satisfy various allowable Q-levels.

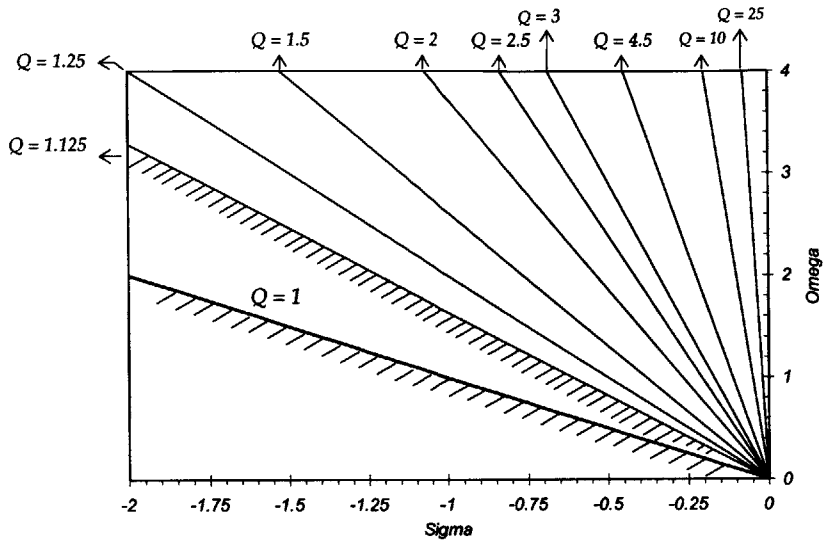

Figure 3-11 Stability margin rule relating the maximum allowable Q-factor to its corresponding σ/ω contour on the complex eigenvalue map

3.3.2 Practical Application of the Analogy

In a practical design framework, it would be desirable to deal with the growth rate of the critical eigenvalue instead of the Q-factor. As the amplification depends both on σ and ω, one should in principle track the relevant pole over the range of operating points as the mass flow is changed, if no further simplification is made.

However, the rotation rate ω of the perturbations could be assumed constant, at least for the initial phases of the design. If that approximation were reasonable, the direct examination of the root locus around neutral stability could be used to extrapolate to the negative plane and determine the necessary growth rate to fulfil the Q-factor requirement.

The Moore-Greitzer solution [10] predicts a constant rotation rate, depending on the harmonic under study and the relative inertias of the various blade passage flows. This is found through

$$\omega_n = \frac{\lambda n}{\mu + \frac{2}{n}} \tag{3.18}$$

where: $\lambda = \sum_{i=1}^{Nstages} \frac{c_{R,i}}{R_{R,i}\cos^2\gamma_{R,i}}$ is the inertia parameter of the rotor

and $\mu = \sum_{i=1}^{Nstages} \frac{c_{R,i}}{R_{R,i}\cos^2\gamma_{R,i}} + \frac{c_{S,i}}{R_{S,i}\cos^2\gamma_{S,i}}$ is that of both rotors and stators.

Indeed, when the Moore-Greitzer configuration is examined the eigenvalues migrate towards neutral stability at constant rotation rate. However, even when the blade-rows are separated from

each other or unsteady losses are incorporated, one finds that this is also a very good approximation for most realistic compressors, i.e. without excessively narrow loss buckets or large inter-blade-row spacings.

This is shown in the parametric study summarised in Figure 3-12, where the first harmonic, critical eigenvalue is tracked for various compressor configurations:

1. The first plot shows the variation in rotation rates due to progressively narrower loss buckets. Each new bucket is generated by multiplying the baseline loss levels by an integer factor (the actual characteristics for each compressor can be found in Figure 3-6). All these cases lie on a fairly constrained, flat region except for the *5x* and *6x* cases. It is unlikely that the loss levels of an existing blade design would be changed by more than a few percents, in an optimisation process.
2. The inter-blade-row spacing is found to have a greater impact on the rotation rate, which increases drastically as the gap is lengthened beyond small fractions of the mean radius. However, these differences take place below σ = -0.5, where the growth rates are very low and the compressor is operating far away from stability and its peak aerodynamic performance. This trend is observed for compressors of any number of stages. Therefore, one can conclude that in the region of interest of an optimisation process ($|\sigma| < 0.5$) the rotation rate also remains essentially flat.
3. The third study (Figure 3-12 [c]) shows the variation in eigenvalue motion for different speed lines. All the stability histories except the two most compressible cases are superimposed on the same, constant rotation path. This is logical, since in the incompressible regime the performance at the different speeds essentially collapses on a single non-dimensional characteristic, which has one set of dynamic attributes. The two distinct speeds are immediately before and after a relative blade Mach number of unity (0.96 and 1.03) , a regime in which the dynamic compressor model hereby presented cannot capture the acoustic effects, despite the fact that the loss model can account for some compressibility changes.
4. Finally, the effect of blade sizing is explored by doubling the chords of both rotor and stator in the 1-stage standard compressor. Because the first harmonic is being considered and $\mu<<1$ due to the small dimensions of the blades (10% R_{mean}), one would expect the rotation rate to be roughly proportional to the sum of the rotor inertia parameters, i.e. $\omega \propto \lambda$. This is indeed the case, as the mean rotation rate increases by approximately 80% when the blade chords are doubled. In both configurations, ω registers variations of under 10% for both blade dimensions. As one moves to multi-stage configurations, the sensitivity to the blade-row inertias becomes less acute.

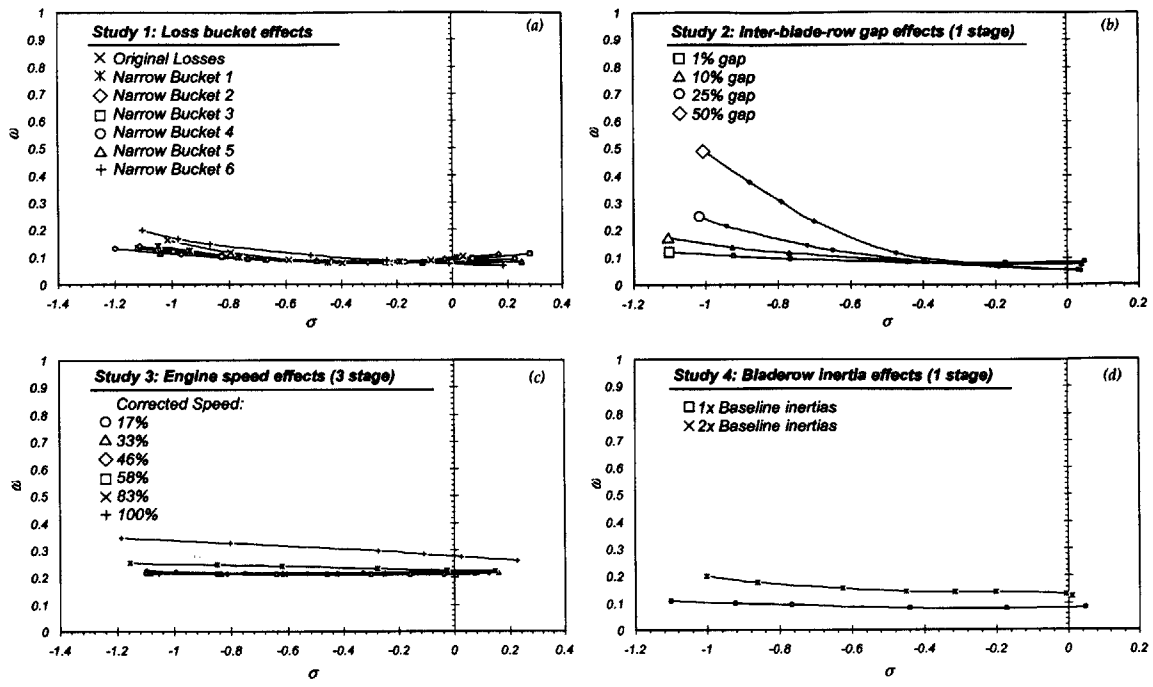

Figure 3-12 Rotation rate sensitivity studies

In summary, the Q-factor analogy can be used together with the assumption that the rotation rate varies negligibly, as long as one starts from a known configuration with reasonable loss levels and wishes to examine variations of the design within the incompressible speed range ($M_{rel} < 0.3$), while allowing for moderate changes in gap elongations and blade profile. To first order, the required growth rate of the least stable eigenvalue at the desired operating point must be of around the same magnitude as its rotation rate.

3.4 Robustness of Dynamic Stability to Flow Changes

The dynamic instability margin and stable flow range metrics, derived so far, would be sufficient to evaluate the compliance of candidate compressors with the dynamic stability requirements if it were possible to always sustain operation along the running line. The issue of robustness arises when excursions away from steady-state, typical of accel/decel operations, are taken into account.

The objective is to quantify the sensitivity of the perturbations with changes in flow along a given speed line. Geometrically, this is related to the curvature of the performance characteristic *at the operating point.*

The magnitude of interest is the percentage increase in quality factor Q due to a percentage decrease in mass flow from the design operating point, i.e. $\partial Q/\partial \phi$. From the definition of resonant amplification (3.16), this can be expressed as

$$\left.\frac{\partial Q}{\partial \phi}\right|_{op.point} = \frac{\partial Q}{\partial \sigma}\frac{\partial \sigma}{\partial \tilde{\phi}}\left.\frac{\partial \tilde{\phi}}{\partial \phi}\right|_{op.point} = \frac{1}{2\phi_{NS}\omega}\left(\frac{1}{(\sigma/\omega)^2}-1\right)\left.\frac{\partial \sigma}{\partial \tilde{\phi}}\right|_{op.point} \tag{3.19}$$

If one chooses to operate at Q = 1 (no resonance), where the magnitude of the growth rate is equal to the rotational frequency, the sensitivity becomes zero. This is consistent, since from that point onwards, there is no disturbance amplification.

Similarly, as the operating point moves towards the zero-damping axis, the rate of change of amplification becomes higher, eventually becoming infinite as σ/ω goes to zero.

In the low-amplification region where one is likely to operate ($Q \sim 1.1$), it can be easily shown that the sensitivity is of order $O(10^1)$. Both the flow coefficient ϕ and the rotation rate ω are of order $O(10^{-1})$. The slope of the ray where the eigenvalue lies is close to unity, but also of order $O(10^{-1})$, which makes the term in brackets of order $O(1)$. The sensitivity of the critical eigenvalue growth rate has been conveniently nondimensionalised to be of order $O(1)$. Depending on the location of the stall point and the value of the rotation rate, the amplification sensitivity $\partial Q/\partial \phi$ can take a range of values between $O(10^1)$ and $O(10^2)$.

A reasonable robustness criterion would be a limit of $\left.\partial Q/\partial \phi\right|_{op.point} \leq 10$. This implies that for a 1% change in mass flow, the disturbances are only amplified a further 10% from their static level.

It has been shown that the disturbance rotation rate can be taken to be invariant along a speed line. The required growth rate σ to ensure sufficient dynamic stability can be worked out using the Q-factor analogy. With these two quantities being fixed, and noticing that, in the resonant region ($|\sigma/\omega| < 1$), the term in brackets is always positive, the robustness in amplification is governed by the sensitivity of the critical eigenvalue growth rate with flow changes. This ties in precisely with the geometric point made above: the *robustness of dynamic stability to flow changes* is largely determined by the equivalent curvature $K_e^{\sigma} = \partial\sigma/\partial\tilde{\phi}$ of the performance characteristic at the operating point.

Computation of the Equivalent Curvature at the Operating Point

The sensitivity of σ at the design operating point must be calculated, but as with the analysis of overall safety, it would not be desirable to resolve the dynamic history around the design point, because of the increased calculation cost.

We can assume that, to first order, the σ-sensitivity or equivalent curvature can be found through the following Taylor series expansion

$$K_{e\,OP}^{\sigma} = K_{e\,NS}^{\sigma} + \left.\frac{\partial K_e^{\sigma}}{\partial \tilde{\phi}}\right|_{NS} \left(\tilde{\phi}_{OP} - \tilde{\phi}_{NS}\right) \tag{3.20}$$

In order to verify this hypothesis, the relation between the σ-sensitivity at the operating point with respect to its curvature and sensitivity at neutral stability can be analysed for the series of compressors used to derive the Equivalent Curvature relation. Various surfaces can then be fitted through the dataset to determine the most accurate analytical representation of this sensitivity relation.

Starting off by no *a-priori* assumptions on the form of this 3D relationship, the objective is to link the Equivalent Curvature at the operating point to the shape of the characteristic at neutral stability

$$K_{e\,OP}^{\sigma} = f\left(K_{e\,NS}^{\sigma}, \left.\frac{\partial K_e^{\sigma}}{\partial \tilde{\phi}}\right|_{NS}\right) \tag{3.21}$$

In an optimisation process, the required curvature sensitivity can be used as a parameter, and it might be desirable to compare the values of the required and actual equivalent curvature sensitivity. In that case, the useful relationship is actually

$$\left.\frac{\partial K_e^{\sigma}}{\partial \tilde{\phi}}\right|_{NS} = g\left(K_{e\,NS}^{\sigma}, K_{e\,OP}^{\sigma}\right) \tag{3.22}$$

The analytic curves fitted to the σ vs $\tilde{\phi}$ lines in order to produce the flow-range relations, can be used again to calculate the curvature of σ at surge and its slope at design point. Visualisation of those same compressors on this 3-dimensional space shows that, as expected from the simple expansion above, they lie in a confined planar region of space, through which a surface can be made to pass.

This surface must have a monotonic growth in both directions. For a fixed curvature $K_{e\,OP}^{\sigma}$ at the operating point, an increase in the curvature $K_{e\,NS}^{\sigma}$ at neutral stability must result in a smaller sensitivity $\partial K_e^{\sigma}/\partial \tilde{\phi}_{NS}$. Similarly, for a constant curvature $K_{e\,OP}^{\sigma}$ at stall, a larger sensitivity $\partial K_e^{\sigma}/\partial \tilde{\phi}_{NS}$ must exist as the design point curvature $K_{e\,OP}^{\sigma}$ increases. In summary,

$$\left.\frac{\partial\left(\partial K_e^{\sigma}/\partial \tilde{\phi}_{NS}\right)}{\partial\left(K_{e\,NS}^{\sigma}\right)}\right|_{K_{e\,OP}^{\sigma}} \prec 0 \quad \forall\left(K_{e\,NS}^{\sigma}, K_{e\,OP}^{\sigma}\right) \tag{3.23}$$

$$\left.\frac{\partial\left(\partial K_e^{\sigma}/\partial \tilde{\phi}_{NS}\right)}{\partial\left(K_{e\,OP}^{\sigma}\right)}\right|_{K_{e\,NS}^{\sigma}} \prec 0 \quad \forall\left(K_{e\,NS}^{\sigma}, K_{e\,OP}^{\sigma}\right) \tag{3.24}$$

An analytical formulation of this surface can be made by the least-squares technique outlined in Appendix C for the loss model. Variations of the following second order surface of symmetric curvature are explored to this end, with terms up to k_2, k_3, k_4 and k_5, respectively.

$$\frac{\partial^2\sigma}{\partial\tilde{\phi}^2} = k_0 + k_1\left.\frac{\partial\sigma}{\partial\tilde{\phi}}\right|_{NS} + k_2\left.\frac{\partial\sigma}{\partial\tilde{\phi}}\right|_{OP} + k_3\left.\frac{\partial\sigma}{\partial\tilde{\phi}}\right|_{NS}\left.\frac{\partial\sigma}{\partial\tilde{\phi}}\right|_{OP} + k_4\left[\frac{\partial\sigma}{\partial\tilde{\phi}}\right]^2_{NS} + k_5\left[\frac{\partial\sigma}{\partial\tilde{\phi}}\right]^2_{OP} \qquad (3.25)$$

The surface should pass through the origin, as an idle compressor with a flat *DEB* history at surge and no σ-curvature cannot have any sensitivity to flow changes – the engine would not be running. Thus, the independent term can be ruled out ($k_o = 0$).

The quadratic terms in the interpolated surface are bound to violate the limits set forth in (3.23) and (3.24), as can be seen in Figure 3-14. As said before, this σ-Sensitivity Surface should have an almost planar character.

The RMS errors in curvature for the different polynomials, grouped into compressibility ranges, are summarised in Figure 3-14. As with the flow-range relation, only the compressors running below the 0.30 relative Mach number threshold are used to generate the analytical relation.

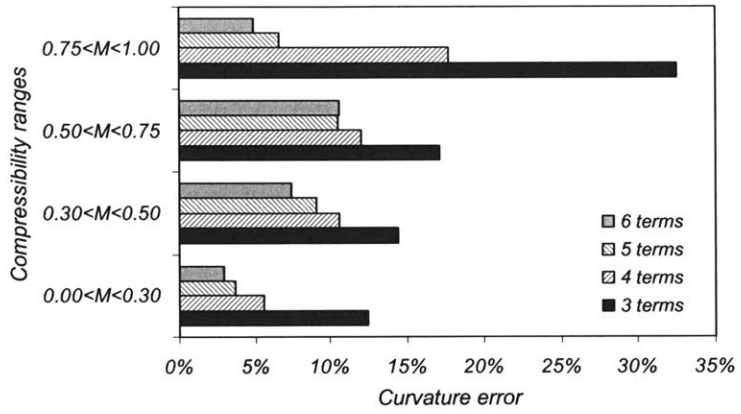

Figure 3-13 Average curvature error with different degrees of compressibility for σ_{OP} = -0.3

The resulting error clearly increases with compressibility, as found with the flow-range curves. The sharpest improvement in accuracy is registered with the addition of the cross-term over the basic linear plane. While the error can be decreased further at the data-points region with the quadratic terms, the function ceases to be physical, as it is not monotonic in both directions any more.

Just like any particular *Equivalent Curvature* relation is only valid for a certain σ-limit, the same is true for these surfaces. A four-dimensional hypersurface can thus be generated, from which only a particular σ-slice is used to assess any given compressor.

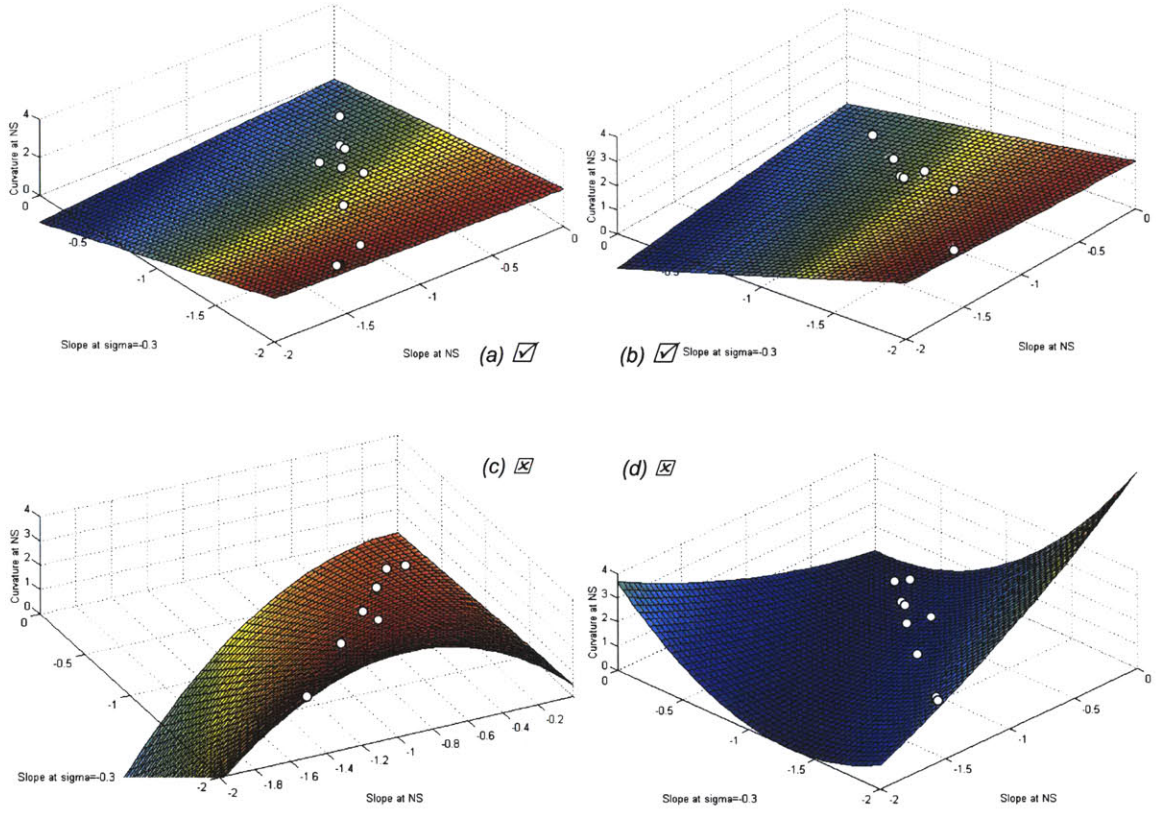

Figure 3-14 Polynomial interpolation surfaces with 3 (a), 4 (b), 5 (c) and 6 (d) terms

The main outcome of this analysis, however, is the realisation that, even though the addition of the first crossed term over the simple planar surface does yield smaller errors at the data points, the use of a linear Taylor expansion to determine the Equivalent Operating Curvature $K_{e,OP}$ is a good, simple approximation to the equivalent curvature variation along the characteristic.

3.5 Summary

Based on the lack of physical relevance of the currently established design practice, a set of metrics related to dynamic stability and robustness has been defined:

- The *dynamic instability margin* is understood by analogy with the concept of disturbance amplifications at resonance, Q, which is related to both σ and ω. The growth rate of the perturbations does not define a degree of stability *per se*, but in conjunction with the rotating frequency of the perturbations. A dynamic instability margin of $Q \leq 1.1$ will be used in subsequent designs, meaning that perturbations are only allowed to grow a further 10% from their static values.

- The *robustness of dynamic stability to flow changes* at any operating point can be assessed through the concept of amplification sensitivity, $\partial Q/\partial\phi$. This quantity determines the increase in amplification factor due to a decrease in mass flow. A plausible dynamic robustness margin of $\partial Q/\partial\phi \leq 10$ will be taken from here onwards. This robustness metric is mostly dominated by the equivalent curvature of the characteristic at the operating point, $K_{e,OP}$.

For a computationally efficient evaluation of these criteria, two standard relations have been uncovered, from physical arguments and examination of the dynamic history of an extensive array of machines.

- The *Equivalent Curvature Relation* provides an expedient way to calculate the stable flow range between the surge point and a particular level of dynamic stability, based on the equivalent curvature of the performance characteristic at neutral stability, given by either $K_e{}^{\sigma}$ (from eigenvalue information) or $K_e{}^{DEB}$ (from DEB analysis). The disturbance-energy concept is shown to be too expensive to ascertain the overall dynamic state of a compressor, which is just as well predicted by the eigenvalue alone (if, as in all the illustrative examples hereby presented, the dynamics are truly governed by *one* stability-critical mode, all others being highly damped). However, *DEB* is the only metric to provide a discrete measure of stability contributions for different blade-rows. This will be exploited in the design process described in Chapter 4.
- The Equivalent Curvature at the operating point is essential for the evaluation of the dynamic stability robustness at design. It can be determined through a quasi-planar surface, which relates the $K^{\sigma}_{e\ NS}$ and $\partial K^{\sigma}_{e\ NS}/\partial\tilde{\phi}$ to the equivalent curvature at any given dynamic stability level, $K^{\sigma}_{e\ OP}$. However, a linear Taylor expansion around the peak of the characteristic is a much more straightforward method to calculate this curvature, with an error of only 12.5%.

As they stand, both relations are only valid, to reasonable accuracy, for low speed machines (M_{rel} <0.3), because of the incompressible character of the dynamic compressor model and its inability to foresee the potentially critical acoustic-like modes in the compression system.

Chapter 4

Integrated Design Process for Stability

4.1 Introduction

4.1.1 The Need for an Integrated Design Methodology

The current industrial practice in axial compressor design tends to disregard stability as a prime design variable. In the initial phases of the design process, current frameworks are clearly more geared towards performance, efficiency, cost and operational issues than stability. It is true that, in most design groups with vast experience in the field, some known trade-offs between aerodynamic performance and stall margin are taken into account during the conception of a new compressor. By and large, however, the stability of the machine is something that is taken care of *a posteriori*, and only through the use of the stall margin, which has been arguably shown to have important deficiencies, apart from being a performance-limiting constraint that ensures static stability on a steady-state basis.

With the more detailed knowledge of dynamic compressor behaviour acquired so far, the development of systematic dynamic stability and robustness metrics, and expedient relations to assess them, the creation of a practical design architecture that accounts for dynamic stability, together with all the traditional aerodynamic requirements, is finally a feasible endeavour.

This Chapter deals with the conception of such methodology, the development of a unified framework for the understanding of the key features governing the compression system dynamics and the practical application of all these ideas to a real design exercise.

4.1.2 A Unified Framework for Compressor Dynamics

It is useful, before the mechanics of the design process are discussed, to step back and re-formulate the principal ideas developed in Chapter 3. In summary, it is hypothesised that, given the

pre-stall dynamics of any particular compressor are linked to the slope of its performance characteristic, the curvature of such characteristic must determine the stable flow range to a certain degree of dynamic stability. A pre-stall dynamics-based measure of a common, equivalent curvature is calculated from both the standard eigenvalue results and the *DEB* analysis. Indeed, a simple relation is found that closely determines the stable flow range to a particular Q-factor level (and hence σlimit) from knowledge of this equivalent curvature, as long as the operating condition is within the incompressible bounds established by the dynamic compressor model's limitations.

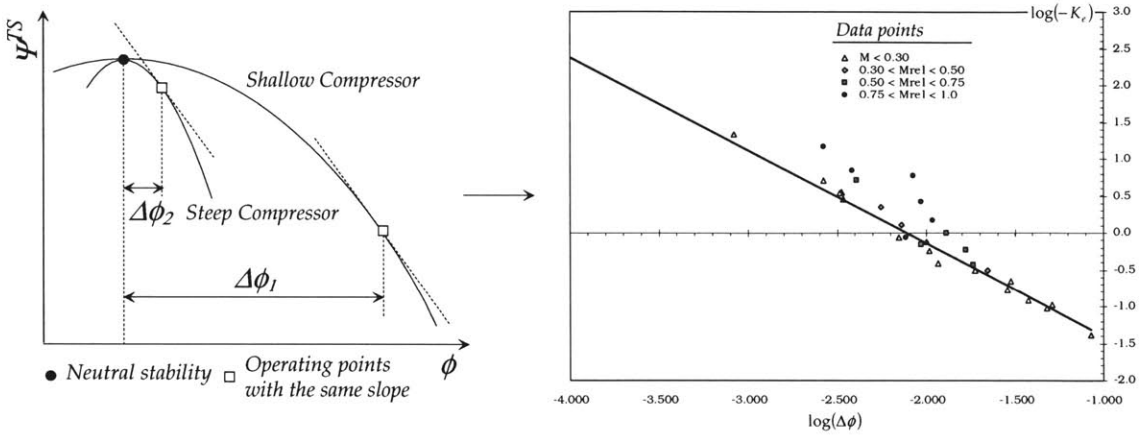

Figure 4-1 Logical path to the Equivalent Curvature relation

Expanding for various *Q*-levels, one can synthesise all the information that is physically relevant to the designer in a single plot, shown below, which is powerful in its simplicity; it is a conceptual summary of the relation between:

1.. Dynamic stability – *Q* 2. Robustness - K_e 3. Stable flow range – $\Delta\phi$

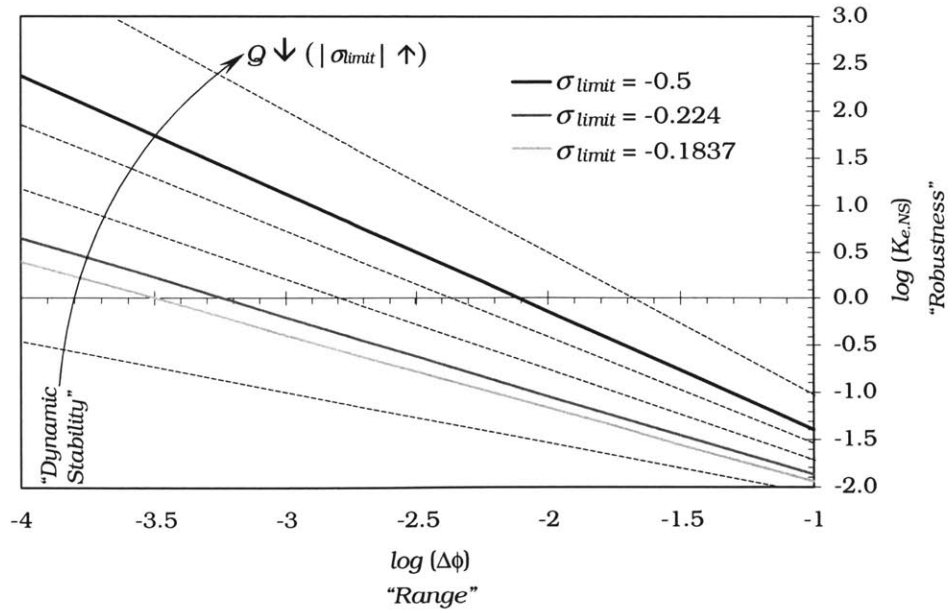

Figure 4-2 Unified Equivalent Curvature Relation for various dynamic stability levels

As said before, the non-dimensional dynamic history with flow changes is a measure of the Equivalent Curvature K_e of the compressor characteristic. In fact, given that the curvature is extrapolated linearly from neutral stability to the desired operating point, $K_{e,NS}$ is also a measure of $K_{e,OP}$, which is basically the robustness of the compressor dynamic stability to flow changes.

In parallel, the significance of a particular growth rate for the critical eigenvalue was elucidated through the Q-factor analogy. For any family of compressors, with a similar disturbance rotation rate ω, operating at different σ-limits is the same as changing the amplification factor Q of the disturbances.

Having specified the level of dynamic stability at which one wants to operate (in terms of Q) the equivalent curvature, measured at the neutral stability condition, can be used to directly obtain the stable flow range between neutral stability and the aforementioned operating point.

Due to time constraints, the Equivalent Curvature relation has only been computed for the three cases shown above, which are necessary for the practical design application described in 4.3. However, this is enough to clarify the nature of the relation as the required degree of dynamic stability increases: for the same curvature of the characteristic, choosing a design with a higher level of dynamic stability (lower allowable Q) implies stable operation at a larger stable flow range from the peak of the characteristic, and therefore a lower aerodynamic performance and efficiency.

This unified framework is the stepping stone by which the feasibility of various candidate compressors within the design optimisation scheme will be quantified.

4.1.3 Organisation of the Chapter

It is envisaged that the preliminary design process of an axial flow compressor will be embedded in a multi-objective optimisation framework, where it will be possible to change geometric, configuration and operational variables between iterations.

- First of all, the core of this scheme is the development of an appropriate cost function that includes measures of loading, dynamic stability and robustness. This is tackled at the onset, with the help of the unified framework discussed above. Once the objective function has been defined, the full sequence of the iteration can be laid out.
- Secondly, a case study is carried out, where the feasibility of a 2-stage non-standard compressor is benchmarked against a set of specified requirements. Design changes are made to this configuration and the resulting improvements in the different constraints are highlighted.
- Finally, an exploration of the use of *DEB* to systematically identify the blade-rows where particular design changes are most effective is performed.

4.2 Cost Function Definition

The convergence of the optimisation algorithm will be based on the minimisation of the following cost function

$$C = C_{\Psi} + C_{Q} + C_{K_e} = \underbrace{\left(\frac{\Delta\Psi^{TS}}{\overline{\Psi}^{TS}}\right)^2}_{\text{"Loading"}} + \underbrace{\left(\frac{\Delta\phi}{\overline{\phi}}\right)^2}_{\text{"Dynamic Stability"}} + \underbrace{\left(\frac{\Delta K_e}{\overline{K}_e}\right)^2}_{\text{"Robustness"}} \tag{4.1}$$

The definition of each of these terms is dealt with in the following sections, having first discussed the performance and stability constraints that the user must specify as design targets.

4.2.1 Design Requirements

A successful candidate in the optimisation process should satisfy the following constraints:

1. A certain performance level at a given speed, presumably to ensure operation along an unknown running line or to achieve a certain aerodynamic load for a determined application. This comes in the form of a required pressure rise Ψ^{TS}_{req} at a prescribed Operating Point, ϕ_{OP}. Adiabatic efficiency could also be incorporated into the optimisation procedure.
2. A dynamic instability margin, specified in terms of the maximum resonant disturbance amplification at the operating condition, Q_{req}.
3. A minimum level of dynamic stability robustness to flow changes at design, ensured through the sensitivity $\partial Q/\partial\phi_{req}$, analogous to the equivalent curvature of the characteristic, $K_{e,OP}$.

While a minimum stable flow range could be asked for, this will be seen to limit the freedom in the mapping of the design space. Fixing the stable flow range represents a crude way of imposing some degree of robustness into the system, by ensuring that flow variations will not bring the machine too close to the stall point. However, the Q-sensitivity constraint already ensures that the system dynamics change within allowable margins when transients are undergone.

Therefore, one could realistically operate very close to the peak of the characteristic, while still retaining a sufficient level of robustness, provided that the relevant dynamic parameters (*DEB* or σ) behave in a shallow enough manner, or in other words, the curvature of the characteristic K_e is small enough. Conversely, operating at a large distance away from the neutral stability condition is no guarantee that the robustness will be above a certain threshold.

The different logical paths to determine the feasibility of a design with fixed and free stable flow range will be highlighted later, demonstrating that a minimum range requirement might constitute a limitation when exploring different designs.

4.2.2 Loading Contribution to the Cost Function

The first task in the aerodynamic evaluation process is the generation of the performance characteristic. One can find the pressure rise at the required operating mass flow and determine whether the design meets the first constraint. The difference in actual and required pressure rise coefficients is used to define the first term in the cost function.

One can choose to penalise under-performance only, thus striving for the highest possible pressure rise. Clearly, a higher-than-required pressure ratio leads to a negative cost, which is beneficial within the optimisation algorithm. In that case, the performance-related cost is

$$C_{\Psi} = \frac{\left(\overline{\Psi}^{TS}_{req} - \overline{\Psi}^{TS}_{OP}\right)}{\overline{\Psi}^{TS}} = \left(\frac{\Delta\overline{\Psi}^{TS}}{\overline{\Psi}^{TS}}\right) \tag{4.2}$$

On the other hand, if one argues that over-performance must come at extra expense or if operation at this speed *must* go through a pre-defined running line, an excess in pressure rise must also contribute to the cost function, in which case this must be quadratic.

$$C_{\Psi} = \left(\frac{\Delta\overline{\Psi}^{TS}}{\overline{\Psi}^{TS}}\right)^2 \tag{4.3}$$

The denominator contains a scaling factor that makes all the terms in the cost function of order one. Otherwise, the optimisation would be biased towards regions in the design space where the largest term in the objective function improves more markedly. It is logical to scale this performance-related contribution by the order of magnitude of the expected variations in pressure rise coefficient.

4.2.3 Dynamic Stability Contribution to the Cost Function

Before an assessment of the stability characteristics can be made, the eigenvalue behaviour around the peak of the characteristic must be resolved. This determines the location of the neutral-stability point and also the non-dimensional slope and curvature of the σ-trace around the performance peak. For each of the points around neutral stability for which the eigenvalue is found, the disturbance-energy balance is also calculated, thus also obtaining the slope and curvature of the *DEB*-history, which are also analogues of the Equivalent Curvature K_e and its derivative $\partial K_e/\partial\phi$.

The unified Equivalent Curvature relation described in 4.1.2 is employed to find the stable flow range between neutral stability and the point where the absolute dynamic stability reaches the required dynamic instability margin, Q_{req}.

However, one must first determine which eigenvalue growth rate yields the required Q-factor. The rotation rate ω of the critical mode is known around the neutral stability condition, and assumed constant throughout the characteristic. The Q-factor analogy gives the required value of the critical growth rate at the operating point through

$$\sigma_{\text{limit}} = \omega\left(Q - \sqrt{Q^2 - 1}\right) \tag{4.4}$$

Based on this value, one can choose a particular line in the unified Equivalent Curvature relation, through which the stable flow range $\Delta\phi$ can be found uniquely. Naturally, one would use the power-law form of the relation, instead of the linear function in logarithmic space, which is more useful for illustration purposes.

Therefore, the flow at which the Q-factor reaches the required level is known.

$$\phi_{\sigma\text{limit}} = \phi_{NS} + \left(-\frac{k_1}{K_{e,NS}}\right)^{1/k_2} \tag{4.5}$$

This provides an indirect route to determine whether the stability constraint is met, without having to actually calculate the value of the quality factor Q at design –the key expensive step one attempts to avoid with the use of equivalent relations. The indirect comparison between the limit-stability flow and the operating point is illustrated in Figure 4-3.

In summary:

- $\phi_{\sigma\text{limit}} > \phi_{OP}$ The resonant amplification at the design flow rate is larger than the tolerable value and the design is not valid.
- $\phi_{\sigma\text{limit}} < \phi_{OP}$ The compressor is more stable than required at the desired operating point, but most importantly, the loading levels are too conservative and more aggressive designs are possible.

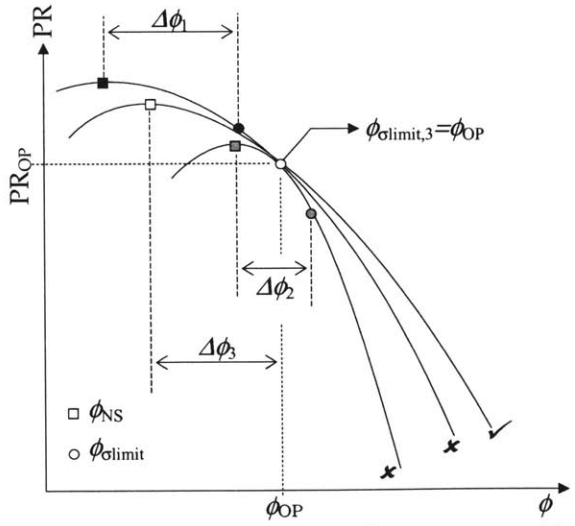

Figure 4-3 Comparison between $\Delta\phi$ computations for compressors with excessive (1), insufficient (2) and correct (3) Q-factors at the operating point

This benchmarking scheme can be used to define the stability contribution to the overall cost function. As in the case of the loading, both excessive and insufficient performance must lead to an increased objective function penalty. The form of the function is the same as before, but with ϕ as the control variable.

$$C_Q = \left(\frac{\phi_{OP} - \phi_{\sigma limit}}{\bar{\phi}} \right)^2 = \left(\frac{\Delta\phi}{\bar{\phi}} \right)^2 \tag{4.6}$$

In this case, the order of magnitude of the required flow coefficient at design can be used as a scaling parameter, making the difference of order one.

Stability Benchmarking with a Fixed Stable flow range

The schematic shown in the previous discussion emphasises that the disturbance amplification at the design flow rate is not only dependent on the equivalent curvature K_e – through which the stable flow range arises – but also on the location of the neutral stability point.

Therefore, different combinations resulting in the same degree of dynamic stability at the operating point may be reached. On one hand, one could exploit compressors with aggressive σ-traces, i.e. highly curved characteristics, and a neutral stability point located very close to the operating flow. In that case, the performance would be close to the peak of the characteristic. On the other hand, a machine with a shallow variation in dynamic behaviour could be chosen, which would imply a characteristic of low curvature. As a result, the stable flow range to stall would be higher, but one would be operating far away from the maximum pressure rise and efficiency.

In light of this reasoning, which is an application of that put forward in 3.1, it is obvious that prescribing a fixed stable flow range between design and neutral stability freezes the location of the peak of the characteristic. Consequently, in order to achieve a certain degree of dynamic stability at the operating point, which is geometrically the slope of the characteristic at that location, the equivalent curvature at the peak is forced to have a concrete value. This implies that the behaviour of the dynamics at neutral stability – either *DEB* or σ – is locked from the onset.

While one could probably attain the required safety margin at design with a fixed stable flow range, it may sometimes not be possible to achieve the required robustness, characterised by the curvature of the characteristic at design. If the stable flow range is floating, one can modify this operating curvature by shifting the location of the neutral stability point and changing the shape of the characteristic. If the stable flow range is fixed from the start, however, the behaviour of the dynamic history is the only degree of freedom to satisfy the robustness requirement.

In summary, specifying a fixed stable flow range is not a sound strategy, as it has no direct physical impact on the dynamic stability and robustness, but still constrains the optimiser to search in a narrow region of the design space.

4.2.4 Dynamic Robustness Contribution to the Cost Function

The final element of the objective function must reflect the robustness of the Q-factor to flow changes around the design operating point. This sensitivity can only be calculated at the flow where the Q-limit is reached. In most candidate compressors, this will not coincide with the design point, where the system dynamics are unknown. This is not a problem, because the stability-related cost C_Q pulls the limit-safety point to the required operating flow condition, ϕ_{OP}. Separately, the third contribution to the cost function should decrease as the amplification sensitivity goes up.

Based on the simple algebraic expressions derived in 3.4, the necessary equivalent curvature at the Q-limit point to achieve the required sensitivity $\partial Q/\partial\phi_{req}$ can be found through

$$K_{e,req} = \left.\frac{\partial\sigma}{\partial\tilde{\phi}}\right|_{Qlimit} = \frac{2\phi_{NS}\omega}{\left(\frac{1}{(\sigma/\omega)^2}-1\right)}\left.\frac{\partial Q}{\partial\phi}\right|_{req} \tag{4.7}$$

The cost term must simply be a comparison between this value and the real equivalent curvature at the Q-limit point, which can be reached by linear expansion from the neutral stability flow,

$$K_{e,Qlimit} = K_e|_{NS} + \left.\frac{\partial K_e}{\partial\phi}\right|_{NS}\cdot\Delta\phi \tag{4.8}$$

The difference between the required and actual equivalent curvatures forms the basis of the robustness-related cost term,

$$C_{Ke} = \left(\frac{K_{e,Qlimit}-K_{e,req}}{\overline{K}_e}\right)^2 = \left(\frac{\Delta K_e}{\overline{K}_e}\right)^2 \tag{4.9}$$

The scaling factor in this case can be chosen to be the order of magnitude of the required curvature. Due to the equivalent curvature being non-dimensional by definition, this tends to be O(1).

4.2.5 Overall Cost Function and Potential Errors

The sum of the loading, dynamic stability and robustness terms forms the overall cost function to be minimised by the optimisation routine,

$$C = C_\Psi + C_Q + C_{Ke} = \left(\frac{\Psi_{req}^{TS}-\Psi_{OP}^{TS}}{\overline{\Psi}^{TS}}\right)^2 + \left(\frac{\phi_{OP}-\phi_{\sigma limit}}{\overline{\phi}}\right)^2 + \left(\frac{K_{e,Qlimit}-K_{e,req}}{\overline{K}_e}\right)^2 \tag{4.10}$$

The quadratic form ensures convergence to the exact constraints, which takes place when the total cost vanishes. If the first order form is used, greater-than-required performance in any of the three criteria returns a negative contribution and the absolute minimum may yield a design with superior performance. However, the adiabatic efficiency, manufacturing bounds and the economics of higher-performance machines should also be taken into account in that case.

Once the root of the cost function has been found, it would be advisable to calculate the full dynamic history up to the design point. The standard relations used to assess Q and $\partial Q/\partial \phi$ in the optimisation are only approximate, and further refinements will surely be necessary.

The main sources of uncertainty are:

- The Equivalent Curvature relation error band for the estimation of the stable flow range.
- The inaccuracy due to the Taylor series expansion to calculate the equivalent curvature at the Q-limit flow condition

4.3 Application of the Integrated Optimisation Scheme

The concepts presented so far are demonstrated with the preliminary design of a 2-stage compressor. The succession of steps leading to the evaluation of the cost function for an arbitrary candidate design, is summarised in Figure 4-4

The performance and stability constraints are outlined in Table 4-1. In principle, the wheel speed and the inlet thermodynamic conditions are fixed, as well as the overall compressor dimensions. The blade positioning, stage configuration, profile characteristics and loss buckets constitute the degrees of freedom in the problem. The design variables for the initial and final configurations are summarised in Table 4-2.

The full iterations for the both the starting design and the converged solution are gone over in detail. In addition, the complete dynamic history is also calculated up to the design point for these two cases, in order to assess the errors introduced by the indirect stability measurements made during the optimisation, through the standard relations.

It should be noted that 3 independent changes have been made between the two configurations. The individual performance variations induced by each of these steps are briefly reviewed at the end, in section 4.3.3.

Ψ_{TS}	*0.9801*
ϕ_{OP}	*0.2715*
Q	*1.1*
$\partial Q/\partial \phi$	*10*

Table 4-1 Design requirements summary of the 2-Stage compressor integrated optimisation for stability

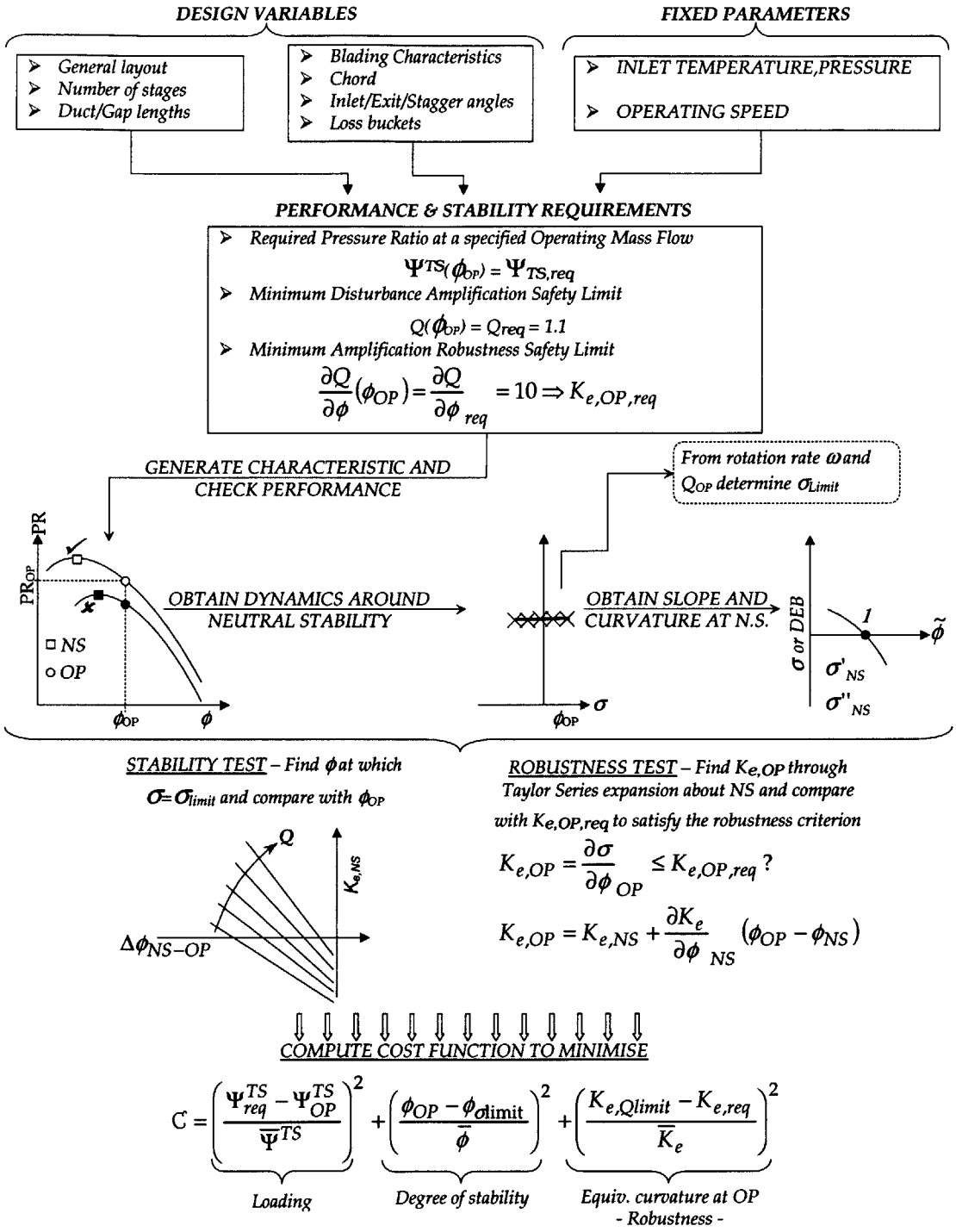

Figure 4-4 Outline of procedures in one optimisation iteration

	Unfeasible Candidate	*Converged Solution*
Stages	2	2
Annulus Geometry	Fixed	Fixed
Wheelspeed [rpm]	4750	4750
$M_{rel,R1}$	0.286	0.286
Intra-stage gaps [%Rmean]	1%	1%
Inter-stage gap [%Rmean]	5%	1%
Loss bucket [x standard]	3x	1x
Rotor chord [%Rmean]	16.41%	12.29%
Stator chord [%Rmean]	10.65%	10.65%

Table 4-2 Design features before and after optimisation

4.3.1 Unfeasible Design Iteration

4.3.1.1 Performance Check

The performance characteristic for the first candidate design is shown below. The compressor is within the unstable regime at the required operating flow. The neutral and limit-stability locations are also shown on the speed line. We can immediately see that neither the pressure ratio nor the minimum stability criteria are met at ϕ_{req}.

The order of magnitude of the difference in pressure-rise coefficient is $O(10^{-1})$, so the performance cost is non-dimensionalised by 0.1, thus becoming:

$$C_{PR} = \left(\frac{PR(\phi_{OP}) - PR_{OP,req}}{\overline{PR}} \right)^2 = \left(\frac{0.7060 - 0.9801}{0.1} \right)^2 = 7.513$$

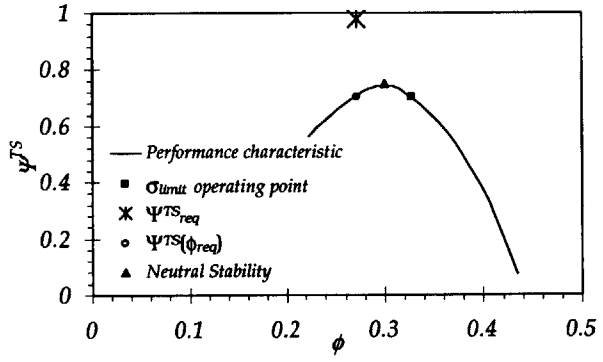

Figure 4-5 Loading check for unfeasible 2-stage compressor

Strictly, if a candidate configuration does not satisfy the expected performance, one could discard it straight away and proceed to modified designs. However, it is advisable to carry out the full dynamic analysis regardless of this, in order to evaluate the contribution to the cost function from the stability constraints. This ensures that gradient-based techniques give rise to changes that enhance the

overall quality of the design, instead of improving the pressure rise until the target is reached and only then moving on to assess the compliance with the stability criteria.

4.3.1.2 Stability Check

Starting at a flow coefficient ϕ about 5% to the left of the peak of the characteristic, the critical eigenvalue is computed up to a growth rate of roughly –0.1, the trace of which is shown below.

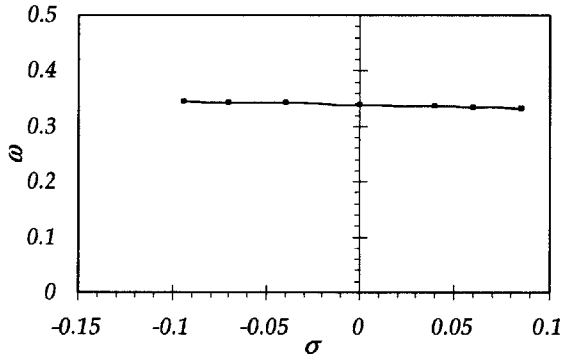

Figure 4-6 Eigenvalue history for unfeasible 2-stage compressor

The average rotation rate around neutral stability is found to be: $\omega_{AVE} = 0.34877$

From the required Q margin for dynamic stability, the growth rate at the limit-safety condition must be:

$$\sigma_{limit} = \omega_{AVE}\left(Q - \sqrt{Q^2 - 1}\right) = \left(1.1 - \sqrt{1.1^2 - 1}\right) = 0.2238$$

This identifies the particular line in the unified Equivalent Curvature relation (Figure 4-1) that applies to this compressor in question. The equivalent curvature at neutral stability must therefore be worked out in order to calculate the stable flow range to the limit-stability flow.

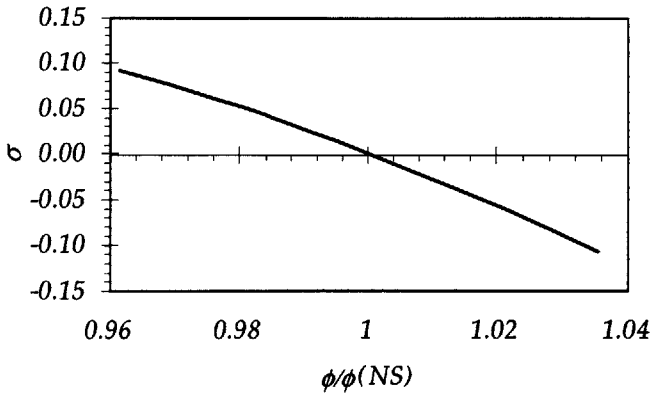

Figure 4-7 Nondimensional σ-history for unfeasible 2-stage compressor

In fact, fitting a polynomial through the σ-trace depicted on Figure 4-7 yields both the equivalent curvature and its rate of change with flow:

$$K_{e,NS} = \left.\frac{\partial \sigma}{\partial \tilde{\phi}}\right|_{NS} = -2.7054 \qquad \left.\frac{\partial K_e}{\partial \tilde{\phi}}\right|_{NS} = \left.\frac{\partial^2 \sigma}{\partial \tilde{\phi}^2}\right|_{NS} = -7.253$$

Through suitable processing of the same data used to generate the σ = *-0.5 Equivalent Curvature* relation in Chapter 3, one can obtain the version corresponding to a σ-limit of -0.224, from which the stable flow range can be read off by simply knowing $K_{e,NS}$ and Q. Instead of the linear logarithmic form portrayed in Figure 4-1, its power-law is given by:

$$K_{e,NS} = \left.\frac{\partial \sigma}{\partial \tilde{\phi}}\right|_{NS} = \frac{-0.050433}{(\phi_{\sigma=-0.224} - \phi_{NS})^{1.3079}}$$

Rearrangement of this expression gives the location of the limit-stability condition:

$$\phi_{\sigma=-0.224} = \left(\frac{-0.050433}{K_{e,NS}}\right)^{1/1.3079} + \phi_{NS} = 0.32816$$

Since $\phi_{\sigma=-0.224} - \phi_{req} \succ 0$, the compressor is not stable enough at the required flow coefficient. For the present case, this is obvious by simple inspection of the characteristic, but when neutral stability lies to the left of the design point, this test becomes indispensable.

This information is sufficient to calculate the stability-related cost. As ϕ_{req} is of order $O(10^{-1})$, the scaling factor is chosen to be 0.1. Alternatively, one can choose ϕ_{req} as the scaling parameter and use a weighting factor within the optimiser to ensure that this cost term is comparable to the others.

$$C_Q = \left(\frac{\phi_{OP} - \phi_{\sigma limit}}{\bar{\phi}}\right)^2 = \left(\frac{0.32816 - 0.2715}{0.1}\right)^2 = 0.3209$$

Range prediction error

The full eigenvalue curve up to the limit-stability point has actually been generated to find the error between the stable flow predicted through the K_e plot and the actual flow at which the Q-factor reaches its safety value. According to the complete trace, shown below, the limit-stability stable flow range is ϕ = 0.327. The stable flow range computed from the true dynamic history is therefore 4.19% smaller than the predicted value within the iteration, as can be seen from the *Equivalent Curvature* plot.

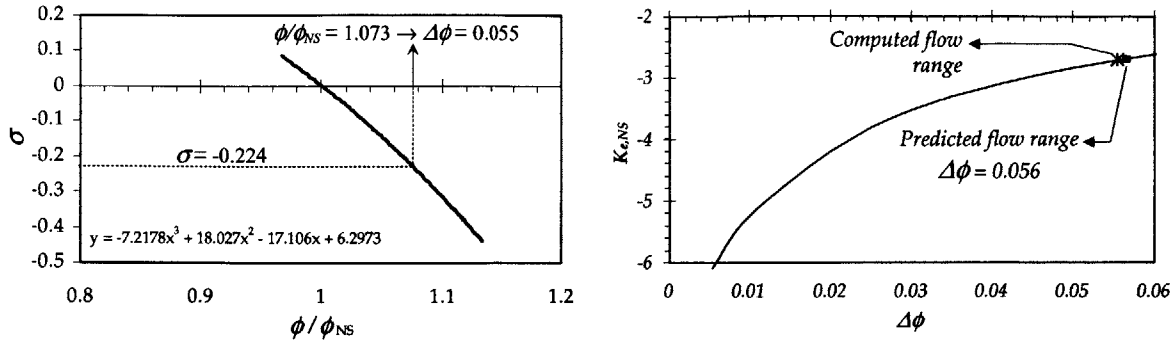

Figure 4-8 Range prediction error for unfeasible 2-stage compressor

4.3.1.3 Robustness Check

Based on the Q-factor sensitivity specified by the robustness constraint, the required equivalent curvature at the limit-stability flow can be easily computed using

$$K_{e,req} = \left.\frac{\partial\sigma}{\partial\tilde{\phi}}\right|_{Qlimit} = \frac{2\phi_{NS}\omega}{\left(\frac{1}{(\sigma/\omega)^2}-1\right)}\left.\frac{\partial Q}{\partial\phi}\right|_{req} = -1.488$$

This must be compared with the actual equivalent curvature at the σ-limit operating point, which is obtained by linear extrapolation from neutral stability:

$$K_{e,Qlimit} = K_e|_{NS} + \left.\frac{\partial K_e}{\partial\phi}\right|_{NS} \cdot \Delta\phi_{NS-Qlimit} = -2.875$$

Thus, the robustness-related cost is:

$$C_\Sigma = \left(\frac{K_{e,OP} - K_{e,OP,req}}{\overline{K}_{e,OP}}\right)^2 = \left(\frac{-2.875+1.488}{1}\right)^2 = 1.925$$

In fact, sufficient information is available to calculate the actual value of the dynamic robustness at the stability-limit condition:

$$\left.\frac{\partial Q}{\partial\phi}\right|_{\sigma=-0.224} = \frac{1}{2\phi_{NS}\omega}\left(\frac{1}{(\sigma/\omega)^2}-1\right)K_e\Big|_{\sigma=-0.224} = -19.32$$

Therefore, even if one allowed the compressor to operate at the mass flow where the stability limit is reached, the Q-sensitivity to flow changes is almost twice the allowed value, Q_{req} = 10; the curvature of the characteristic is too high.

Robustness Prediction Error

The only parameters that can introduce uncertainty into the calculation of the Q-sensitivity are the eigenvalue rotation rate and the equivalent curvature. It is clear that the higher the rotation rate, the worse the sensitivity, other variables remaining fixed. A larger equivalent curvature also contributes to a larger sensitivity, which is expected from geometric considerations. These effects can be expressed as

$$\frac{\partial}{\partial\omega}\left(\left|\frac{\partial Q}{\partial\phi}\right|\right)>0 \qquad \frac{\partial}{\partial K_e}\left(\left|\frac{\partial Q}{\partial\phi}\right|\right)=\frac{\partial}{\partial\left(\partial\sigma/\partial\tilde{\phi}\right)}\left(\left|\frac{\partial Q}{\partial\phi}\right|\right)>0 \tag{4.11}$$

The full eigenvalue migration has been resolved up to the Q-factor limit, revealing that there is a slight increase in rotation rate as the mass flow goes up. In fact, the true rotation rate at the σ-limit is 4.3% higher than the average of the points around neutral stability.

The real value of the equivalent curvature K_e^{σ} at the stability limit can be calculated analytically from the complete dynamic history shown in Figure 4-8. The prediction from the Taylor series is found to be 14.4% smaller than the real value. Such error lies within the expected band of uncertainty for compressors with $M_{rel} < 0.3$, as explained in 3.4.

These two inaccuracies produce errors of the same sign in robustness, so that the actual sensitivity $\partial Q/\partial\phi$ is 17.18% larger than the value derived through approximations.

4.3.1.4 Overall Cost Function and Required Changes

The sum of the performance, stability and robustness contributions to the cost function gives:

$$C = C_{\Psi} + C_Q + C_{Ke} = 7.513 + 0.3209 + 1.925 = 9.759$$

This is the quantity to minimise. In order to do so, the following changes are implemented in the next design iteration, which will be proved feasible:

- The loss bucket is reduced to the levels of the *standard* compressor.
- The inter-stage gap is reduced from 5% to 1%, as this is known to decrease the growth rate of critical eigenvalue, thus stabilising the compression system.
- The chord of both rotors is decreased by about 4% of the mean radius, thus diminishing the blade passage inertia and bringing down the rotation rate of the disturbances. By the Q-factor analogy, this improves both the disturbance amplification and the robustness for any fixed level of critical perturbations' growth rate σ.

4.3.2 Successful Design Iteration

For the improved design, it is not necessary to go over the detailed calculations for each of the terms in the objective function. Instead, the key features are pointed out along the discussion.

Having reduced the loss levels, the new compressor characteristic satisfies the performance requirement exactly, its peak being situated at a lower mass flow than design. The compressor dynamics also behave in a more shallow fashion, as demonstrated by the larger stable flow range to the stability limit, which in this converged design coincides with the operating point.

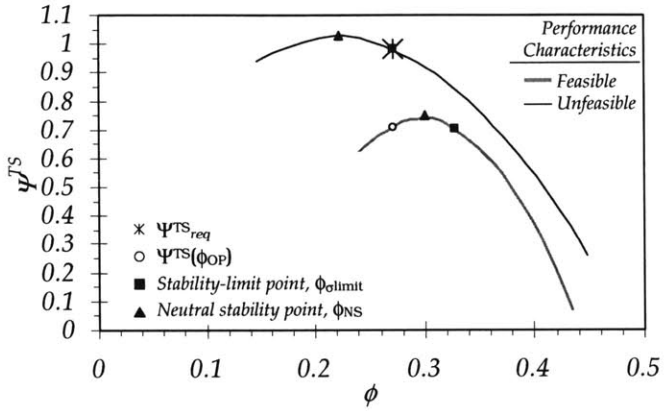

Figure 4-9 Loading check for feasible 2-stage compressor

The critical eigenvalue path around neutral stability shows that the rotation rate of the least stable system mode is smaller than the one of the previous design, as depicted by Figure 4-10. For the same disturbance amplification safety-factor Q, the growth rate of the critical eigenvalue must be around two thirds of its rotation rate. Hence, a smaller value of σ is required to satisfy the stability constraint and the design mass flow can be closer to the peak performance. The σ-limit is found to be –0.184.

The rate at which the eigenvalue or the *DEB* approach neutral stability is clearly smaller for the feasible design (see Figure 4-11). Geometrically, this is translated into a smaller curvature of the characteristic, which is patent from the comparative plot above. The non-dimensional dynamic history at zero-stability is shallower than on the first compressor. Thus, the Equivalent Curvature relation for the new σ-limit predicts a stable flow range that places the stability constraint exactly on the design operating flow rate.

As far as the robustness margin is concerned, it must be pointed out that the curvature at neutral stability is smaller than on the previous design. Because the σ-limit is also lower than before, it follows that the equivalent curvature at design must have been reduced, too.

The linear expansion does predict an equivalent operating curvature $K_{e,OP}$ that is 70% smaller than that of the first design. This, combined with a slower rotation rate, necessarily implies an improved robustness. Indeed, the amplification sensitivity has been reduced to 10, the prescribed margin for $\partial Q/\partial\phi$.

Having satisfied all three constraints exactly, the optimisation cost of the design is zero and the process is terminated.

$$C = C_{\Psi} + C_{Q} + C_{Ke} = 0$$

Benchmarking of the optimised design with a complete dynamic analysis, like the one hereby presented, should always be carried out. Approximation inaccuracies are inevitable due to the use of the standard relations to predict range and sensitivity, as well as the variation of the rotation frequency away from neutral stability.

For this particular compressor, careful inspection of the actual σ-history reveals that the K_e relation under-predicts the range by 6.1%, which makes the design point slightly less stable than required.

Similarly, the equivalent curvature at design, calculated through the linear expansion, is 4.1% smaller than in reality, whereas the rotation rate at the operating mass flow is 4%higher than around neutral stability. These errors produce counteracting variations in Q-factor sensitivity, which is found to be 2.64% higher than the predicted value.

	Predicted from standard relations	*Computed values from pre-stall dynamics*
Ψ_{TS}	0.9801	0.9801
Q	1.1	1.1671
$\partial Q/\partial\phi$	10	10.264

Table 4-3 Predicted and computed performance values for optimised solution

If necessary, these discrepancies can be ironed out by final, small design variations based on the *DEB* power distribution along the different blade-rows. The use of this localised information for this purpose, and also for systematic decision-making within the optimisation process, is discussed in section 4.4.

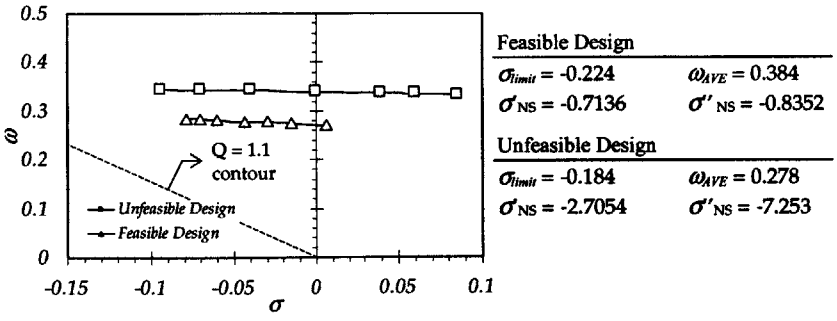

Figure 4-10 Comparison of eigenvalue migration paths

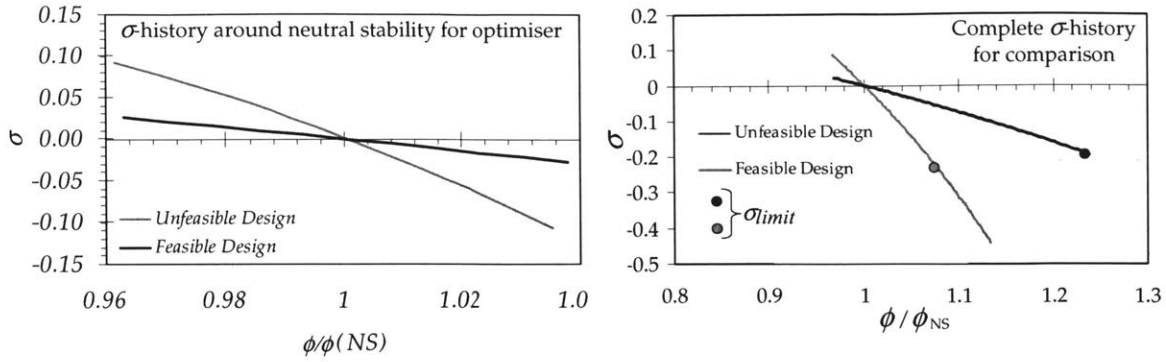

Figure 4-11 Reduced and complete dynamic history for the 2-stage compressor before and after optimisation

4.3.3 Effects of Individual Changes in Intermediate Iterations

A full parametric study of the changes in design feasibility with different variables is beyond the time constraints and scope of this thesis. First of all, the unified Equivalent Curvature relation is not available for any arbitrary Q-limit, as the extension to cover the entire domain is a consuming task. Secondly, the large dimensionality of this multi-variable optimisation means that the effects are highly coupled, and therefore generalisations cannot be made without an extensive battery of design explorations. The example shown here simply proves that the integrated algorithm can be applied successfully, with high savings in computation time.

Despite these limitations, it is interesting to comment on the evolution of the design point, as the modifications of the baseline configuration are implemented one at a time. Figure 4-12 shows a summary of the convergence history.

- Iteration 2 - Lower loss buckets to 1x standard level

  The reduction in loss buckets for all blade-rows shifts the performance up towards the required pressure ratio. The resulting characteristic actually produces the necessary pressure ratio at the desired flow rate. The limit-stability flow is about 6% higher than the design value, but the less aggressive dynamic history – due to the shallower loss buckets – brings the Q-factor sensitivity down to only 15% above the robustness limit.

- Iteration 3 – Rotor 1&2 chords reduced from 16.4% to 12.3% of the mean radius

  The re-dimensioning of the blades does not produce variations in aerodynamic performance in the simplified mean line solver. In reality, the reduced surface would lead to smaller profile losses and the lower solidity would have an impact on the flow turning achieved through the blade-row.

The stability benefits due to the lower disturbance rotation rate, discussed in 4.3.3, contribute to an improved Q-factor at design, but still above the required level. The actual σ improvement is unknown, because the dynamics are not solved for at the design point. The robustness is practically the same as before.

- Iteration 4 – Inter-stage gap reduced from 5% to 1% of the mean radius

  The stabilising effect described in 2.5.3.2 is exploited to achieve the last improvement in dynamic stability. The rotation rate is unaffected with respect to the previous iteration, and the eigenvalue growth rate σ at a fixed flow is increased, reaching the required value at a flow coefficient that is 4% lower than in the previous iteration. The equivalent curvature of the characteristic is reduced enough to decrease the Q-factor sensitivity, indicative of the dynamic robustness, to the prescribed margin.

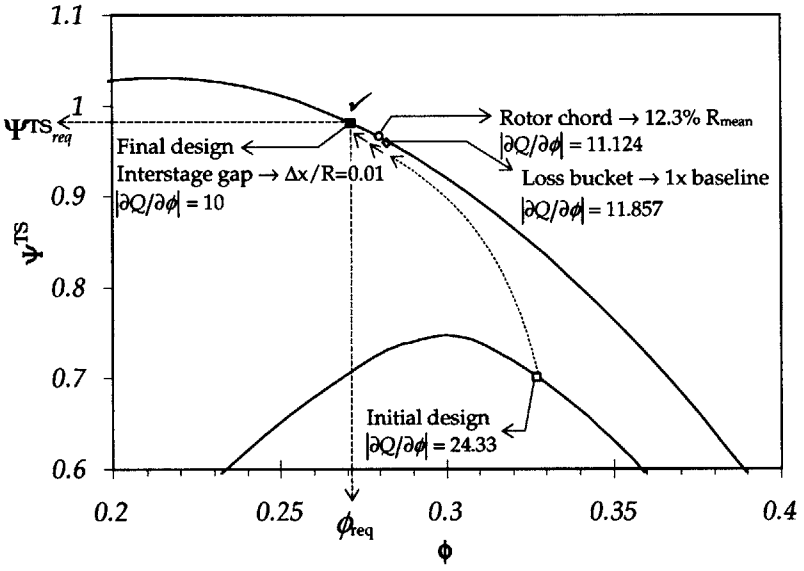

Figure 4-12 Evolution of limit-stability point for successive optimisation steps

As the optimiser progresses towards the converged solution, the loading becomes more aggressive for the same level of dynamic safety. The change in loss buckets has the largest effect in this area, leading to almost a 50% improvement in loading. The rest of the changes do not affect the performance characteristic, but enable safe operation closer to the peak, yielding an additional increase in loading of about 4% from the second to the final iteration.

4.4 Use of DE power distribution within the integrated scheme

In demonstrating the integrated optimisation process, it appears that the disturbance-energy balance concept has lost all relevance, as the entire design can be assessed by examination of the eigenvalue history only. The additional expense of carrying out the *DE* control-volume analysis seems unjustified on this basis. As was said before, though, this only happens if the dynamics of the system are governed by one single critical resonance mode, all others being markedly more damped. When this assumption does not apply, or compressible acoustic mode become dominant, *DEB* is the only quantity that encapsulates the dynamic state of the system in a single number.

In addition, the disturbance-energy power distribution is also the only metric that allows one to identify the blade-rows that introduce more disturbance-kinetic energy into the system. When iterating over a multi-stage configuration with tens of degrees of freedom, this information can be used as an expedient way to direct design changes to the blade-rows with the highest *DE* power. The refinement of the sample optimised solution presented in 4.3.2 is carried out following this criterion, a technique that was already explored in Fréchette [4], along with a systematic examination of the *DE* redistribution in a multi-stage environment when localised design modifications are applied.

The *DE*-Power distribution at the required operating point (see Figure 4-13 [a]) shows all blade-rows acting as *DE* sinks, rotor-two being the weakest. One could erroneously identify this blade-row as the stability-critical one. However, it is the power distribution at neutral stability that must be used to decide which blade-row to act upon (see Figure 4-13[b]), because this gives the true contribution of each blade-row to the pre-stall dynamics. Indeed, it reveals that the second rotor is the least sensitive to flow changes and that, as the machine enters the unstable regime, rotors and stators act as disturbance sinks and sources, respectively. The second stator is the largest contributor towards the instability of the system.

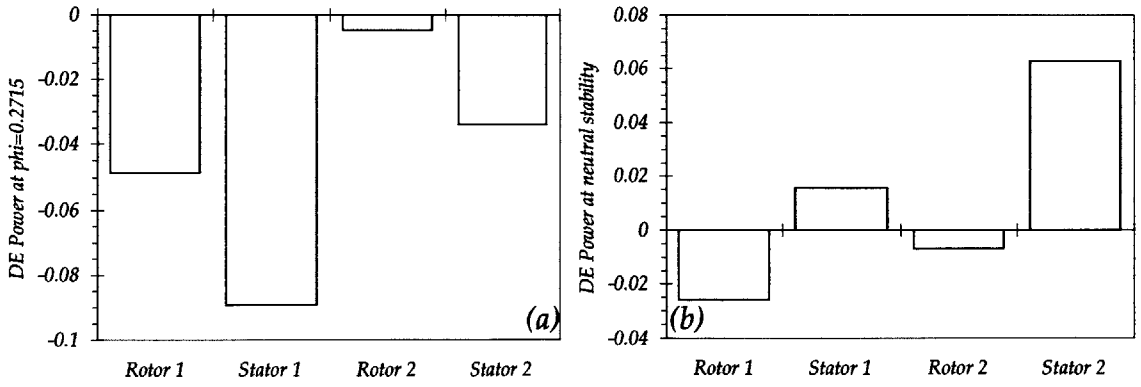

Figure 4-13 Disturbance-energy power distribution for unrefined solution at design and neutral stability mass flow

In order to demonstrate that modifications to second stator lead to the most pronounced dynamic benefit, the loss bucket of each blade-row in the compressor is reduced by 15% in turn, leaving the others unaltered.

The performance characteristics of the initial optimiser solution and the four individual enhancements are compared in Figure 4-14. The additional pressure ratio is more marked when improving the stators' loss buckets. This can be attributed to their higher inlet flow incidences, which are 3.5 and 4 degrees higher than those of their respective rotor.

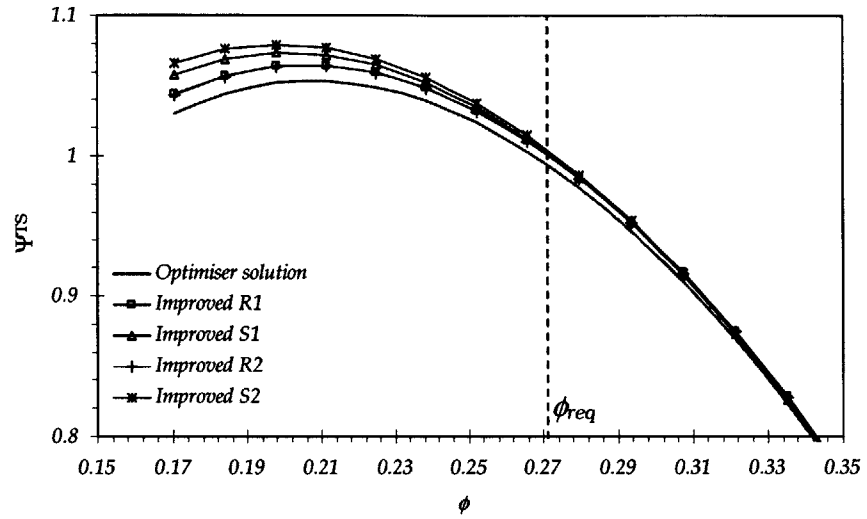

Figure 4-14 Performance variation for individual blade-row enhancements from initial optimiser solution

In terms of pre-stall dynamics, the improved loss characteristics lead to a negligible variation in disturbance rotation rate, of 0.7% in average. Therefore, any improvement in critical eigenvalue growth rate at the design flow results in a reduction of resonant disturbance amplification, Q. The dynamic evolution for each variant shows that the second stator, as conjectured, has the highest shift in σ(see Figure 4-15).

At the same time, the flow coefficient at neutral stability is reduced practically linearly with the improvement in critical eigenvalue growth rate. As a result, the location of the design point on the non-dimensional stability history is higher in the ϕ/ϕ_{NS} axis, which would deteriorate the robustness, if the equivalent curvature $\partial\sigma/\partial\tilde{\phi}$ did not change. However, the non-dimensional σ-traces also become shallower for the improved-stator 1 & 2 variants (see Figure 4-16). In conclusion, the robustness is also most greatly enhanced by modification of stator two.

The relative improvements are more clearly pictured in Figure 4-17. The increased dynamic stability and robustness bear a direct relationship with the highest *DE* powers. This demonstrates that it is essential to use *DE* information to apply modifications to new iterations in the design process.

The resulting power distribution with an improved second stator (Figure 4-18) registers a 160% growth in sink power for this blade-row at design, while the others experience relatively minor changes. At neutral stability, the blade-row only has about a quarter of its initial source intensity. The peak in instability contribution is shifted to stator one, previously the second most powerful blade-row, tripling its initial power.

The re-distribution of disturbance-energy after a particular design change is adopted was attempted by Fréchette [4] through a preliminary dissection of the impact of various design modifications on the *DE* power map.

The *DE* power of a blade-row depends on both the mean flow and the perturbation flow field. In that sense, alterations that modify the background flow impact the *DE* powers of all the downstream blade-rows. On the other hand, the variations in potential perturbation waves are felt throughout the system, whereas vortical changes in the disturbance field are convected downstream only. The systematic prediction of the *DE* power redistribution is therefore a highly coupled problem, which lies beyond the scope and time constraints of this thesis.

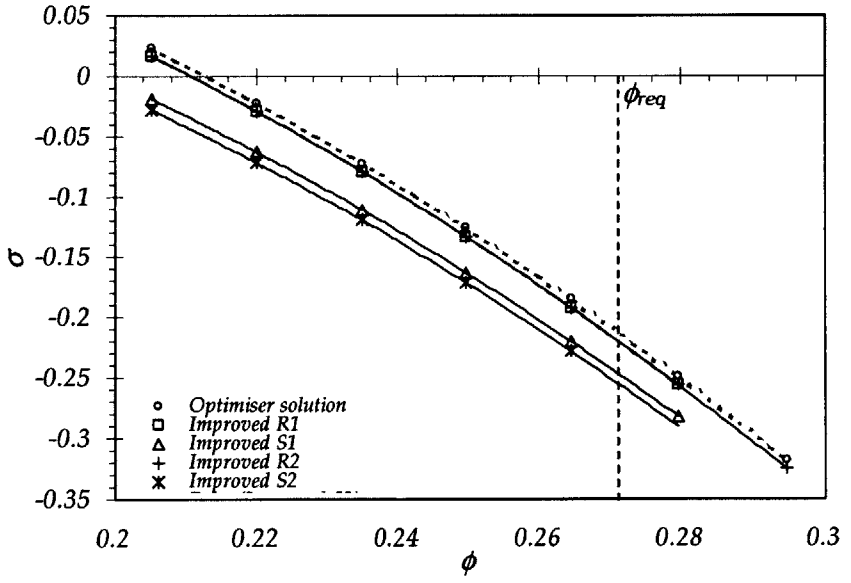

Figure 4-15 Dimensional σ-histories for individual blade-row enhancements from initial optimiser solution

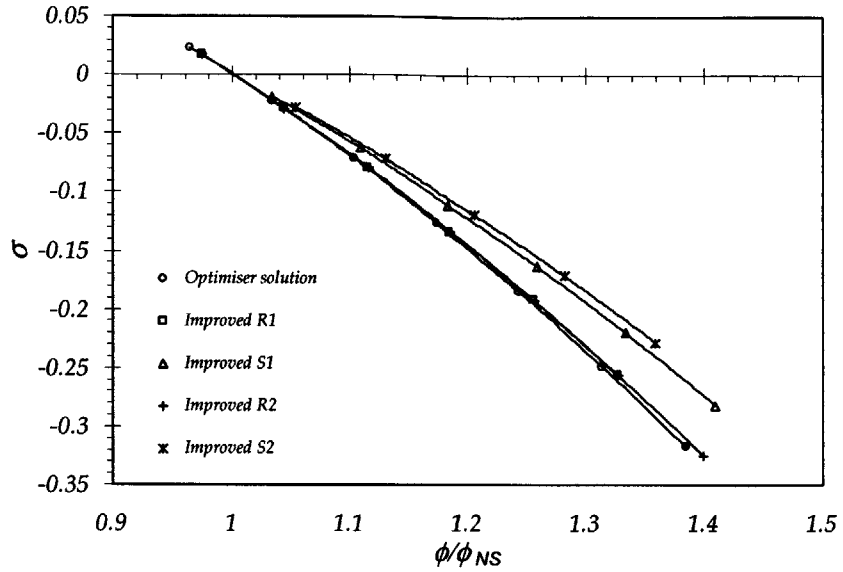

Figure 4-16 Non-dimensional σ-histories for individual blade-row enhancements from initial optimiser solution

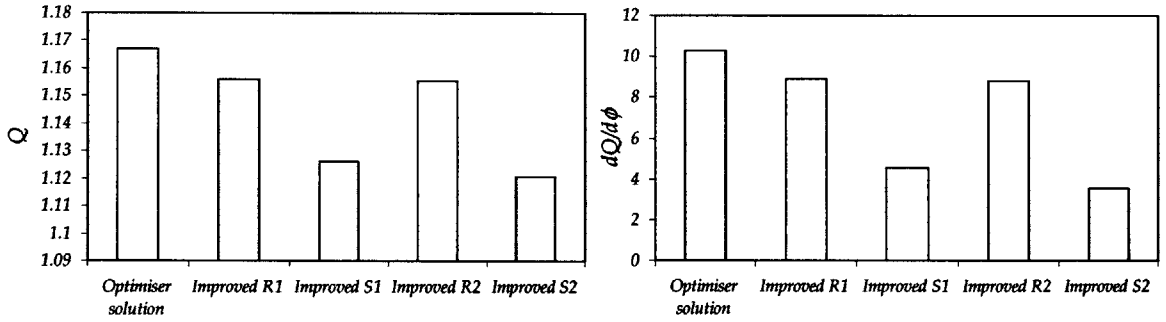

Figure 4-17 Dynamic stability and robustness for individual blade-row enhancements from initial optimiser solution

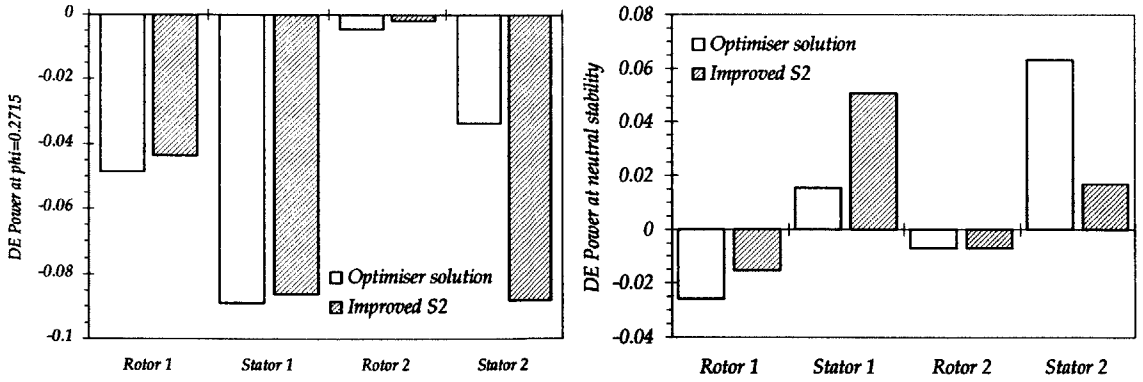

Figure 4-18 Comparison of DE-power distributions between initial optimiser solution and enhanced stator 2 configuration

4.5 Summary

A new philosophy that departs from the traditional compressor design methods applied in industry has been developed and demonstrated in this Chapter.

- In aid of physical clarity, the unified framework relating the stable flow range, dynamic stability and robustness metrics under the Equivalent Curvature relation, devised in Chapter 3, has been re-formulated in a more user-friendly manner.
- Based on this, a cost function has been defined that captures the compliance of a candidate design with the loading, stability and robustness requirements. The use of the standard relations to evaluate each cost term has been delineated.
- The methodology has been successfully implemented in the preliminary design of a 2-stage compressor, for which the full pre-stall dynamics have been calculated in order to quantify the errors introduced by use of the standard relations to find the stable flow range and equivalent curvature at the operating point. For the sample successful design iteration, the Q-factor and the robustness $\partial Q/\partial \phi$ are under-predicted by 6.1% and 2.64%, respectively, well within the incompressible uncertainty bands of the Equivalent Curvature framework, defined in Chapter 3.
- Design modifications on particular blade-rows should be implemented on those possessing the highest *DE* power. It has been shown that such strategy yields the highest improvements in all three cost criteria – performance, stability and robustness.

In terms of design guidelines, the dynamic effects due to the resizing of the inter-blade-row gaps pointed out in Chapter 2 have been exploited in the present design exercise. Apart from the obvious performance and dynamic benefits of lower-magnitude, shallower loss buckets, one important divergence with the recommendations issued by Blanvillain [1] concerns the impact of blade-row inertia on the system stability. While it is true that the critical growth rate of the disturbances is not greatly modified, their rotation rate is appreciably reduced, at least in compressors with few stages. Together with the Q-factor analogy, this implies an improvement in dynamic stability for operation at a fixed flow condition.

The computational savings of this new methodology have been clearly emphasised throughout the discussion; resolving the dynamic history at the design point is no longer necessary to assess the degree of stability. The scheme, however, also has some limitations, namely:

- Operation is restricted to low-speed, incompressible flow conditions.

- Even within the required relative Mach numbers, the use of the Equivalent Curvature relation to find the stable flow range, and the linear prediction of K_e at the operating point introduces errors in the estimation of compressor stability and robustness. A full computation of the dynamic characteristics of the converged solution is suggested.
- A faster progression through the design space towards the final solution is achieved by using the *DE* powers to systematically apply modifications to particular blade-rows. However, one cannot predict the redistribution of disturbance-energy for the following iteration *a priori*.

Chapter 5

Conclusions and Future Work

5.1 Summary and conclusions

Each chapter in this thesis addresses a distinct aspect in the sequence towards the final optimisation problem. Concluding remarks concerning each of these stepping-stones are therefore summed up separately.

5.1.1 Application of the Disturbance-Energy Analysis within the Existing Dynamic compressor model Framework

The methods development task undergone in Chapter 2 is geared to the successful implementation of Fréchette's [4] *DE* control-volume scheme within Spakovszky's [12] dynamic compressor model. The required analytical and numerical techniques are put in place to achieve this, highlighting the key issues related to flow field mapping resolution and computational costs. With respect to the latter, two issues should be pointed out:

- Blanvillain [1] previously identified a system, lightly damped eigenvalue as being critical to machine stability. The first harmonic of this mode is the pole with which to evaluate the compressor's disturbance-energy balance.
- The available search algorithms are only computationally efficient as long as the critical eigenvalue growth rate is below 15% of the rotor frequency, i.e. in the immediate vicinity of the neutral stability condition. Under this condition, the solution to the dynamic eigenvalue problem can be reached in a timescale of seconds, for one-stage machines, or a few minutes, for multi-stage configurations. Solution for higher damping levels entails the re-location of the initial guess for the eigenvalue, which requires user insight and therefore is not attractive for a large-scale, automated multi-objective optimisation. The

need for reliable methods relating the cheap, low-damping information to stability metrics at design is patent.

The full pre-stall dynamic analysis is successfully benchmarked against Fréchette's [4] results for the Moore-Greitzer compressor [10] and Blanvillain's studies on the effects of gap sizing on the stability characteristics [1].

- The critical eigenvalue growth rate σ and *DEB* predict the onset of instability analogously. However, because of the integral nature of the energy-based metric, its magnitude is found to be size-dependent and therefore not as general as the eigenvalue to depict the overall dynamic state of the compressor. However, the *DE* powers are an integral tool to determine the contributions of each individual blade-row to the overall system stability.
- As pointed out by Blanvillain [1], increasing the intra-stage gap size results in enhanced stability. A maximum improvement in system damping of 6% for the standard 2-stage configuration has been achieved for an extension of $\Delta x/R$ = 8% for gaps 2 and 4. This is achieved through a uniform reduction in *DE* powers: sources are seen to diminish in strength, whereas sinks become stronger.
- Conversely, elongation of inter-stage gaps leads to a deterioration in stability. For the same 2-stage machine, a peak penalty in critical eigenvalue growth rate is incurred with a gap length of $\Delta x/R$ = 16%. In this case, the adjacent blade-rows concentrate the dynamic improvement in the form of reduced *DE* powers, while the other two register power increases.

5.1.2 Stability and Robustness Metrics Definition and Standard Relations for their Assessment

After a review of the shortcomings of the present surge-margin paradigm, a more physically relevant description of the compression system dynamics is formulated:

- The sensitivity of the dynamics, measured through either σ or *DEB* is shown to be an indicator of the Equivalent Curvature K_e of the performance characteristic. A general relation is uncovered that predicts the stable flow range to a certain degree of dynamic stability based only on K_e. This applies as long as operation is within the incompressible capabilities of the available dynamic compressor model (M_{rel} < 0.3), and represents an indirect method to assess the stability at any flow condition based on the economical, low-damping information that can be easily obtained through Spakovszky's dynamic compressor model.

- The complete set of relations for the different stability levels have been brought together in the unified Equivalent Curvature map, which embodies all of the above concepts by linking the stable flow range, dynamic stability and robustness under a common framework.

With a view to applying this information to practical designs, new dynamics-based metrics to determine the degree of dynamic stability and its robustness to flow changes are developed.

- The concept of resonant disturbance amplification under aerodynamic forcing, Q, is exploited as an absolute stability metric. Through this concept, the dynamic stability is linked to *both* the growth and the rotation rates of the critical eigenvalue. In synthesis, if σ and ω are roughly equal, the quality factor Q is about unity, i.e. no amplification of disturbances exists beyond their static values. A safety limit of $Q \leq 1.1$ is suggested as a suitable margin; in this case, the critical eigenvalue growth rate σ needs to be around two thirds of its rotation rate ω and of the opposite sign.
- The sensitivity of the disturbance amplification to flow changes is the logical measure of dynamic robustness, for which a limit of $\partial Q/\partial \phi \leq 10$ can be postulated. Although the point at which the compressor stalls, the safety factor Q and the disturbance rotation rate all influence the robustness, this sensitivity is largely governed by the equivalent curvature of the characteristic at the operating point, $K_{e,OP}$.

5.1.3 Integrated Design Optimisation Scheme for Stability

A systematic roadmap for the combined evaluation of aerodynamic and stability-related performance within a multi-objective optimisation has been devised and demonstrated on a sample 2-stage compressor.

- The cost function to minimise is defined as:

$$C = C_{\Psi} + C_{Q} + C_{Ke} = \left(\frac{\Delta\Psi}{\overline{\Psi}^{TS}}\right)^2 + \left(\frac{\Delta\phi}{\overline{\phi}}\right)^2 + \left(\frac{\Delta K_e}{\overline{K}_e}\right)^2$$

The loading is evaluated at the required operating flow. The stability compliance is ascertained indirectly, by determining the stable flow range to the required damping limit at which the amplification margin is reached through Equivalent Curvature measurements at neutral stability. The required K_e for sufficient dynamic robustness is then computed at that location.

- The full optimisation is carried out, at first, only with the aid of the standard relations. Comparison of this with the actual system dynamics at design reveals that the converged solution has a 6.1% error in disturbance amplification and a 2.64% error in robustness. These are due to the uncertainty band in the Equivalent Curvature relation and the assumption that K_e varies linearly along the characteristic.
- Blanvillain [1] stated that changing blade-row inertias had no appreciable dynamic benefit in terms of critical eigenvalue growth rate. While that is true, a reduction in inertia leads to a lower rotation rate, so the true dynamic state of the machine *is* affected even if σ remains the same, since the disturbance amplification Q is effectively reduced.
- The disturbance-energy map is essential to speed up the optimisation process, directing design modifications to the blade-rows with higher *DE* power. It has been proved that there exists a direct correlation between the relative powers of the different blade-rows and the resulting improvements in both stability and robustness as each of them is enhanced in turn.

5.2 Recommendations for future work

The limitations of the design framework developed hereby have been highlighted throughout the thesis, and make patent the need for further developments on both the conceptual and implementation sides.

5.2.1 Dynamic compressor model Refinements towards the Application of the *DEB* to a Wider Range of Dynamic Systems and Operating Conditions

Three important lines of work should be initiated to mitigate the key deficiencies of the disturbance-energy analysis in the form that has been used so far:

- A thorough application of the *DEB* scheme should encompass the contributions to the disturbance flow field of more than just the stability-critical eigenvalue. A cumulative *DEB* approach should thus be devised.
- Compressibility effects should be incorporated into the dynamic compressor model and the internal-energy contributions to the *DE* balance accounted for in the overall metric of dynamic stability. The physical relevance of the Q-factor analogy in these instances should be reviewed.
- A systematic analysis of the behaviour of the perturbation modeshapes when design changes are effectuated in an initial compressor configuration should be carried out. This should evolve into a predictive capability to foresee the re-distribution of disturbance-energy powers throughout the design process.

5.2.2 Extensions to the Equivalent Curvature Relation

The modelling enhancements described in the previous section should be employed in the refinement of the equivalent curvature relation. In particular, the contribution of the acoustic-like compressibility modes to the equivalent curvature should be explored, with a view to potentially bring the range prediction error of the presently scattered, high-speed compressors within the incompressible bounds.

In parallel, thorough parametric studies should be conducted to quantify the inaccuracies in range prediction due to the design features that *can* be captured by the dynamic compressor model, such as, for example, gap length. Physical understanding of the deviations introduced by these parameters could be used to potentially define correction factors or correlations to apply to the basic relation.

5.2.3 Integrated Design Optimisation for Enhanced Stability

The above improvements should be brought together within the integrated scheme described in Chapter 4. It is expected that the errors introduced by the evaluation of the dynamic stability and robustness objectives will decay as the new modelling additions are implemented, thus minimising the need for expensive benchmarking of the optimiser solutions with true dynamic histories.

The understanding of the *DE* re-distribution due to design variations should be embedded in the optimisation architecture, to guide the convergence path more efficiently.

Most importantly, the methodological insights developed by Perrot [11], principally those regarding the use of state-of-the-art multi-variable optimisation methods and the use of profile alterations to engineer precise aerodynamic characteristics, should be merged with the framework derived in this thesis.

In so doing, the inner optimisation loop of the integrated design philosophy (see Figure 1-1) envisioned at the start of the Joint Project shall be completed, hopefully revolutionising the field of axial compressor design for enhanced stability in the not-too-distant future.

Appendix A

Analytical Derivation of the Disturbance-Energy Conservation Law

A.1 Conservation law for Disturbance-Energy

Fréchette [4] used an analogy with analytical acoustic theory to derive a Reynolds Transport Equation for an energy-like quantity representing both the extra internal and kinetic energy due to perturbation velocities and pressure. As well as the formal identification of disturbance-energy, the derivation also presents the form of its 'power sources' and fluxes.

We shall concern ourselves with 2-D, inviscid, incompressible flow fields. Unsteadiness is accounted for by suitable linearisation of the governing equations.

To that effect, small perturbations of physical quantities are taken about their average values, i.e. $\phi(x,t)=\bar{\phi}+\delta\phi(x,t)$. The mean flow quantities, calculated via the mean line solver described in section 2.4.1, are assumed to be steady ($\partial\bar{\phi}/\partial t=0$) and spatially invariant ($\partial\bar{\phi}/\partial\theta=0$ & $\partial\bar{\phi}/\partial z=0$).

The steps leading to the linearised form are shown in detail for the continuity equation for illustrative purposes.

$$\frac{\partial\rho}{\partial t}+\bar{V}\cdot\nabla\rho=0 \qquad (A.1)$$

This can be rewritten as

$$\frac{\partial\rho}{\partial t}+\nabla\left(\rho\bar{V}\right)-\rho\cdot\nabla\bar{V}=0 \qquad (A.2)$$

For incompressible flow ($\nabla\bar{V}=0$), this reduces to

$$\frac{\partial\rho}{\partial t}+\nabla\left(\rho\bar{V}\right)=0 \qquad (A.3)$$

Applying small-perturbation theory to this expression, one gets

$$\frac{\partial(\bar{\rho}+\delta\rho)}{\partial t}+\cdot\nabla\left[(\bar{\rho}+\delta\rho)\left(\bar{\vec{V}}+\delta\vec{V}\right)\right]=0 \qquad (A.4)$$

After expanding, one can neglect products of perturbations and derivatives of mean flow quantities, obtaining the *Linearised Continuity Equation*

$$\frac{\partial\delta\rho}{\partial t}+\bar{\vec{V}}\cdot\nabla\delta\rho+\bar{\rho}\cdot\nabla\delta\vec{V}=0 \qquad (A.5)$$

The same procedure can be carried out starting from the unsteady Euler equation for momentum and the entropy transport theorem. The final form of the linearised equations is

- *Momentum:* $$\bar{\rho}\frac{\partial\left(\delta\vec{V}\right)}{\partial t}+\bar{\rho}\bar{\vec{V}}\cdot\left[\nabla\cdot\left(\delta\vec{V}\right)\right]=-\nabla(\delta p) \qquad (A.6)$$
- *Entropy Transport:* $$\frac{\partial(\delta s)}{\partial t}+\bar{\vec{V}}\cdot\nabla\cdot(\delta s)=0 \qquad (A.7)$$

Through appropriate combination of the three linearised equations, Fréchette showed that for incompressible flow the quantity $\varepsilon=\rho(\delta V)^2/2$ obeys the following conservation law

$$\frac{\partial\varepsilon}{\partial t}+\nabla\cdot\left(\bar{\mathrm{I}}+\varepsilon\bar{\vec{V}}\right)=0 \qquad (A.8)$$

where: $$\bar{\mathrm{I}}=\delta P\delta\vec{V} \qquad (A.9)$$

If one carries out a similar compressible analysis, *DE* is found to possess an internal-energy-like term of the form $(\delta P)^2/2\overline{\rho a}^2$. However, in the simplified incompressible case, *DE* is simply the additional fluid kinetic energy per unit volume due to the perturbation velocities.

In fact, (A.8) can be rewritten in terms of substantial derivatives, yielding:

$$\frac{\partial\varepsilon}{\partial t}+\nabla\cdot\left(\bar{\mathrm{I}}+\varepsilon\bar{\vec{V}}\right)=\frac{\partial\varepsilon}{\partial t}+\nabla\cdot\left(\varepsilon\bar{\vec{V}}\right)+\nabla\cdot\bar{\mathrm{I}}=\frac{\partial\varepsilon}{\partial t}+\left[\varepsilon\left(\nabla\cdot\bar{\vec{V}}\right)+\bar{\vec{V}}\cdot\nabla\varepsilon\right]+\nabla\cdot\bar{\mathrm{I}}=\frac{\partial\varepsilon}{\partial t}+\bar{\vec{V}}\cdot\nabla\varepsilon+\nabla\cdot\bar{\mathrm{I}}$$

$$\frac{D\varepsilon}{Dt}+\nabla\cdot\bar{\mathrm{I}}=0 \qquad (A.10)$$

The flux term $\bar{\mathrm{I}}$, known as the *Disturbance-Energy Intensity*, represents the time rate of change of disturbance-pressure work per unit area exerted on a given cross-section of the compressor.

A.2 Integral Disturbance-Energy Theorem

In view of an application of the *DE* transport concept in a control-volume analysis, the conservation law is best viewed in integral form over a generic volume *V*.

$$\iiint_V \left(\frac{D\varepsilon}{Dt} + \nabla \cdot \bar{\bar{\mathrm{I}}} \right) dV = \iiint_V \left(\frac{\partial \varepsilon}{\partial t} + \bar{\bar{V}} \cdot \nabla \varepsilon + \nabla \cdot \bar{\bar{\mathrm{I}}} \right) dV = 0 \qquad (A.11)$$

If the boundaries of integration are fixed in time, then the partial time derivative can be taken to apply to the integral as a whole. This immediately returns the standard Reynolds Transport Theorem form

$$\frac{\partial}{\partial t} \iiint_V \varepsilon dV + \iiint_V \left(\bar{\bar{V}} \cdot \nabla \varepsilon + \nabla \cdot \bar{\bar{\mathrm{I}}} \right) dV = 0 \qquad (A.12a)$$

Use of Gauss's divergence theorem, recalling again the zero volumetric strain for incompressible flow, yields the equivalent expression

$$\frac{\partial}{\partial t} \iiint_V \varepsilon dV + \iiint_V \left(\nabla \cdot \left(\varepsilon \bar{\bar{V}} \right) + \nabla \cdot \bar{\bar{\mathrm{I}}} \right) dV = \frac{\partial}{\partial t} \iiint_{CV} \varepsilon dV + \oiint_{CV} \left(\varepsilon \bar{\bar{V}} + \bar{\bar{\mathrm{I}}} \right) \cdot \vec{n} dA = 0 \qquad (A.12b)$$

Further caveats related to the physical interpretation of this expression, together with its conceptual implementation in a control-volume form are given in 2.3.2.

Appendix B

Analytical Evaluation of the Terms Contributing to the DE Balance

B.1 Fluxes

The annulus integration of the *DE* flux can be split into the disturbance-pressure work on the surface and the disturbance-kinetic energy entering the control volume through the boundary of interest. Both can be solved analytically for any axial location. Thus,

$$\mathcal{F} = \mathcal{F}_P + \mathcal{F}_{KE} = \iint_A \delta P \delta V_x dA + \iint_A \rho \frac{(\delta V)^2}{2} V_x dA \tag{B.1}$$

The local magnitude and phase of the perturbations is known from previous calculation of the modeshapes. The circumferential variation of any of the perturbation variables is simply a sinusoid of n lobes and corresponding angular phase.

Thus, we can express the disturbance velocities and pressure as

$$\delta V_x(\theta)\big|_{x1} = |\delta V_x|_{x1} \sin(n\theta - \varphi_{Vx}) \tag{B.2}$$

$$\delta V_\theta(\theta)\big|_{x1} = |\delta V_\theta|_{x1} \sin(n\theta - \varphi_{V\theta}) \tag{B.3}$$

$$\delta P(\theta)\big|_{x1} = |\delta P|_{x1} \sin(n\theta - \varphi_P) \tag{B.4}$$

Substituting for these perturbations and recalling the definition of the elemental annular area, the pressure-work flux term can therefore be rewritten as

$$\mathcal{F}_P = \int_0^{2\pi} |\delta P| \sin(n\theta - \varphi_P) |\delta V_x| \sin(n\theta - \varphi_{Vx}) \left(\frac{R_{ext}^{\,2} - R_{\text{int}}^{\,2}}{2} \right) d\theta =$$

$$= \left(\frac{R_{ext}^{\,2} - R_{\text{int}}^{\,2}}{2} \right) |\delta P| |\delta V_x| \int_0^{2\pi} (\sin n\theta \underbrace{\cos \varphi_P}_{a} - \underbrace{\sin \varphi_P}_{b} \cos n\theta)(\sin n\theta \underbrace{\cos \varphi_{Vx}}_{c} - \underbrace{\sin \varphi_{Vx}}_{d} \cos n\theta) d\theta \tag{B.5}$$

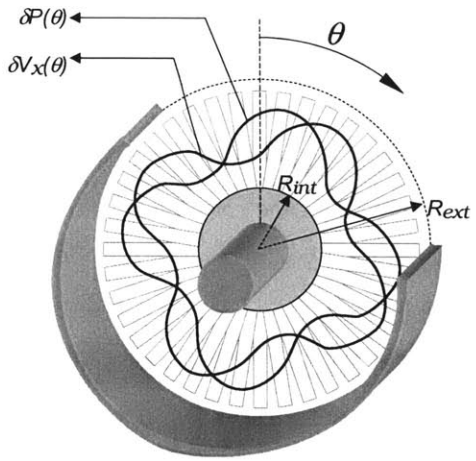

Figure B-1 Flux integration schematic

Expanding,

$$\mathcal{F}_P = \left(\frac{R_{ext}^{\,2} - R_{\text{int}}^{\,2}}{2}\right)\|\delta P\|\delta V_x\|\Big[\underbrace{ac\int_0^{2\pi}\sin^2 n\theta d\theta}_{\pi} - \underbrace{(ad+bc)\int_0^{2\pi}\sin n\theta\cos n\theta d\theta}_{0} + \underbrace{bd\int_0^{2\pi}\cos^2 n\theta d\theta}_{\pi}\Big] \qquad (B.6)$$

So finally the integral can be expressed only as an algebraic expression of the area and the perturbations' magnitudes and phases.

$$\mathcal{F}_P = \pi\left(\frac{R_{ext}^{\,2} - R_{\text{int}}^{\,2}}{2}\right)\|\delta P\|\delta V_x|(\cos\varphi_P\cos\varphi_{Vx} + \sin\varphi_P\sin\varphi_{Vx}) = \frac{A}{2}|\delta P\|\delta V_x|\cos(\varphi_P - \varphi_{Vx}) \qquad (B.7)$$

A similar analysis can be pursued with $\mathcal{F}_{KE}$. In this case, however, $(\delta V)^2$ is always positive, oscillating about a non-zero value. This is physically sensible, as it would not be logical to see kinetic energy taking negative values anywhere in the flow field.

$$\begin{aligned}\mathcal{F}_P &= \iint_A \rho\frac{(\delta V)^2}{2}V_x dA = \frac{\rho V_x}{2}\iint_A(\delta V)^2 dA = \frac{\rho V_x\left(R_{ext}^{\,2} - R_{\text{int}}^{\,2}\right)}{4}\int_0^{2\pi}\left(\delta V_x^{\,2} + \delta V_\theta^{\,2}\right)d\theta = \\ &= \frac{\rho V_x\left(R_{ext}^{\,2} - R_{\text{int}}^{\,2}\right)}{4}\int_0^{2\pi}\left(\left[|\delta V_x|\cos(n\theta - \varphi_{Vx})\right]^2 + \left[|\delta V_\theta|\cos(n\theta - \varphi_{V\theta})\right]^2\right)d\theta \qquad (B.8)\end{aligned}$$

$$\mathcal{F}_P = \frac{\rho V_x A}{4}|\delta V_x|^2|\delta V_\theta|^2$$

The overall expression for the *DE* flux therefore becomes

$$\mathcal{F} = \frac{A}{2}\left(|\delta P\|\delta V_x|\cos(\varphi_P - \varphi_{Vx}) + \frac{\rho V_x}{2}|\delta V_x|^2|\delta V_\theta|^2\right) \qquad (B.9)$$

B.2 Unsteady Term - DEB

The volumetric rate of change of *DE* requires the evaluation of an $\mathcal{F}_{KE}$ – like integral over a continuous axial domain. It has been chosen to carry out this analysis in small control volumina covering the length between any two consecutive intervals within a gap. The other instance in which this quantity must be evaluated arises in the calculation of blade-row powers, but the analysis is exactly the same, except that the control volume is now bounded by the last point in the row's inlet gap and the first point of its exit gap.

The order of integration can be chosen as follows

$$DEB = \frac{\partial}{\partial t}\iiint_V \rho \frac{(\delta V)^2}{2} dV = \frac{1}{2}\iiint_V \rho \frac{\partial (\delta V)^2}{\partial t} dV = \iiint_V \rho \delta V \frac{\partial \delta V}{\partial t} dV = \int_{xin}^{xout} \iint_{A(x)} \rho \delta V \frac{\partial \delta V}{\partial t} dA dx \quad (B.10)$$

The dynamic compressor model is formulated in the frequency domain. Therefore, the time-derivative can be re-expressed in terms of its corresponding Laplace transform, yielding

$$DEB = \mathrm{Re}\left[\int_{xin}^{xout} \iint_{A(x)} \rho(x) \delta V(s,x,\theta) s \delta V(s,x,\theta) dA dx\right] = \mathrm{Re}\left[\int_{xin}^{xout} \iint_{A(x)} \rho(x) s \delta V^2(s,x,\theta) dA dx\right] \quad (B.11)$$

Now, the area integral can be evaluated exactly, so DEB becomes the line integral of a known function in x,

$$DEB = \mathrm{Re}\left[s \int_{xin}^{xout} \rho(x) \iint_{A(x)} (\delta V)^2 dA dx\right] = \mathrm{Re}\left[s \int_{xin}^{xout} \left(\frac{\rho(x) A(x)}{2} |\delta V_x(x)|^2 |\delta V_\theta(x)|^2\right) dx\right] \quad (B.12)$$

The integral is a positive real quantity, so the unsteady term is simply

$$DEB = \frac{\sigma}{2} \int_{xin}^{xout} \mathrm{K}(x) dx \quad (B.13)$$

where

$$\mathrm{K}(x) = \rho(x) A(x) |\delta V_x(x)|^2 |\delta V_\theta(x)|^2 \quad (B.14)$$

The control volume is discretised into three points (inlet, mid-section and exit), at each of which the values of density, radius and perturbation velocities are taken. The modeshapes are only solved for at boundary data points, so linear interpolation is employed to find the intermediate values. While this is accurate enough for an elemental gap volume, in the absence of a blade passage flow model, linear variation of disturbances is also assumed for the calculation of blade powers.

When the control volume is within a gap, the area and density will be constants, because of the discrete nature of the mean line calculation. When dealing with a blade-row, average values will be taken for the mid-point.

This is sufficient for the calculation of $K(x)$ at the three points of interest. A parabola is then fitted through these three points and the integral (B.13) is evaluated analytically.

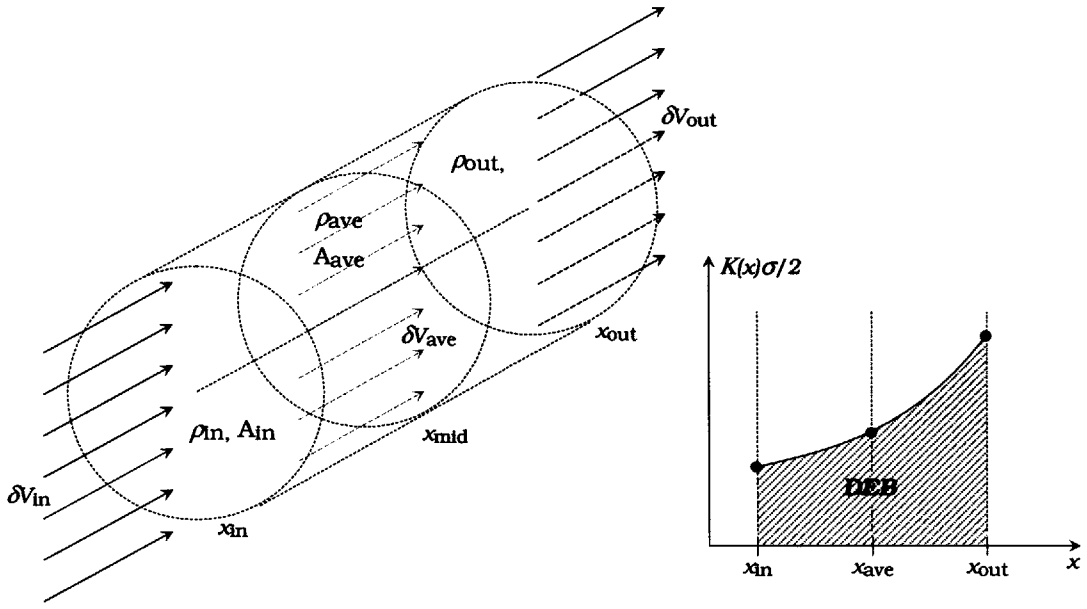

Figure B-2 Unsteady term integration procedure

Appendix C

1-D Mean Line Flow Analysis

This section provides a concise overview of the process followed to resolve the compressor background velocity and pressure fields. The essential iterative scheme for compressible flow matching at the blade-rows is described in detail. The analytical mapping of loss and deviation buckets is dealt with in Appendix C.

C.1 Geometric Model and Input Parameters

The initial information needed to carry out the mean flow analysis consists of:

- Inlet thermodynamic conditions: $P_{o,in}$, $T_{o,in}$
- Operating point mass flow, engine rotational speed and inlet swirl: $\dot{m}$, Ω, α_{in}
- Range of mass flow used to generate the compressor characteristic: $\dot{m}_{\min}$, $\dot{m}_{\max}$
- Number of stages: N_{stages}
- Length of inlet and exit ducts, and inter-blade-row gaps: $L_{g,1},\ldots,L_{g,Ngaps}$
- Average hub and tip radius for each duct/gap: $r_{h,1},\ldots,r_{h,Ngaps}, r_{t,1},\ldots,r_{t,Ngaps}$
- Blade chords, stagger, inlet & exit metal angles: $c_{rot,i}, \gamma_{rot,i}, \beta_{in,rot,i}, \beta_{out,rot,i}, c_{sta,i}, \gamma_{sta,i},\ldots$

A geometric simplification is made in considering all gaps to have constant hub and tip radii. Both ducts and gaps are treated equally in the numbering system; *Gap 1* denotes the inlet duct whereas *Gap (2 Nstages + 1)* refers to the exit duct. A single value for all flow and thermodynamic quantities at the Euler radius is computed for each gap, using the turbomachinery equations and compressible flow theory to bridge the blade-rows separating them.

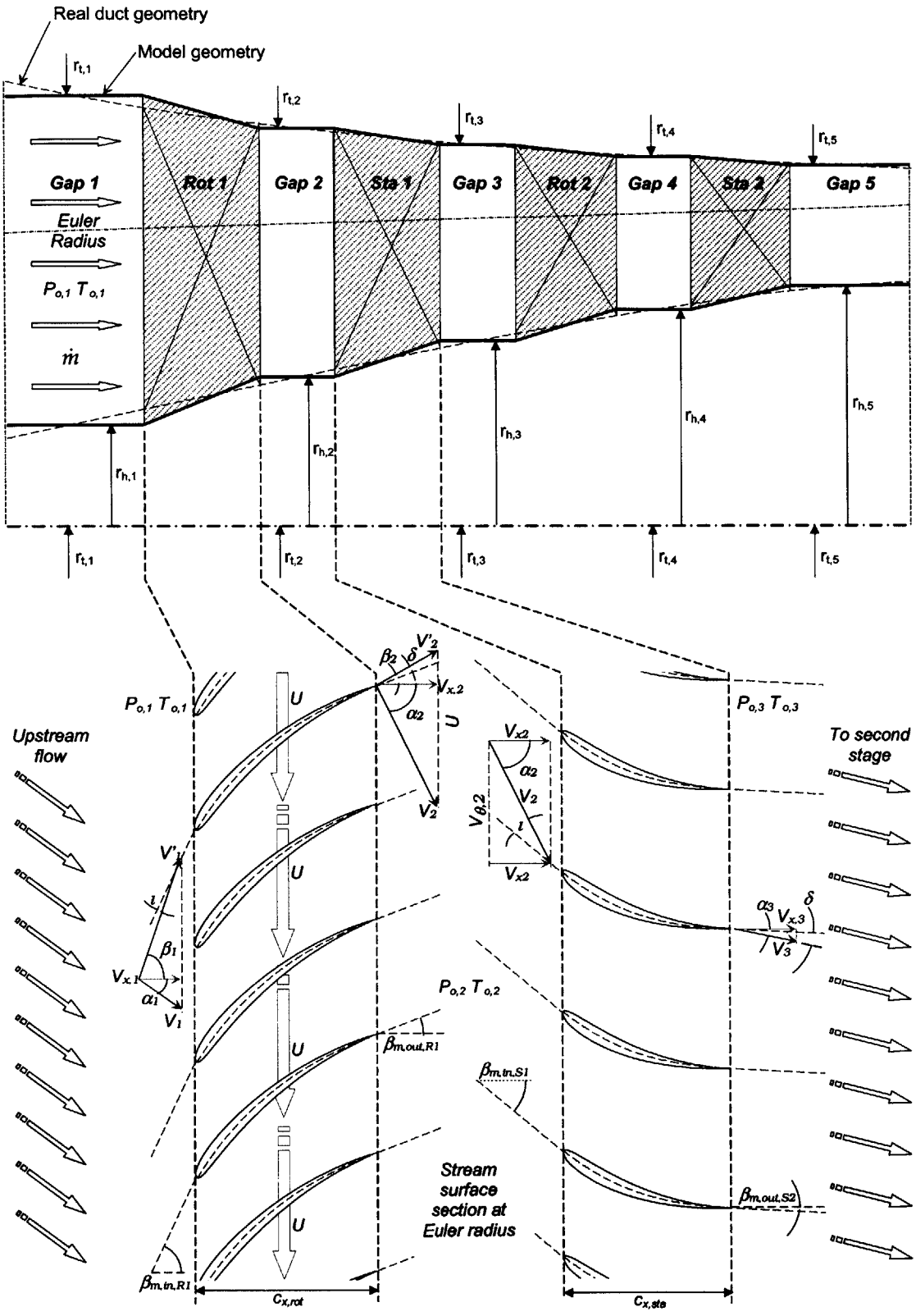

Figure C-1 Mean flow model – nomenclature and definitions

C.2 Flow through a Generic Rotor

The Euler turbomachinery equations are not sufficient to determine the blade exit velocities without an iterative procedure. Density and Mach number vary with each other, and mass conservation at rotor exit must be invoked to close the problem. The combination of density and velocity in any iteration must hold the pre-specified operating mass flow rate, i.e.

$$\dot{m}_i = \rho_i V_{x,i} A_i = \rho_{i+1} V_{x,i+1} A_{i+1} = \dot{m}_{i+1} \tag{C.1}$$

where i is the iteration number.

One can start by postulating an absolute axial velocity at rotor exit. A plausible initial guess is to set the axial velocity equal to its value upstream of the rotor.

$$V_{x,2}^1 = V_{x,1} \tag{C.2}$$

The blade-relative flow exit angle is calculated from the blade metal exit angle and the deviation, due to the boundary layer growth over the profile, and remains constant throughout the convergence history, for a given set of upstream conditions

$$\beta_2 = \beta_{out,rot,1} + \delta_{rot,1} \tag{C.3}$$

An elaborate procedure has been developed to extract δ from a 3D surface capturing changes in both incidence and inlet relative Mach number; this is described in further sections.

Having obtained values for $V_{x,2}^i$ and $\beta_{out,rot,1}$ the absolute tangential velocity at exit arises from straightforward manipulation of the velocity triangles

$$V_{\theta,2}^i = U - V'_{\theta,2} = \Omega \overline{R}_2 - V_{x,2}^i \tan\beta_2 \tag{C.4}$$

The change in absolute tangential velocity across the rotor leads directly to the increase in stagnation temperature through the Euler work equation

$$T_{o,2}^i = T_{o,1} + \frac{U}{c_p}\left(V_{\theta,2}^i - V_{\theta,1}\right) \tag{C.5}$$

From this, one can calculate the ideal total pressure rise by the isentropic flow relations, from which the stagnation pressure loss, ΔP_o, must be deducted. Like the deviation, this is accounted for by an accurate distribution of ΔP_o with incidence and inlet relative Mach number, using the same analytical procedure to map the point on the surface corresponding to the desired operating condition.

$$P_{o,2}^i = P_{o,1}\left(\frac{T_{o,2}^i}{T_{o,1}}\right)^{\frac{\gamma}{\gamma-1}} - \Delta P_{o,rot,1} \tag{C.6}$$

Compressible flow relations enable one to deduce the static pressure, temperature and density at rotor exit as follows,

$$T_2^i = T_{o,2}^i - \frac{V_2^{i2}}{2c_p} \qquad P_2^i = P_{o,2}^i - \left(T_{o,2} - \frac{V_2^{i2}}{2c_p} \right)^{\frac{\gamma}{\gamma-1}} \qquad \rho_2^i = \frac{P_2^i}{RT_2^i} \tag{C.7}$$

The final step in the iteration is to check whether mass conservation at the downstream station is satisfied. A variety of control variables can be selected. As the axial velocity after the rotor is used as the variable of iteration, one can calculate the required value of $V_{x,2}^{req}$ required to enforce continuity.

$$V_{x,2,req}^i = \frac{\dot{m}}{\rho_2^i A_2} \tag{C.8}$$

Typically, one will find that the required value of axial velocity will be different than the initial guess for the iteration step. The starting value for iteration *i+1* can be chosen to be the required velocity at the end of iteration *i*, so that

$$V_{x,2}^{i+1} = V_{x,2,req}^i \tag{C.9}$$

The process can be carried on *ad infinitum*, by simply repeating steps (C.4) through (C.9), until a pre-specified tolerance level has been reached.

C.3 Flow through a Generic Stator

The compressible flow iteration to bridge a stator is exactly the same as that presented above for a generic rotor, with the exception that all velocities involved in the calculation are in the absolute frame and that stagnation temperature remains constant across the blade-row, since no mechanical work is exerted on the fluid and the flow is assumed adiabatic.

$$T_{o,3}^i = T_{o,2} \tag{C.10}$$

Appendix D

Loss and Deviation Models

D.1 Definitions

Because of the exploratory nature of this work, mean flow calculations and dynamic stability analyses have to be performed for a wide range of compressor configurations and operating points. It is envisaged that loss and deviation information corresponding to the machine at hand will be provided by the user in the form of tabulations relating the aforementioned quantities to blade-relative incidence and Mach number.

$$\varpi = \varpi(\iota, M_{in,rel}) \qquad \delta = \delta(\iota, M_{in,rel}) \tag{D.1}$$

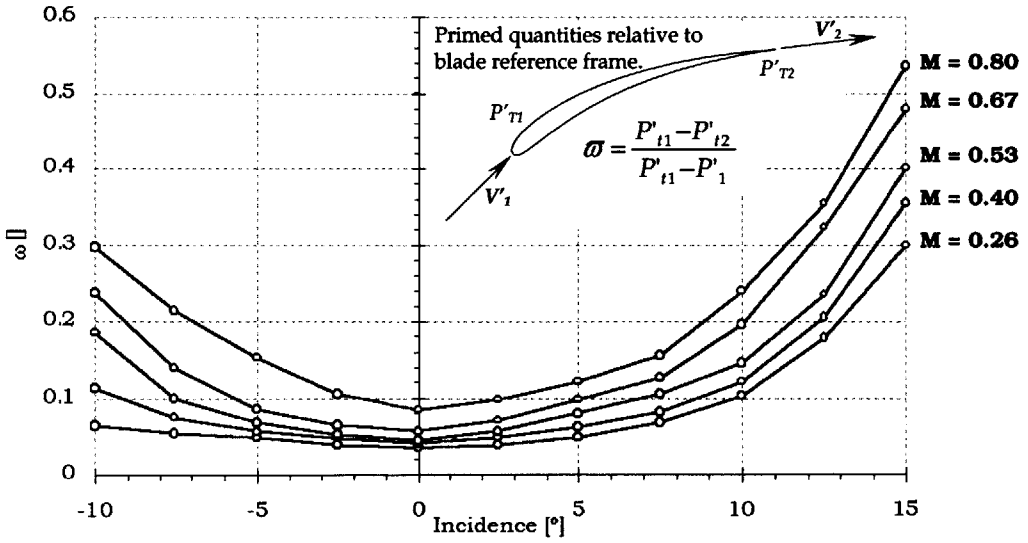

Figure D-1 Sample loss dataset obtained from CFD or empirical tests

The relative stagnation pressure loss suffered by blade-rows can be expressed by the following loss coefficient, where the relative stagnation pressure drop is nondimensionalised by the dynamic head

$$\varpi = \frac{P'_{t1} - P'_{t2}}{P'_{t1} - P'_{1}} \qquad (D.2)$$

In an incompressible simplification, this reduces to

$$\varpi = \frac{P'_{t2} - P'_{t1}}{\frac{1}{2}\rho V'^{2}_{1}} \qquad (D.3)$$

While this is the standard term in which loss information is presented, the description used for the dynamic compressor model involves non-dimensionalisation by the wheelspeed

$$L = \frac{P'_{t2} - P'_{t1}}{\rho U^{2}} \qquad (D.4)$$

D.2 3D Interpolation Technique

It is obvious that only a limited amount of data can be generated by either experimental or computational means. The case for a reliable interpolation technique to any specified flow condition is thus established.

In addition to obtaining the relevant ϖ and δ values, the method should also be capable of delivering the local derivative of the loss with respect to the relative air angle, a necessary variable for the generation of the transmission matrices used in the dynamic compressor model.

One could, in principle, solve for the loss or deviation values in the neighbourhood of each operating point at which a solution is to be found, extracting a functional behaviour applicable to its vicinity. This has two major drawbacks:

- A low number of data points and high noise levels can potentially make a local expansion imprecise.

- For any arbitrary point, the interpolation should be carried out for multiple points in the neighbourhood, in order to determine the loss derivative by, say, finite-difference-type approaches.

It is much more feasible to obtain an analytic expression for each of the two surfaces. A two-variable polynomial can be used to map the surface dataset in a least-square sense. Various numbers

of terms were tried and the final form of the equation permits enough directions of curvature to map typical loss and deviation buckets, while retaining computational efficiency.

$$\varpi = k_0 + k_1 i + k_2 M_{in,rel} + k_3 M_{in,rel} i + k_4 M_{in,rel} i^2 + k_5 {M_{in,rel}}^2 \qquad (D.5)$$

In order to find the values of the coefficients for a given data-set, a least-squares formulation yields

$$\begin{bmatrix} \varpi_1 \\ \varpi_2 \\ \cdots \\ \varpi_n \end{bmatrix} = \begin{bmatrix} 1 & i_1 & M_{in,rel_1} & M_{in,rel_1} i_1 & M_{in,rel_1} {i_1}^2 & {M_{Ri1}}^2 \\ 1 & i_2 & M_{in,rel_2} & M_{in,rel_2} i_2 & M_{in,rel_2} {i_2}^2 & {M_{Ri2}}^2 \\ \cdots & \cdots & \cdots & \cdots & \cdots & \cdots \\ 1 & i_n & M_{in,rel_n} & M_{in,rel_n} i_n & M_{in,rel_n} {i_n}^2 & {M_{Rin}}^2 \end{bmatrix} \cdot \begin{bmatrix} k_0 \\ k_1 \\ k_2 \\ k_3 \\ k_4 \\ k_5 \end{bmatrix} \qquad (D.6)$$

In a more compact form, this can be expressed as

$$\vec{\omega} = [A]\vec{k} \qquad (D.7)$$

The standard procedure for calculation of the coefficients whilst minimising the sum of the magnitudes of the errors at each data-point is as follows,

$$[A]^T \vec{\omega} = [A]^T [A]\vec{k} \quad \Rightarrow \quad \vec{k} = \left([A]^T [A]\right)^{-1} [A]^T \vec{\omega} \qquad (D.8)$$

After application of this method, the analytic topology corresponding to the data and domain presented in Figure D-1 is shown below, from which direct calculation of the loss coefficient and its derivatives at any point is possible.

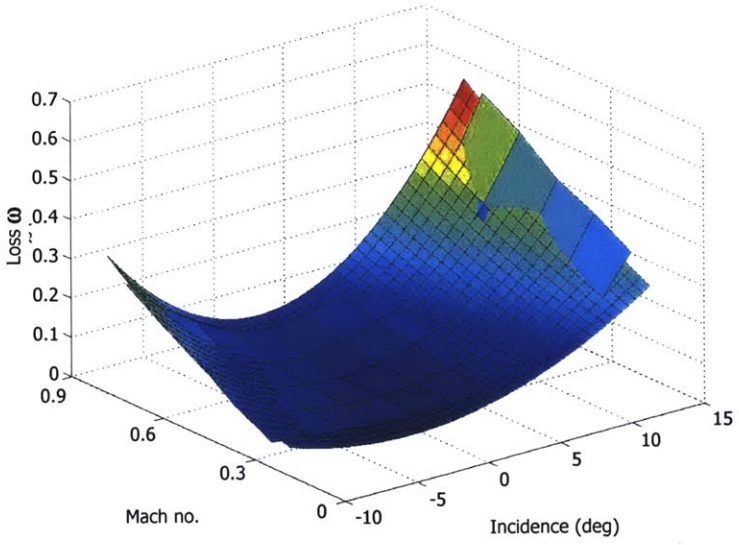

Figure D-2 Analytic surface mapping of experimental/computational data

D.3 Mapping Inaccuracies

The accuracy of the analytic surface fit depends highly on the behaviour of the initial data and its conformance with the curvature possibilities offered by the polynomial. In any case, the resulting surface is always continuous in all derivatives.

The *standard* loss and deviation buckets used for the sample analyses presented in this thesis were specifically chosen to produce low loss levels. The error ranges from –10% to +12.5%, being within ±5% over most of the domain, as seen below.

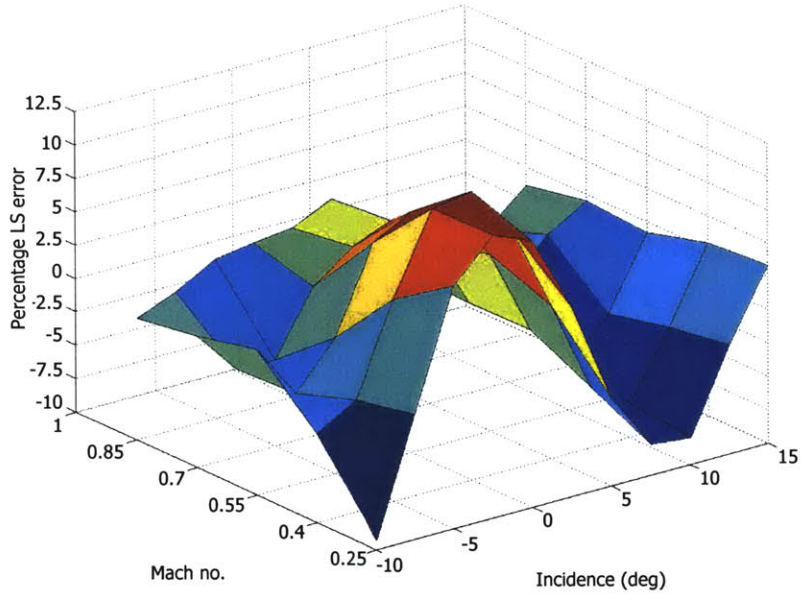

Figure D-3 Least-Squares mapping error for sample experimental data

D.4 Evaluation of Loss Sensitivity from the Analytic Surface

While the two loss-coefficients ϖ and L differ by the non-dimensionalisation parameter, obtaining the loss-sensitivity with respect to the tangent of the inlet angle, $\partial L/\partial \tan\beta_1$, which is necessary for the dynamic analysis, requires further manipulation.

For a start, one can only calculate analytically the slope of the 3D loss surface used in the mean line model, $\partial\varpi/\partial\iota\big|_M$. By virtue of the truncated expansion *(D.5)*,

$$\frac{\partial\varpi}{\partial\iota} = k_1 + k_3 M_{in.rel} + 2k_5 \iota M_{in.rel} \qquad (D.9)$$

It is straightforward, however, to switch to

$$\frac{\partial L}{\partial\iota} = \frac{V'^2_1}{2U^2}\left(\frac{\partial\varpi}{\partial\iota}\right) \qquad (D.10)$$

To reach the required derivative, an expression for $\partial \tan \beta_1 / \partial \iota$ must be devised in view of the application of the chain rule

$$\frac{\partial L}{\partial \tan \beta_1} = \frac{\partial L}{\partial \iota} \frac{\partial \iota}{\partial \tan \beta_1} \tag{D.11}$$

The inlet-relative air angle is simply the sum of the blade metal angle and the flow incidence at the leading edge. Therefore, the tangent of the inlet flow angle can be expressed as

$$\tan \beta_1 = \tan\left(\beta_{in,blade} + \iota\right) = \frac{\tan \iota + \tan \beta_{in,blade}}{1 - \tan \iota \tan \beta_{in,blade}} \tag{D.12}$$

From here, one finds immediately that

$$\frac{\partial \tan \beta_1}{\partial \iota} = \frac{1}{\cos^2 \iota \left(1 - \tan \beta_{in,blade} \tan \iota\right)} + \frac{\tan \beta_{in,blade} \left(\tan \iota + \tan \beta_{in,blade}\right)}{\cos^2 \iota \left(1 - \tan \beta_{in,blade} \tan \iota\right)^2} \tag{D.13}$$

And the loss derivative of interest becomes

$$\frac{\partial L}{\partial \tan \beta_1} = \frac{\frac{V'^2_1}{2U^2}\left(k_1 + k_3 M_{in.rel} + 2k_5 \iota M_{in.rel}\right)}{\frac{1}{\cos^2 \iota \left(1 - \tan \beta_{in,blade} \tan \iota\right)} + \frac{\tan \beta_{in,blade} \left(\tan \iota + \tan \beta_{in,blade}\right)}{\cos^2 \iota \left(1 - \tan \beta_{in,blade} \tan \iota\right)^2}} \tag{D.14}$$

Bibliography

[1] BLANVILLAIN, E. "Dynamic Stability Analysis of a Multi-Stage Axial Compressor with Design Implications". Master's Thesis, Department of Aeronautics and Astronautics, Massachusetts Institute of Technology, Feb. 2003.

[2] CAMP, T., AND DAY, I. "A Study of Spike and Modal Stall Phenomena in a Low-Speed Axial Compressor", in *ASME Turbo Expo, Orlando, FL,* Paper 97-GT-526, June 1997.

[3] CUMPSTY, N. *Compressor Aerodynamics.* Addison-Wesley Publishing Company, 1998

[4] FRÉCHETTE, L.G. "Implications of Stability Modeling for High-Speed Axial Compressor Design". Master's Thesis, Department of Aeronautics and Astronautics, Massachusetts Institute of Technology, Feb. 1997.

[5] GREITZER, E.M. "Review – Axial Compressor Stall Phenomena", *Journal of Fluids Engineering* (Jun. 1980), Vol. 102, pp. 134-168.

[6] GREITZER, E.M. "Stability of Pumping Systems – The 1980 Freeman Scholar Lecture", *Journal of Fluids Engineering* (Jun. 1981), Vol. 163, pp. 193-240.

[7] GYSLING, D.L. "Dynamic Control of Rotating Stall in Axial Flow Compressors Using Aeromechanical Feedback", GTL Report No.219, Massachusetts Institute of Technology, Aug.1993.

[8] KERREBROCK, J.L. *Aircraft Engines and Gas Turbines,* 2nd ed. The MIT Press, Cambridge, Massachusetts, 1992.

[9] LONGLEY, J. "A Review of Nonsteady Flow Models for Compressor Stability", *ASME J. of Turbomachinery* (Apr. 1994), pp. 202-215.

[10] MOORE, F., AND GREITZER, E. "A Theory of Post-Stall Transients in Axial Compressors: Part I – Development of the Equations", *ASME J. of Engineering for Gas Turbines and Power, Vol.108* (1986), pp. 68-76.

[11] PERROT, V. "A Design Optimization Framework for Enhanced Compressor Stability Using Dynamic System Modeling", Master's Thesis, Department of Aeronautics and Astronautics, Massachusetts Institute of Technology, Aug. 2003

[12] SPAKOVSZKY, Z. *Applications of Axial and Radial Compressor Dynamic System Modeling*, PhD Thesis, Department of Aeronautics and Astronautics, Massachusetts Institute of Technology, 2000.

[13] SPAKOVSZKY, Z. "Backward Traveling Rotating Stall Waves in Centrifugal Compressors", *ASME Journal of* Turbomachinery (Oct. 2003), Vol. 125 No. 4